NATIONAL ADVISORY COMMITTEE FOR AERONAUTICS

TECHNICAL NOTE

No. 1478

WIND-TUNNEL INVESTIGATION OF THE STABILITY AND CONTROL CHARACTERISTICS OF A COMPLETE MODEL EQUIPPED WITH A VEE TAIL

By Edward C. Polhamus and Robert J. Moss

Langley Memorial Aeronautical Laboratory
Langley Field, Va.

Washington
November 1947

NATIONAL ADVISORY COMMITTEE FOR AERONAUTICS

TECHNICAL NOTE NO. 1478

WIND-TUNNEL INVESTIGATION OF THE STABILITY AND CONTROL CHARACTERISTICS OF A COMPLETE MODEL EQUIPPED WITH A VEE TAIL

By Edward C. Polhamus and Robert J. Moss

SUMMARY

A wind-tunnel investigation was conducted to determine the low-speed stability and control characteristics of a complete model equipped with a vee tail. Tail dihedral angles of 35°, 47°, and 55° were tested and the results compared with results of tests of a conventional-tail arrangement used with the same wing-fuselage combination. The area of the vee tail was slightly greater than that of the conventional-tail assembly (approx. 2 percent), and the vee tail was mounted on a small dorsal trunk (10 percent of vee-tail area). The total wetted area of the vee-tail assembly, therefore, was approximately 12 percent greater than that of the conventional-tail assembly. The aspect ratio of the vee tail was equal to that of the horizontal tail but greater than that of the vertical tail.

The 47° vee tail was the best of those tested when both longitudinal and lateral stability were concerned, and it contributed 40 percent more longitudinal and directional stability and 90 percent more dihedral effect than the conventional tail.

The increase in directional stability was due to the dorsal trunk and to the fact that the vee tail had a greater aspect ratio than the vertical tail.

The increase in longitudinal stability was caused by the increase in stabilizer effectiveness and the decrease in the rate of change of effective downwash with angle of attack due to the high tail position and the favorable effect of sidewash at the tail. A method of predicting the sidewash effect is presented in an appendix.

INTRODUCTION

Interest has been displayed in vee tails, particularly for high-speed aircraft, because of: (1) the possibility of a reduction in drag of the empennage due to an improved tail-fuselage juncture and due to a reduction in tail area and (2) the location of the tail out of the wing wake without encountering difficult structural problems. The isolated-tail theory (reference 1) indicates that an isolated vee-tail surface producing stability parameters equal to those produced by an isolated conventional-tail assembly (and having equal effective aspect ratios) must have an area equal to that of the conventional-tail assembly. When the vee tail is used with a wing-fuselage combination, additional factors such as the downwash and sidewash associated with the wing-fuselage vortex pattern must be considered. Inasmuch as the effects of these factors are difficult to evaluate theoretically, an experimental investigation was made of a vee tail used with a wing-fuselage combination. This vee tail had the same tail length and approximately the same total area as the sum of the horizontal and vertical tail surfaces of a conventional tail that was previously investigated with the same wing-fuselage combination. The vee tail, however, was mounted on a small dorsal trunk, the area of which was approximately 10 percent of the area of the vee tail. The effect of this dorsal trunk on lateral stability should be considered when comparing the vee and conventional tails. The aspect ratio of the vee tail was equal to that of the horizontal tail but was greater than that of the vertical tail.

The investigation included stability and control tests, with and without wing flaps, for tail dihedral angles of 35°, 47°, and 55°.

SYMBOLS

The system of axes used for the presentation of the data together with an indication of the sense of the positive forces and moments is presented in figure 1. All moments are presented about the center of gravity. Pertinent symbols are defined as follows:

C_L lift coefficient (Lift/qS)

C_D drag coefficient (Drag/qS)

C_m pitching-moment coefficient $\left(\frac{\text{Pitching moment}}{qS\bar{c}}\right)$

C_l rolling-moment coefficient $\left(\frac{\text{Rolling moment}}{qSb}\right)$

C_n yawing-moment coefficient $\left(\frac{\text{Yawing moment}}{qSb}\right)$

C_Y lateral-force coefficient $\left(\frac{\text{Lateral force}}{qS}\right)$

S wing area, square feet

b wing span, feet

$\bar{c}$ wing mean aerodynamic chord (M.A.C.), feet

q dynamic pressure, pounds per square foot $\left(\rho V^2/2\right)$

ρ mass density of air, slugs per cubic foot

V free-stream velocity, feet per second

M Mach number

α angle of attack of fuselage center line, degrees

ϵ angle of downwash, degrees

ϵ_e effective downwash (downwash that alone has same effect as downwash and sidewash)

i_t stabilizer setting (angle between line of intersection of tail panels and fuselage center line), degrees

ψ angle of yaw, degrees

δ control-surface deflection with reference to fixed surface and measured in plane normal to fixed surface, degrees

Γ_t tail dihedral angle with reference to horizontal, degrees

Subscripts:

t tail

e elevator

r rudder

f flap

m measured value

δ_e, i_t, δ_r, α, ψ denote partial derivative of a coefficient with respect to δ_e, i_t, δ_r, α, ψ, respectively; for example, $C_{m_{\delta_e}} = \frac{\partial C_m}{\partial \delta_e}$

MODEL AND APPARATUS

The model equipped with a 47° vee tail is shown mounted in the Langley 300 MPH 7- by 10-foot tunnel in figures 2 and 3 and a three-view drawing of the model as tested is presented in figure 4. Details of the vee-tail panel are presented in figure 5; details of the conventional-tail assembly are shown in figures 6 and 7.

The model was constructed of wood attached to metal reinforcing members with Cycleweld cement except for the all-metal control surfaces. The tail-control surfaces and wing flaps were 20-percent-chord plain flaps and the ailerons were 15-percent-chord plain flaps. All controls were flat-sided from the hinge line to the trailing edge and all control gaps were sealed.

Specific model configurations referred to herein are as follows:

(a) High-speed configuration
Flaps retracted
Landing gear retracted

(b) Landing configuration
Flaps deflected 60°
Landing gear extended

The tests were conducted in the Langley 300 MPH 7- by 10-foot tunnel, which is a closed rectangular tunnel with a contraction ratio of 14:1 and is powered by a 1600-horsepower synchronous motor.

TESTS

Test Conditions

Tests in the high-speed configuration were run at dynamic pressures of 88.5 and 165.2 pounds per square foot. Tests in the

landing configuration were run at a dynamic pressure of 33.5 pounds per square foot. The corresponding approximate values of Mach number and Reynolds number (based on a wing mean aerodynamic chord of 1.202 ft) were as follows:

Dynamic pressure (lb/sq ft)	Mach number	Reynolds number
33.5	0.15	1.28×10^6
88.5	.25	2.08×10^6
165.2	.35	2.82×10^6

The Reynolds number was computed using a turbulence factor of unity. The degree of turbulence of the tunnel is not known quantitatively but is believed to be small because of the high contraction ratio.

Corrections

All data have been corrected for tares caused by the model-support struts. Jet-boundary corrections were computed as follows (reference 2), where the subscript m refers to the measured values:

$$\alpha = \alpha_m + 0.88C_{L_m}$$

$$C_D = C_{D_m} + 0.0128C_{L_m}^2$$

$$C_m = C_{m_m} + 0.0222C_{L_m} \qquad \text{(for flaps undeflected)}$$

$$C_m = C_{m_m} + 0.0227C_{L_m} \qquad \text{(for flaps deflected)}$$

$$C_l = 0.98C_{l_m}$$

$$C_n = C_{n_m} - 0.0173C_{l_m}C_{L_m}$$

All force and moment coefficients were corrected for blocking by the method presented in reference 3. An increment in drag coefficient has been added in order to account for the horizontal buoyancy effected by the longitudinal static pressure gradient in the tunnel.

RESULTS AND DISCUSSION

An outline of the figures presenting the results is as follows:

Lift characteristics.- The lift characteristics of the model with the vee tail are presented in figures 8 to 13 and are summarized in the following table:

Γ_t (deg)	$C_{L_{max}}$ trimmed	C_{L_α}
$\delta_f = 0^\circ$		
35	0.76	0.085
47	.86	.088
55	.81	.085
$\delta_f = 60^\circ$		
35	1.19	.090
47	1.15	.086
55	1.18	.083

Horizontal tail characteristics.- Mean values describing the effectiveness of the elevator and stabilizer for the different dihedral angles are plotted against tail dihedral angle in figures 19 and 20, respectively. The values at $\Gamma_t = 0^\circ$ that are presented were

obtained by multiplying the values obtained with a conventional horizontal tail of the same aspect ratio (data obtained in the Langley 300 MPH 7- by 10-foot tunnel) on the same wing-fuselage combination by the ratio of tail areas. Also presented in these figures are the theoretical variations based on the isolated-tail theory of reference 1. The experimental and theoretical results are in fair agreement, but the general trend of the experimental results seems to indicate that there may be a slight increase in effectiveness at the higher dihedral angles over that predicted by the theory.

Downwash at the tail.- The average effective-downwash values for the various tail dihedral angles are presented in figure 14. These values were evaluated from tail-on and tail-off pitching moments; and, since the pitching moment contributed by a vee tail depends on sidewash as well as downwash, the effective downwash, rather than the actual downwash existing in the vertical plane, is obtained. The effective downwash is defined as the downwash that alone would produce the same pitching moment as that produced by the actual downwash and sidewash. A method of estimating the effect of sidewash on effective downwash and longitudinal stability is presented in the appendix.

Figure 21 shows the effect of tail dihedral angle on the rate of change of effective downwash angle with angle of attack. Two theoretical variations with dihedral angle are also included. One curve takes into account the change in tail height and was determined from the charts of reference 4 by assuming the tail height to be equal to the height of the tail mean aerodynamic chord. The other curve includes both the effect of tail height and the effect of sidewash (see appendix) and is in fair agreement with the experimental data.

Rudder effectiveness.- Values of the rudder-effectiveness parameter $C_{n_{\delta_r}}$ obtained from figures 15 to 17 are plotted against tail dihedral angle Γ_t in figure 22. The theoretical variation of $C_{n_{\delta_r}}$ with Γ_t, as estimated from the isolated-tail theory of reference 1, is also presented. The increase in effectiveness is probably due to the rudder induced load carried by the dorsal trunk. Also presented in figure 22 are the variations of $C_{l_{\delta_r}}$ and $C_{l_{\delta_r}}/C_{n_{\delta_r}}$ with Γ_t. The ratio of adverse rolling moments to favorable yawing moments produced by rudder deflection is greater for the vee tail than for the conventional tail.

Static longitudinal stability.- The neutral-point locations for both the cruising and landing configurations are presented in figure 23.

The tail-off neutral points and the assumed center-of-gravity position at 25 percent M.A.C. about which the moments were measured are also indicated. The curves indicate that the model with the vee tail has greater longitudinal stability than the model with the horizontal tail for the three tail dihedral angles tested. The 47° tail, which according to isolated-tail theory should contribute the same longitudinal stability as the horizontal tail tested, actually contributes 40 percent more longitudinal stability than the horizontal tail. The variation of $\left(C_{m_\alpha}\right)_t$ with Γ_t is presented in figure 24. For comparison, the horizontal-tail contribution $\left(\Gamma_t = 0°\right)$ was increased by the ratio of the vee-tail area to the horizontal-tail area. Also presented in this figure is the theoretical variation of $\left(C_{m_\alpha}\right)_t$ with Γ_t, and it can be seen that the decrease in longitudinal stability with dihedral angle is overestimated. The overestimated decrease in stability can be accounted for by the increase in stabilizer effectiveness and the decrease in the rate of change of effective downwash with angle of attack due to the increased tail height and the favorable effect of sidewash. A method of estimating this sidewash effect is presented in the appendix.

Static directional and lateral stability.- The static lateral-stability parameters determined from pitch tests at yaw angles of 5° and -5° for both the high-speed and the landing configurations are plotted against angle of attack in figure 18. In the high-speed configuration a large amount of directional and lateral stability exists for all three dihedral angles and the maximum stability would appear to occur at some angle between 47° and 55°. In the landing configuration the high static directional stability and the dihedral effect are indicated for angles of attack below 6°. Above 6° there is a slight loss of dihedral effect and a large loss in directional stability. It will be noted that the 47° vee tail, which is the best of those tested, contributed approximately 40 percent more longitudinal and directional stability and 90 percent more dihedral effect than the conventional tail. The increase in directional stability, however, is due to the fact that the aspect ratio of the vee tail is greater than that of the vertical tail and due to the dorsal trunk upon which the vee tail was mounted. The effect of this trunk can be seen in figure 25, which presents the actual and theoretical variations of the tail contribution to directional stability $\left(C_{n_\psi}\right)_t$ and to dihedral effect $\left(C_{l_\psi}\right)_t$ with tail dihedral angle. The reasons for the large contribution to directional stability of this small trunk (approx. 10 percent of the vee-tail area) are that the trunk increases the effective aspect ratio of the vee tail in yaw. Since tail effectiveness is proportional to $\sin^2\Gamma_t$, this trunk is more effective per unit area than the vee tail.

The high dihedral effect (equivalent to approx. 16.5° of wing geometric dihedral for the 47° tail) is due to the high geometric dihedral of the tail.

CONCLUSIONS

From low-speed wind-tunnel tests of a complete model equipped with a vee tail having tail dihedral angles of 35°, 47°, and 55° and from comparisons with tests of a conventional tail used with the same wing-fuselage combination, the following conclusions with regard to static stability and control were reached:

1. The 47° vee tail appeared to be the best of those tested when both longitudinal and lateral stability were concerned.

2. The 47° vee tail, the area of which was approximately the same (2 percent greater) as the conventional tail assembly but was mounted on a small dorsal trunk (10 percent of vee-tail area), contributed 40 percent more longitudinal and directional stability and 90 percent more dihedral effect than the conventional tail.

3. The increase in directional stability was due to the dorsal trunk and to the fact that the vee tail had a greater aspect ratio than the vertical tail.

4. The increase in longitudinal stability was caused by the increase in stabilizer effectiveness and the decrease in the rate of change of effective downwash with angle of attack due to the high tail position and the favorable effect of sidewash at the tail.

5. The measured variations of stabilizer and elevator effectiveness with tail dihedral angle agreed fairly well with the isolated-tail theory.

Langley Memorial Aeronautical Laboratory
National Advisory Committee for Aeronautics
Langley Field, Va., July 31, 1947

APPENDIX

METHOD OF ESTIMATING SIDEWASH EFFECT ON LONGITUDINAL STABILITY

Symbols

α	angle of attack of airplane in plane of symmetry
$(\alpha_N)_{tail}$	angle of attack of tail panel in plane normal to chord plane of tail surface
ϵ	induced angle (downwash) in plane of symmetry
ϵ_N	induced angle in plane normal to chord plane of tail surface
$(C_L)_{tail}$	lift coefficient of tail measured in plane of symmetry
$\left(C_{L_\alpha}\right)_N$	lift-curve slope of tail in plane normal to chord plane of tail surface
Γ_t	dihedral angle of tail surface
$(C_m)_{tail}$	airplane pitching moment due to tail lift
$\frac{b_t}{2}$	span of one vee-tail panel
$\bar{c}_w$	M.A.C. of wing
$\bar{c}_t$	M.A.C. of tail
c_t	local chord of tail
l_t	tail length measured from c.g. to $\bar{c}_t/4$
S_t	actual (not projected) area of tail
S_w	wing area
q	free-stream dynamic pressure
q_t	effective dynamic pressure at tail
w	total induced velocity in vertical plane $(w_T + w_B)$

w_T velocity in vertical plane induced by trailing vortices (downwash)

w_B velocity in vertical plane induced by bound vortex (downwash)

w_S velocity in plane normal to vertical plane induced by trailing vortices (sidewash)

w_N total induced velocity in plane normal to tail panel

w_{T_N} velocity in normal plane induced by trailing vortices

X tail length measured from $\bar{c}_w/4$ to $\bar{c}_t/4$

s wing vortex semispan

v tangential velocity of a vortex at Y for unit circulation

Y distance from vortex center to point in question

V velocity at tail parallel to X-axis

Method

When the longitudinal stability contributed by a vee tail is calculated, the effect of sidewash should be included. The following derivation of the longitudinal-stability equation includes this effect. The angle of attack in the plane normal to the tail panel is as follows (see fig. 26):

$$(\alpha_N)_{tail} = \alpha \cos \Gamma_t - \epsilon_N \tag{1}$$

and

$$(C_L)_{tail} = (C_{L_\alpha})_N (\alpha_N)_{tail} \cos \Gamma_t \tag{2}$$

By substituting equation (1) in equation (2)

$$(C_L)_{tail} = (C_{L_\alpha})_N \left(\alpha \cos \Gamma_t - \epsilon_N\right) \cos \Gamma_t \tag{3}$$

Now

$$\left(C_m\right)_{tail} = \left(C_L\right)_{tail} \frac{l_t}{\bar{c}_w} \frac{S_t}{S_w} \frac{q_t}{q} \tag{4}$$

and by substituting equation (3) in equation (4)

$$\left(C_m\right)_{tail} = \left(\alpha \cos \Gamma_t - \epsilon_N\right) \left(C_{L_\alpha}\right)_N \cos \Gamma_t \frac{l_t}{\bar{c}_w} \frac{S_t}{S_w} \frac{q_t}{q}$$

or

$$\left(C_{m_\alpha}\right)_{tail} = \left(\cos \Gamma - \frac{\partial \epsilon_N}{\partial \alpha}\right) \left(C_{L_\alpha}\right)_N \cos \Gamma_t \frac{l_t}{\bar{c}_w} \frac{S_t}{S_w} \frac{q_t}{q} \tag{5}$$

Since all available theoretical and experimental induced angles are presented as downwash angles, ϵ, equation (5) will be revised by replacing $\frac{\partial \epsilon_N}{\partial \alpha}$ with $\frac{\partial \epsilon}{\partial \alpha}$ and a correction factor. Since $\epsilon = \frac{w}{V}$ and $\epsilon_N = \frac{w_N}{V}$,

$$\frac{\partial \epsilon_N}{\partial \alpha} = \frac{\partial \epsilon}{\partial \alpha} \frac{w_N}{w} \tag{6}$$

By substituting equation (6) in equation (5)

$$\left(C_{m_\alpha}\right)_{tail} = \left(\cos \Gamma_t - \frac{\partial \epsilon}{\partial \alpha} \frac{w_N}{w}\right) \left(C_{L_\alpha}\right)_N \cos \Gamma_t \frac{l_t}{\bar{c}_w} \frac{S_t}{S_w} \frac{q_t}{q} \tag{7}$$

A more convenient form of equation (7) is

$$\left(C_{m_\alpha}\right)_{tail} = \left(1 - \frac{\partial \epsilon}{\partial \alpha} \frac{w_N}{w \cos \Gamma_t}\right) \left(C_{L_\alpha}\right)_N \cos^2 \Gamma_t \frac{l_t}{\bar{c}_w} \frac{S_t}{S_w} \frac{q_t}{q} \tag{8}$$

Values of $\frac{\partial \epsilon}{\partial \alpha}$ may be obtained from the charts of reference 4 by use of a tail height equal to the height of the M.A.C. of the tail. Values of $\frac{w_N}{w \cos \Gamma_t}$ may be obtained as follows:

$$\frac{w_N}{w \cos \Gamma_t} = \frac{w_B \cos \Gamma_t}{w \cos \Gamma_t} + \frac{w_{T_N}}{w \cos \Gamma_t}$$

and

$$\frac{w_N}{w \cos \Gamma_t} = \frac{w_B}{w} + \frac{w_{T_N}}{w_T \cos \Gamma_t} \frac{w_T}{w}$$

or

$$\frac{w_N}{w \cos \Gamma_t} = \frac{w_B}{w} + \frac{w_{T_N}}{w_T \cos \Gamma_t} \left(1 - \frac{w_B}{w}\right) \tag{9}$$

An approximate value $\frac{w_B}{w}$ may be obtained from the following equation which was derived from the equation for downwash due to the bound and trailing vortices given in reference 5:

$$\frac{w_B}{w} = \frac{s^2}{s^2 + X^2 + X\sqrt{X^2 + s^2}} \tag{10}$$

Equation (10) is for a point midway between the two trailing vortices in the plane of the horseshoe vortex but is sufficiently accurate for these calculations.

The factor $\frac{w_{T_N}}{w_T \cos \Gamma_t}$ (equation (9)) may be determined graphically as follows: By assuming a horseshoe vortex of span equal to 90 percent of the wing span (see fig. 27), the induced velocities due to the trailing vortices in the normal and vertical planes are obtained at various spanwise stations of the tail. Inasmuch as only velocity ratios are desired, the tangential velocity v of the vortex at the first spanwise point investigated may be drawn to any convenient length.

At any other point the velocity may then be easily drawn since it is inversely proportional to the distance Y from the vortex center to the point in question. At each spanwise station the induced velocities w_{T_N} and $w_T \cos \Gamma_t$ due to both trailing vortices are obtained and then the factor $\frac{w_{T_N}}{w_T \cos \Gamma_t}$ is weighted according to the local chord and integrated over the span in order to obtain an average value to substitute in equation (9). This procedure need be done for only one panel since it will be the same for both.

From figure 27 it can be seen that $\frac{w_{T_N}}{w_T \cos \Gamma_t}$ is less than unity and that the reduction is due to the sidewash w_S.

REFERENCES

1. Purser, Paul E., and Campbell, John P.: Experimental Verification of a Simplified Vee-Tail Theory and Analysis of Available Data on Complete Models with Vee Tails. NACA ACR No. L5A03, 1945.

2. Gillis, Clarence L., Polhamus, Edward C., and Gray, Joseph L., Jr.: Charts for Determining Jet-Boundary Corrections for Complete Models in 7- by 10-Foot Closed Rectangular Wind Tunnels. NACA ARR No. L5G31, 1945.

3. Thom, A.: Blockage Corrections in a Closed High-Speed Tunnel. R. & M. No. 2033, British A.R.C., 1943.

4. Silverstein, Abe, and Katzoff, S.: Design Charts for Predicting Downwash Angles and Wake Characteristics behind Plain and Flapped Wings. NACA Rep. No. 648, 1939.

5. von Kármán, Th., and Burgers, J. M.: General Aerodynamic Theory - Perfect Fluids. Mathematical Foundation of the Theory of Wings with Finite Span. Vol. II of Aerodynamic Theory, div. E, ch. III, W. F. Durand, ed., Julius Springer (Berlin), 1935, p. 142. (Reprint of 1943.)

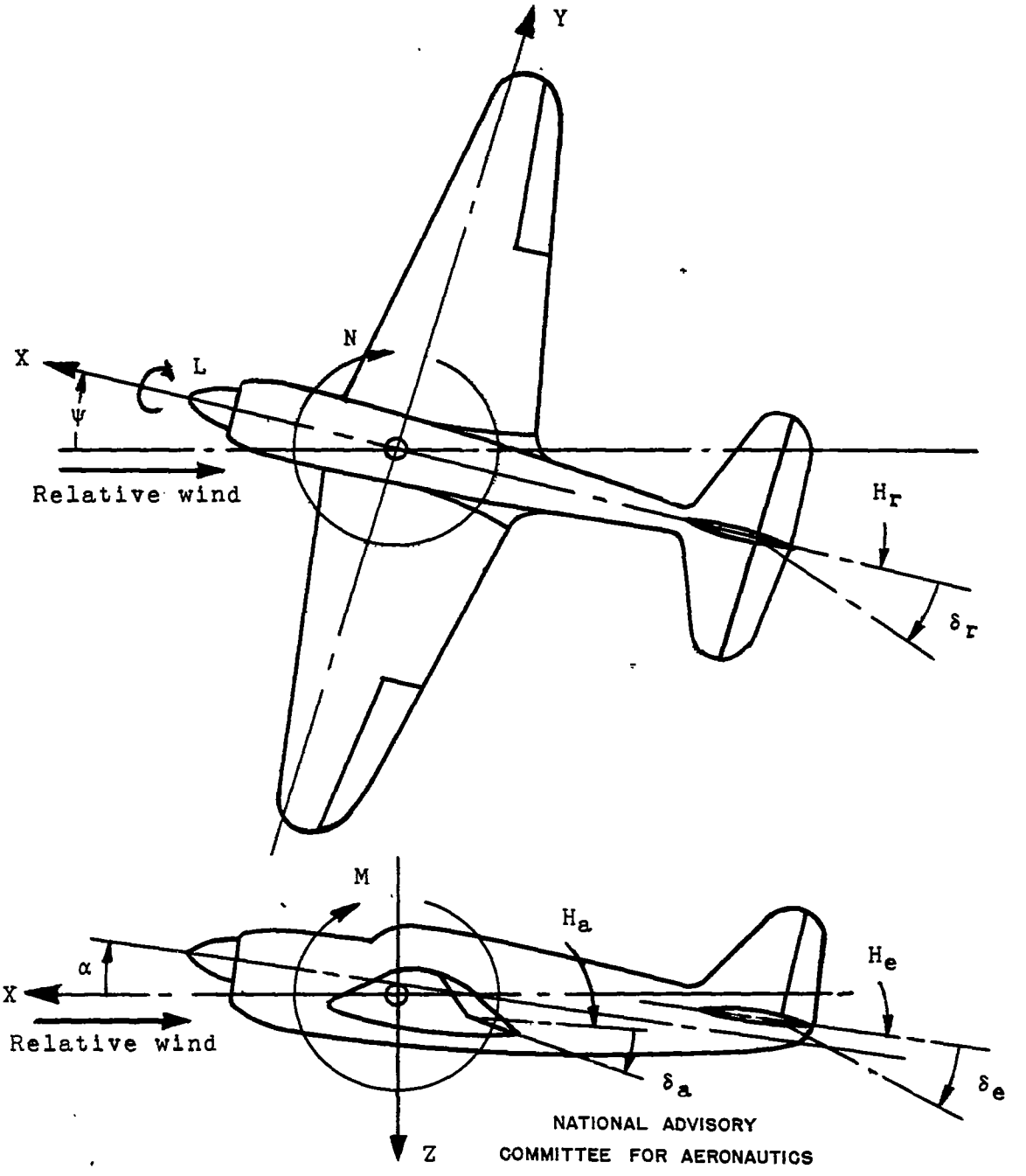

Figure 1.- System of axes and control-surface hinge moments and deflections. Positive values of forces, moments, and angles are indicated by arrows. Positive values of tab hinge moments and deflections are in the same directions as the positive values for the control surfaces to which the tabs are attached.

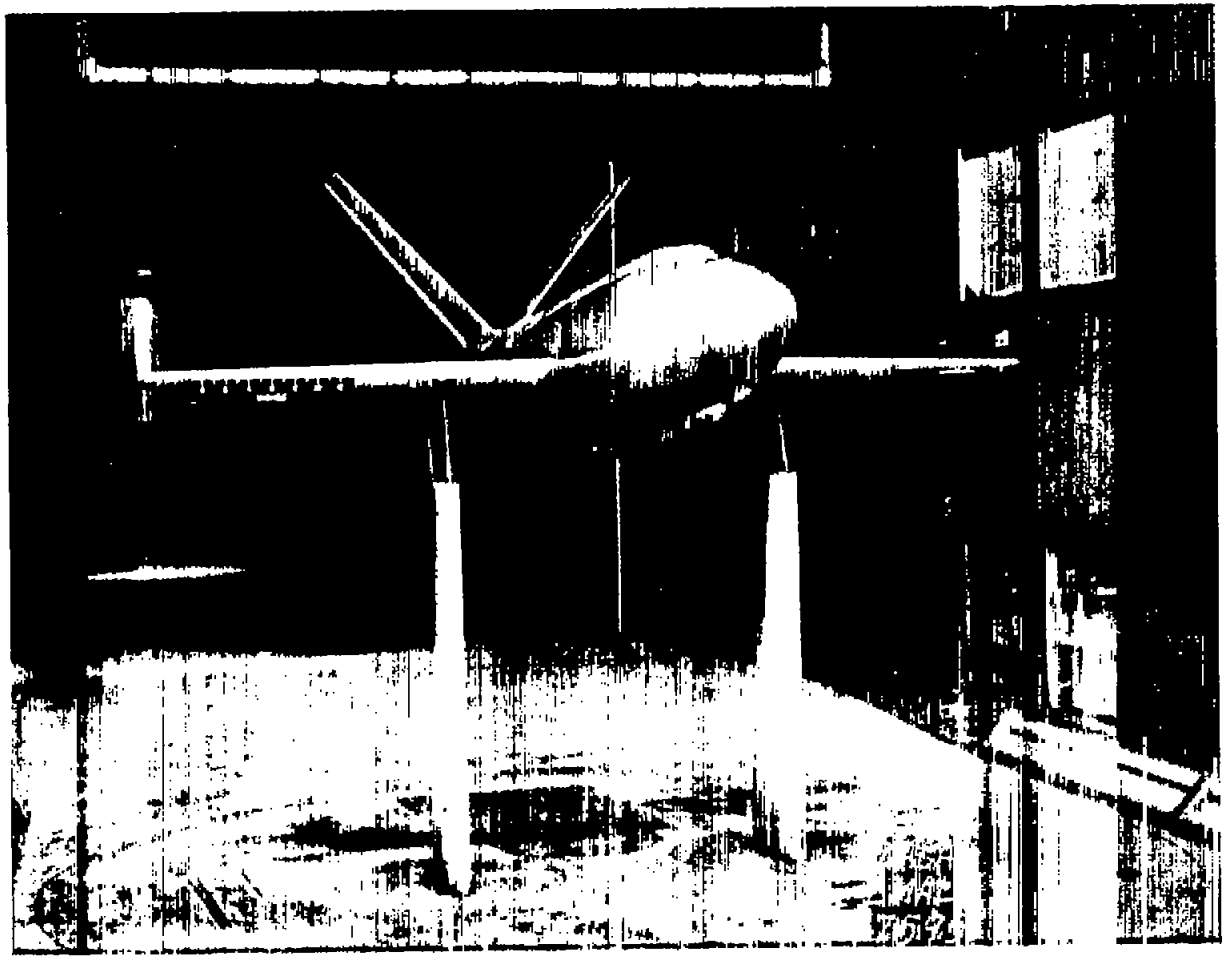

Figure 2.- Front view of model mounted in the Langley 300 MPH 7- by 10-foot tunnel.

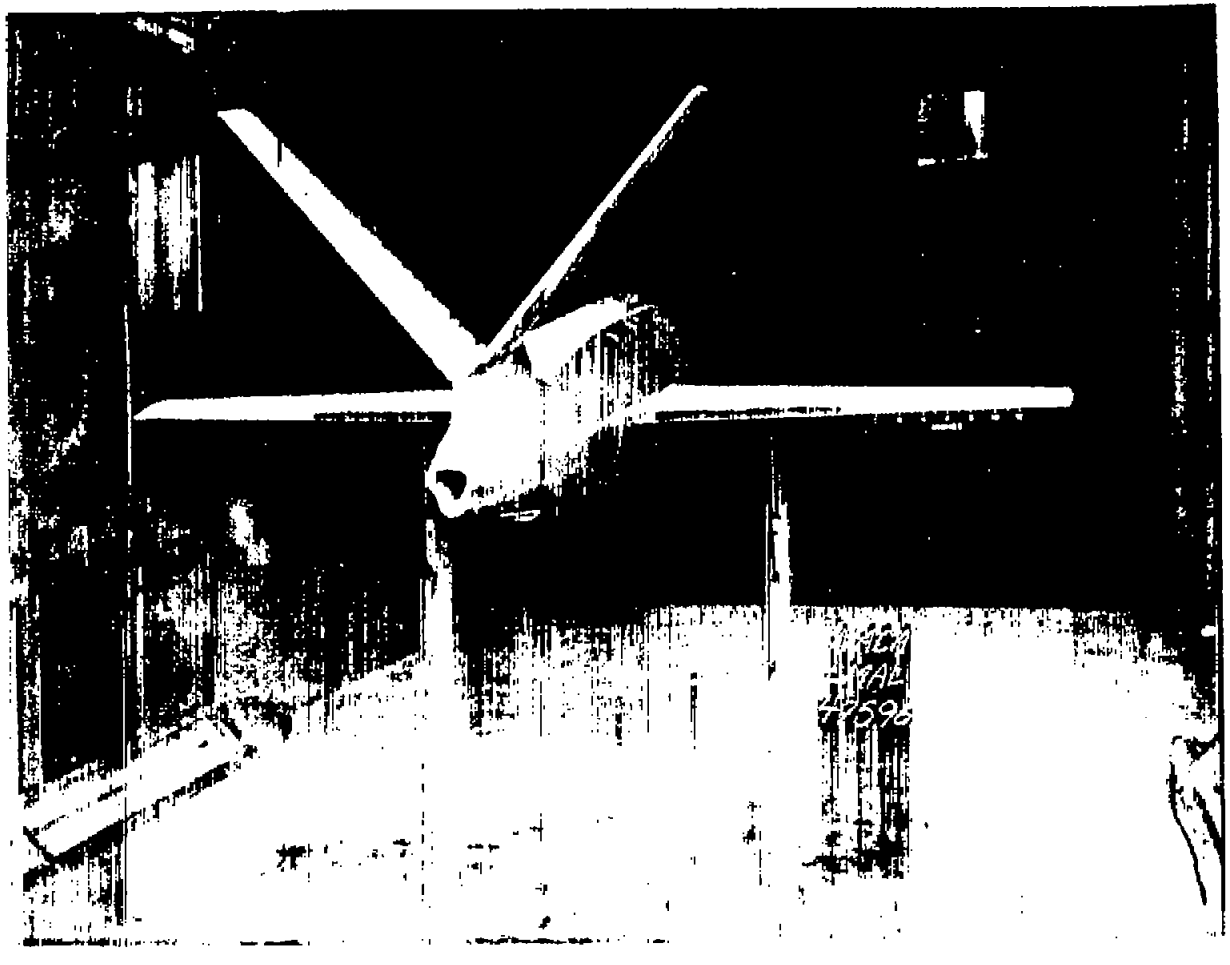

Figure 3.- Rear view of model mounted in the Langley 300 MPH 7- by 10-foot tunnel.

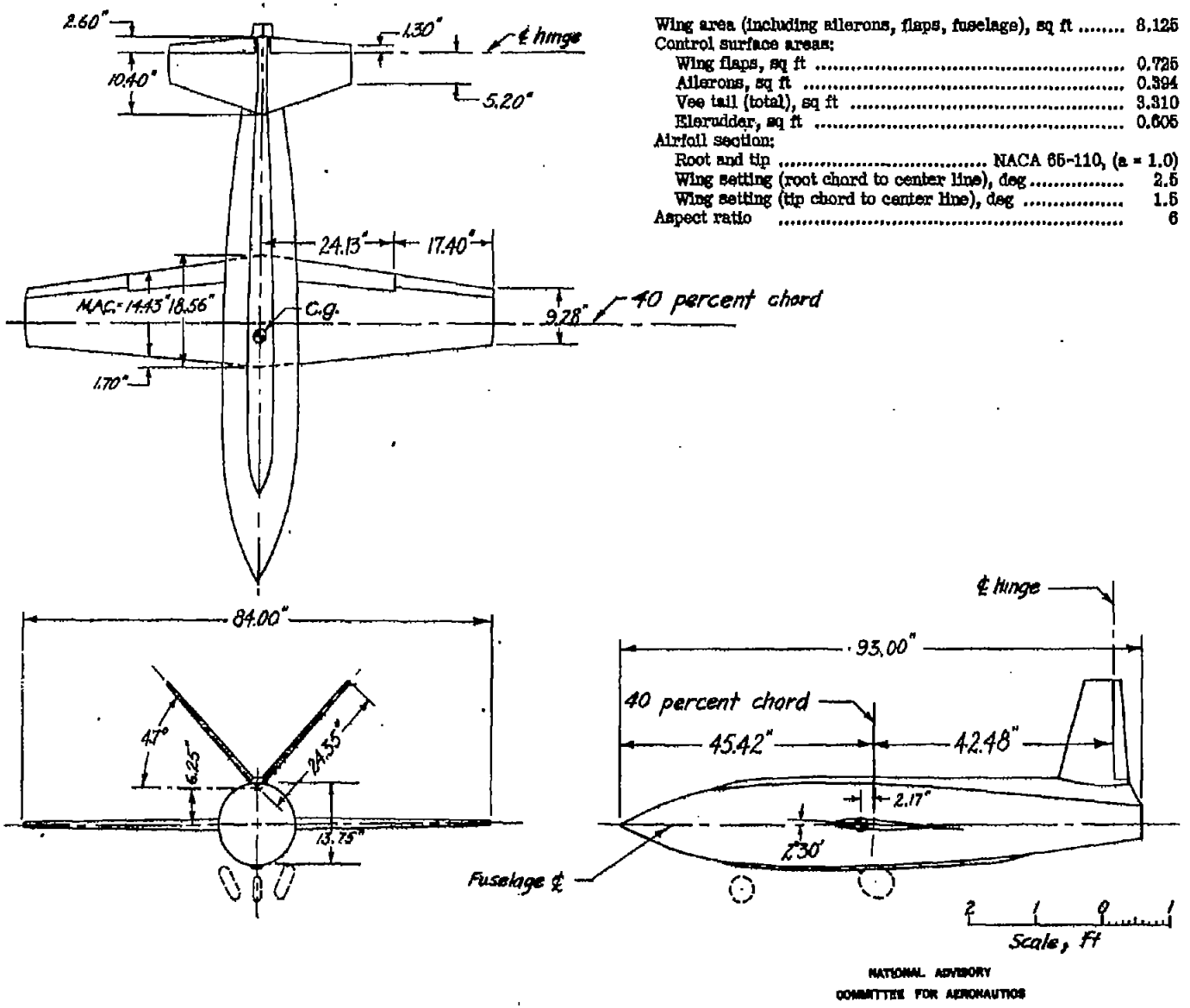

Wing area (including ailerons, flaps, fuselage), sq ft	8.125
Control surface areas:	
Wing flaps, sq ft	0.725
Ailerons, sq ft	0.394
Vee tail (total), sq ft	3.310
Elerudder, sq ft	0.605
Airfoil section:	
Root and tip	NACA 65-110, (a = 1.0)
Wing setting (root chord to center line), deg	2.5
Wing setting (tip chord to center line), deg	1.5
Aspect ratio	6

Figure 4.- Three-view drawing of the model.

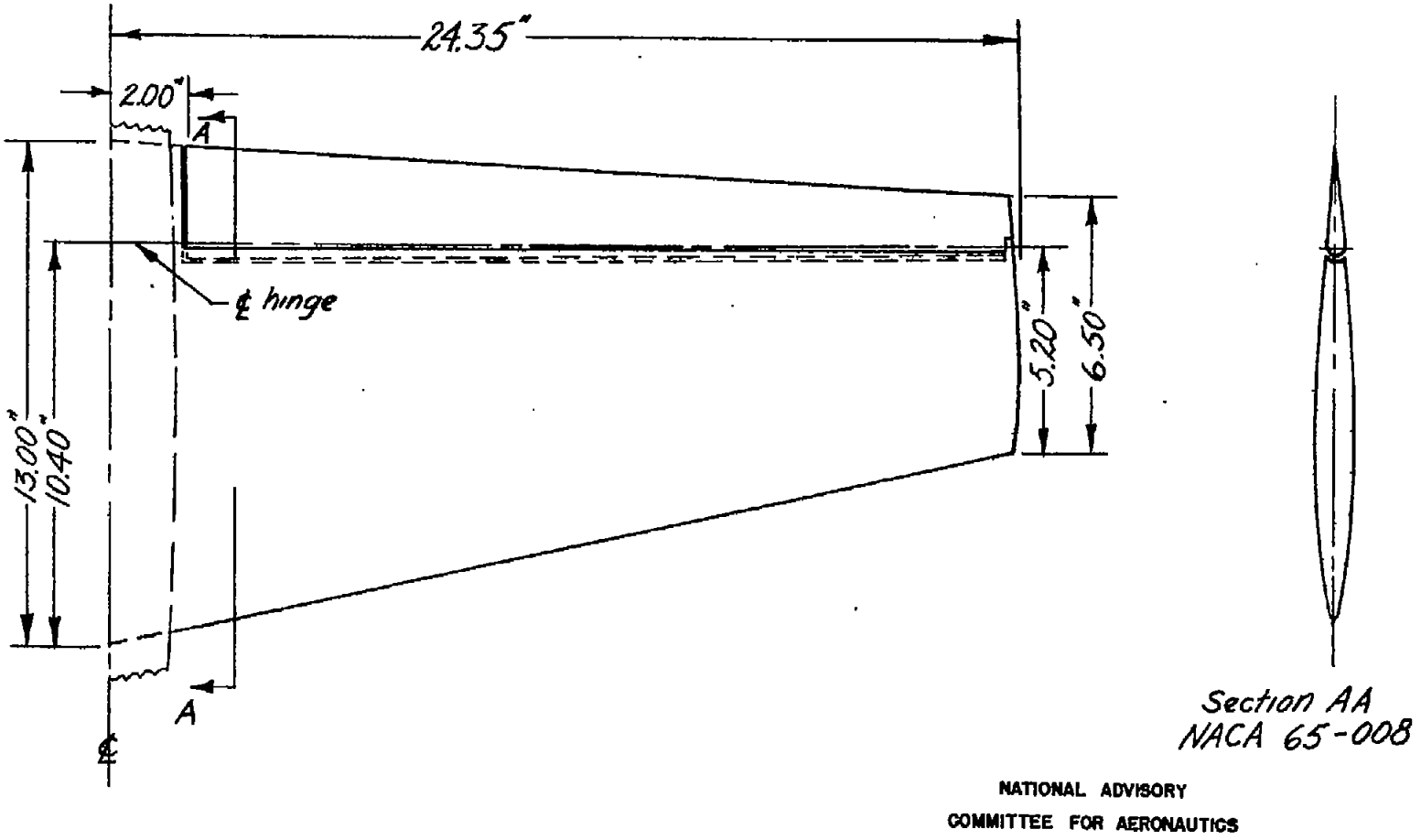

Figure 5.- Vee-tail panel. Area (total, not including trunk), 3.31 square feet; area (dorsal trunk), 0.32 square feet; aspect ratio, 5.0.

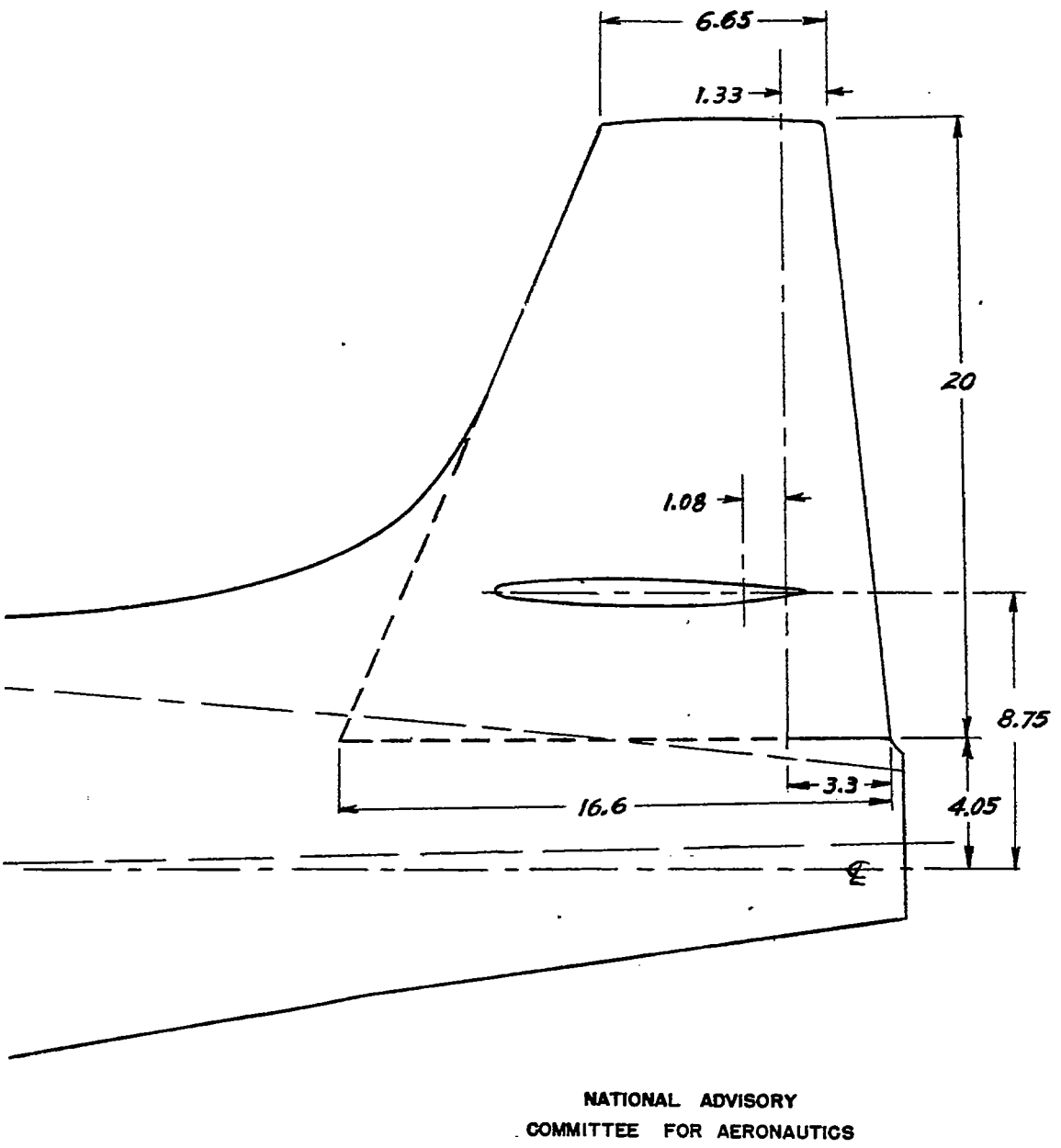

Figure 6.- Vertical tail. Area (total), 1.60 square feet; aspect ratio, 1.74.

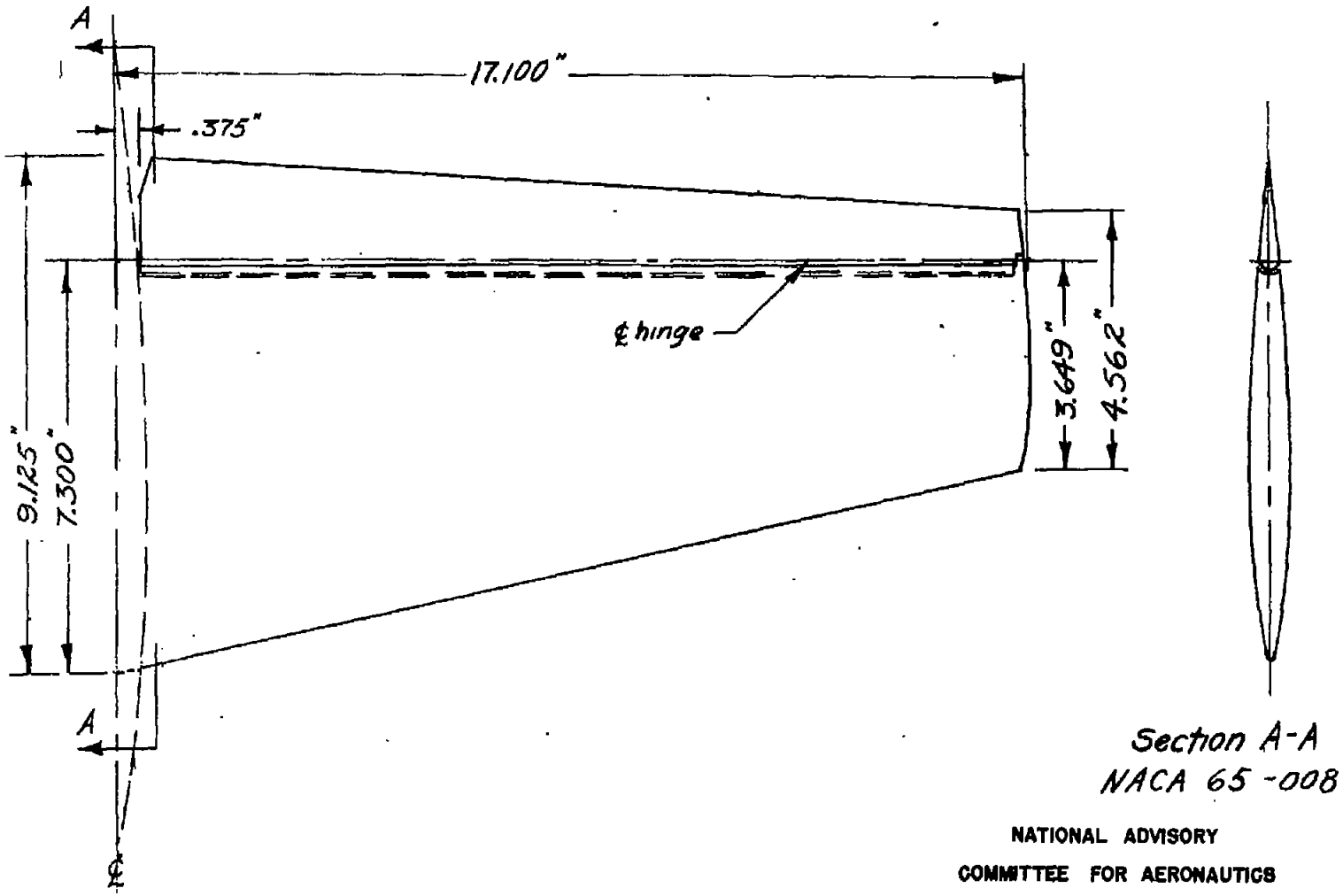

Figure 7.- Horizontal tail. Area (total), 1.625 square feet; aspect ratio, 5.0; trailing edge angle, 10°.

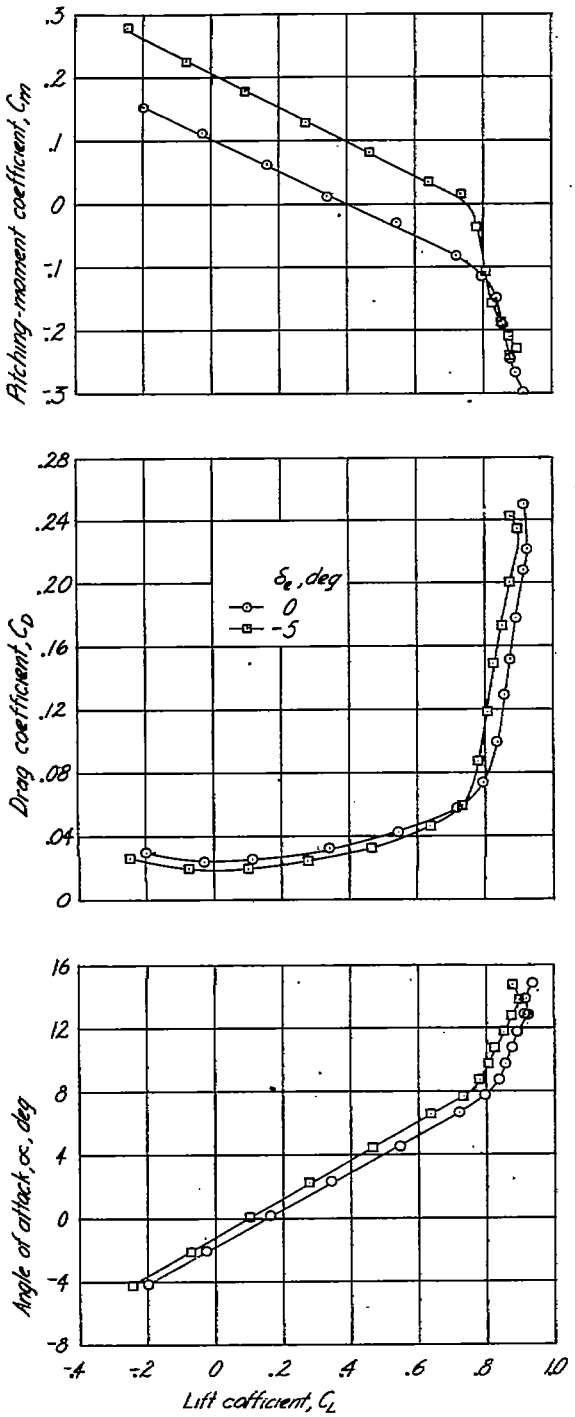

(a) $\delta_f = 0°$; $M = 0.35$.

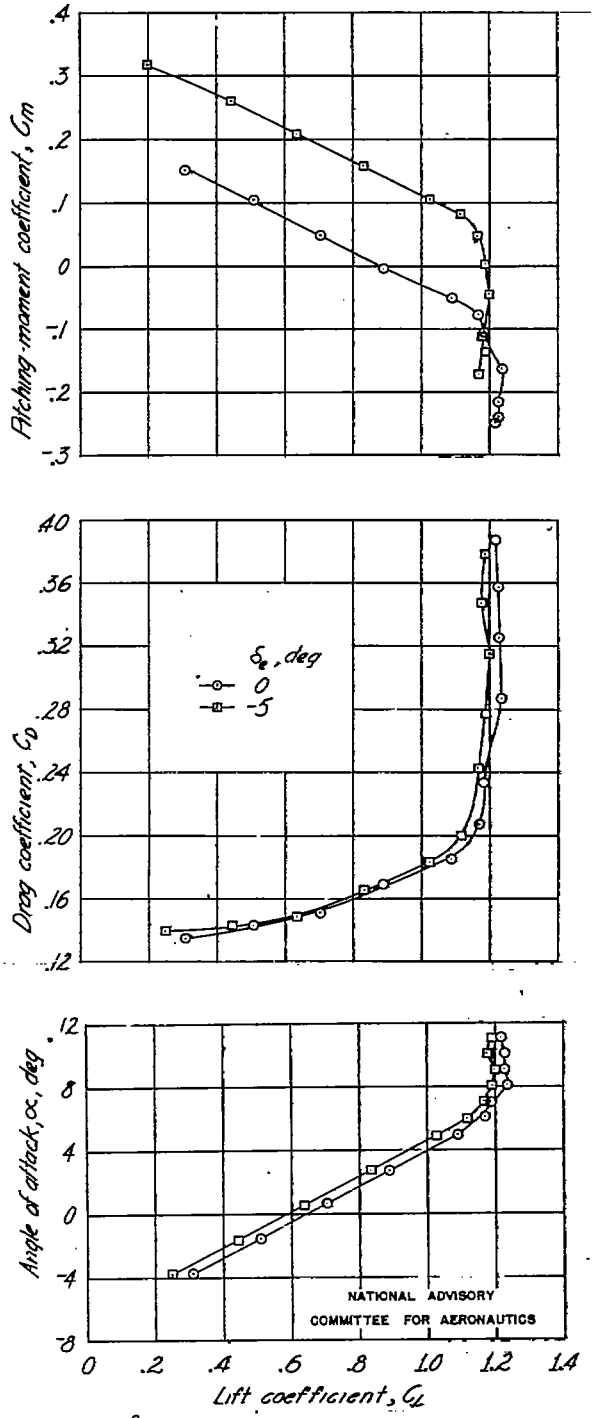

(b) $\delta_f = 60°$; $M = 0.15$.

Figure 8.- Effect of elevator deflection on the aerodynamic characteristics in pitch of the model with a 35° vee tail.

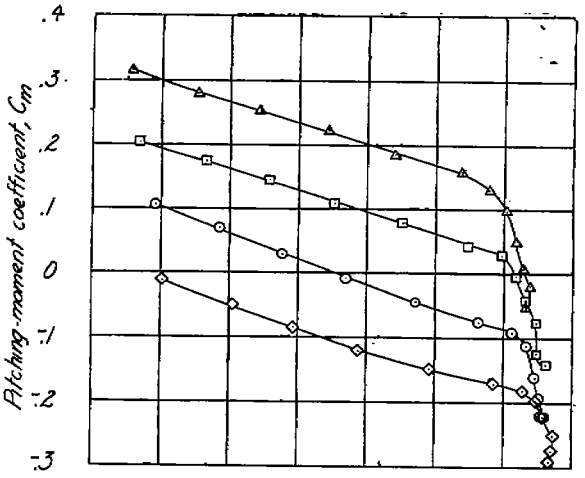

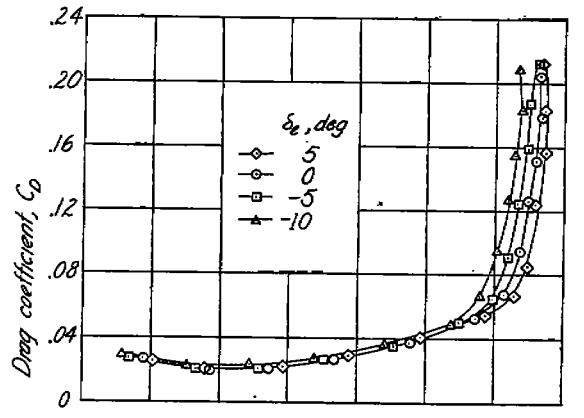

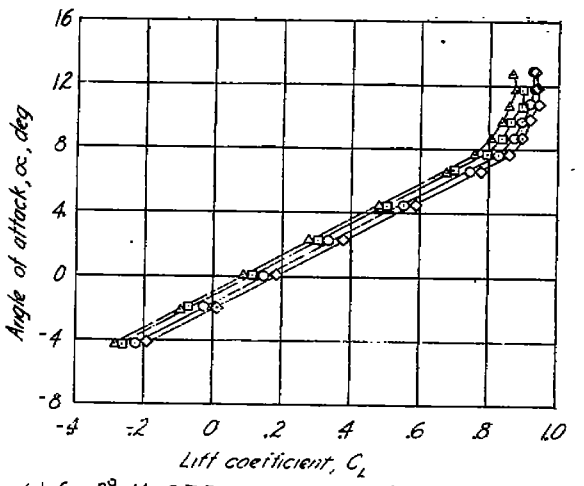

(a) $\delta_f = 0°$; $M = 0.35$.

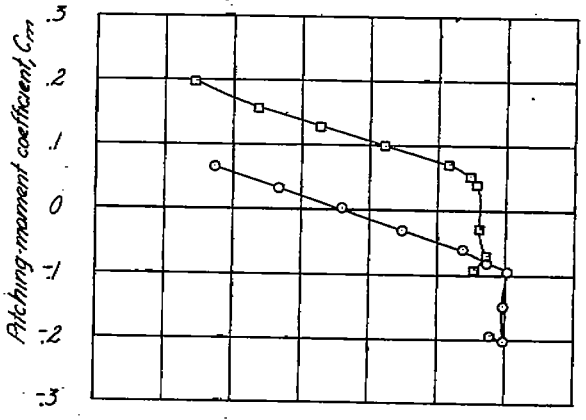

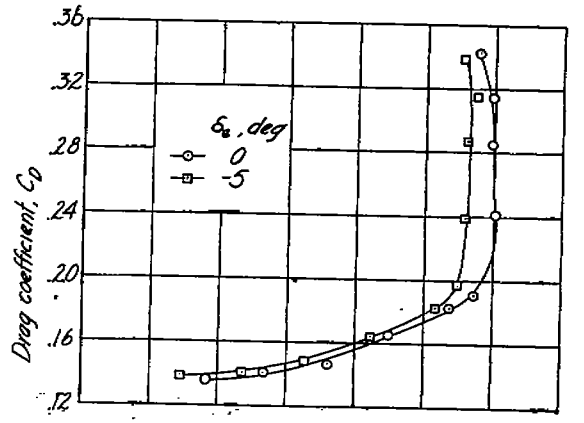

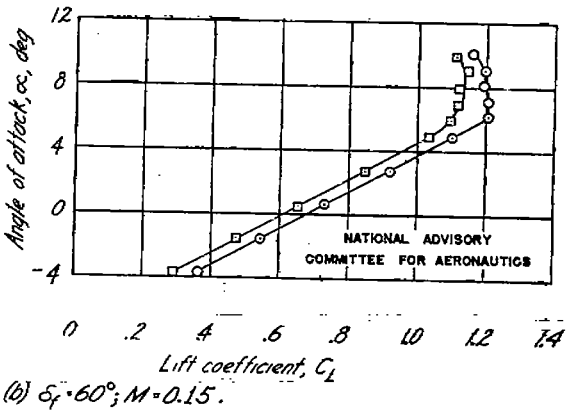

(b) $\delta_f = 60°$; $M = 0.15$.

Figure 9.- Effect of elevator deflection on the aerodynamic characteristics in pitch of the model with a 47° vee tail.

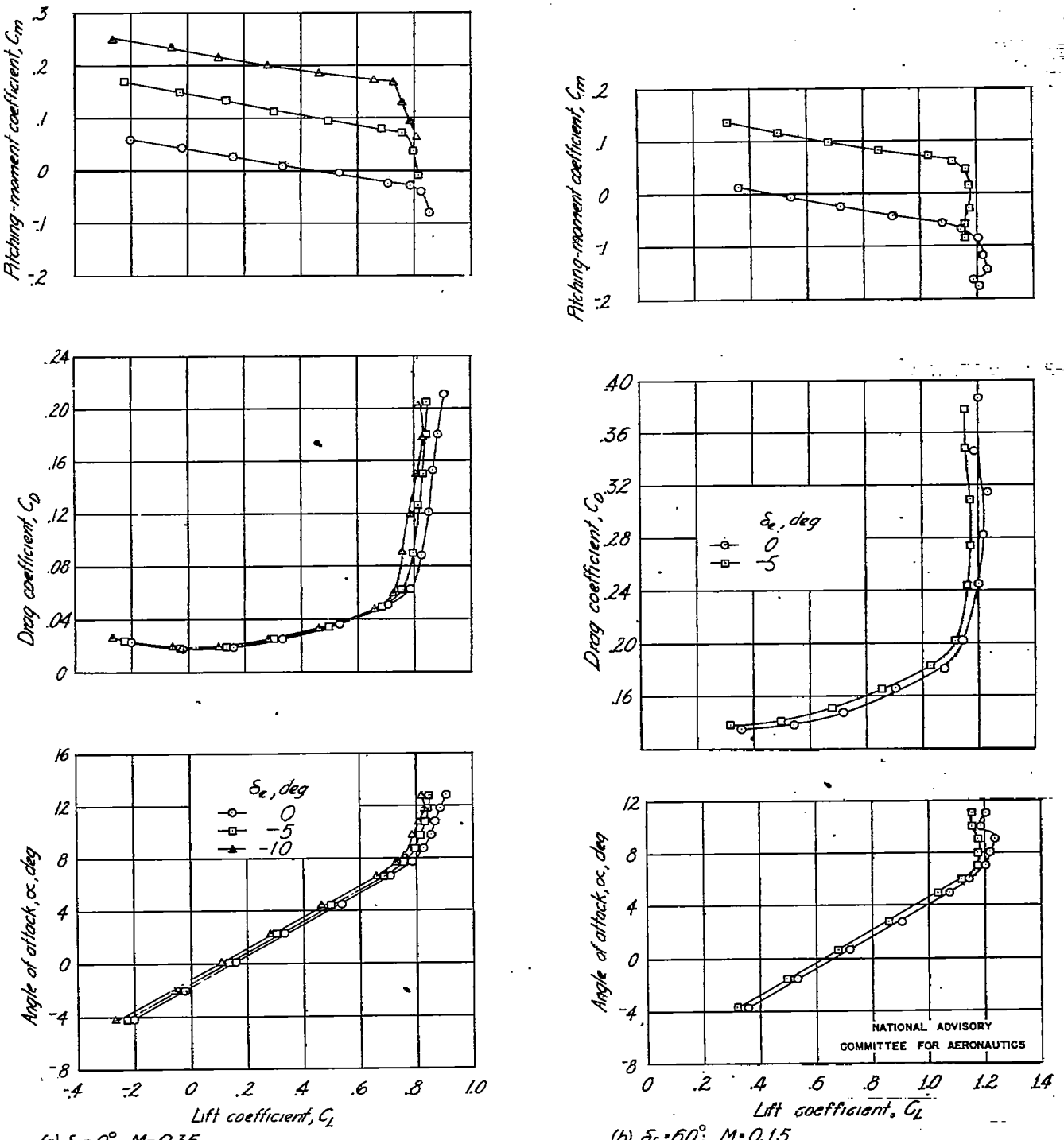

Figure 10.- Effect of elevator deflection on the aerodynamic characteristics in pitch of the model with a 55° vee tail.

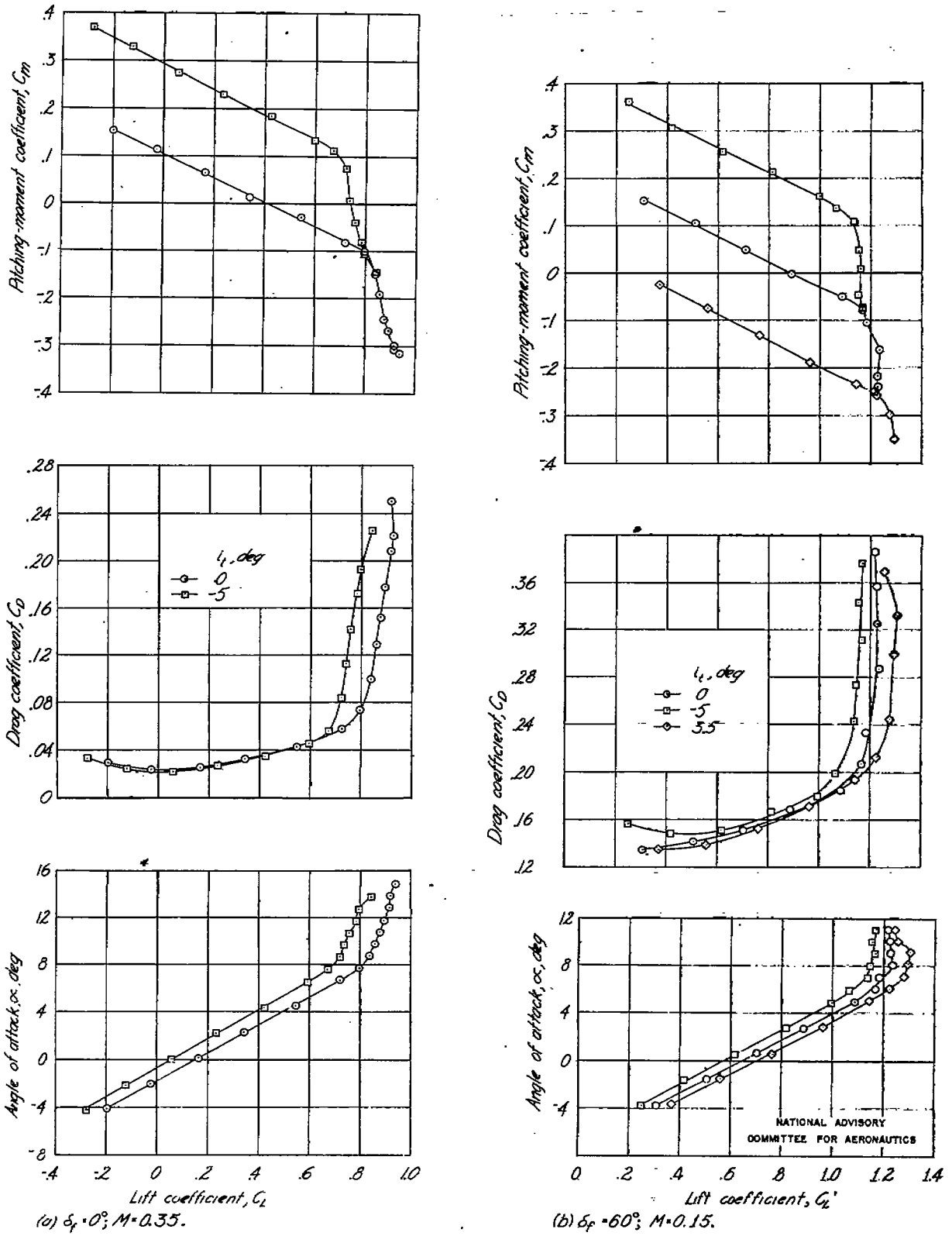

Figure 11.- Effect of stabilizer setting on the aerodynamic characteristics in pitch of the model with a 35° vee tail.

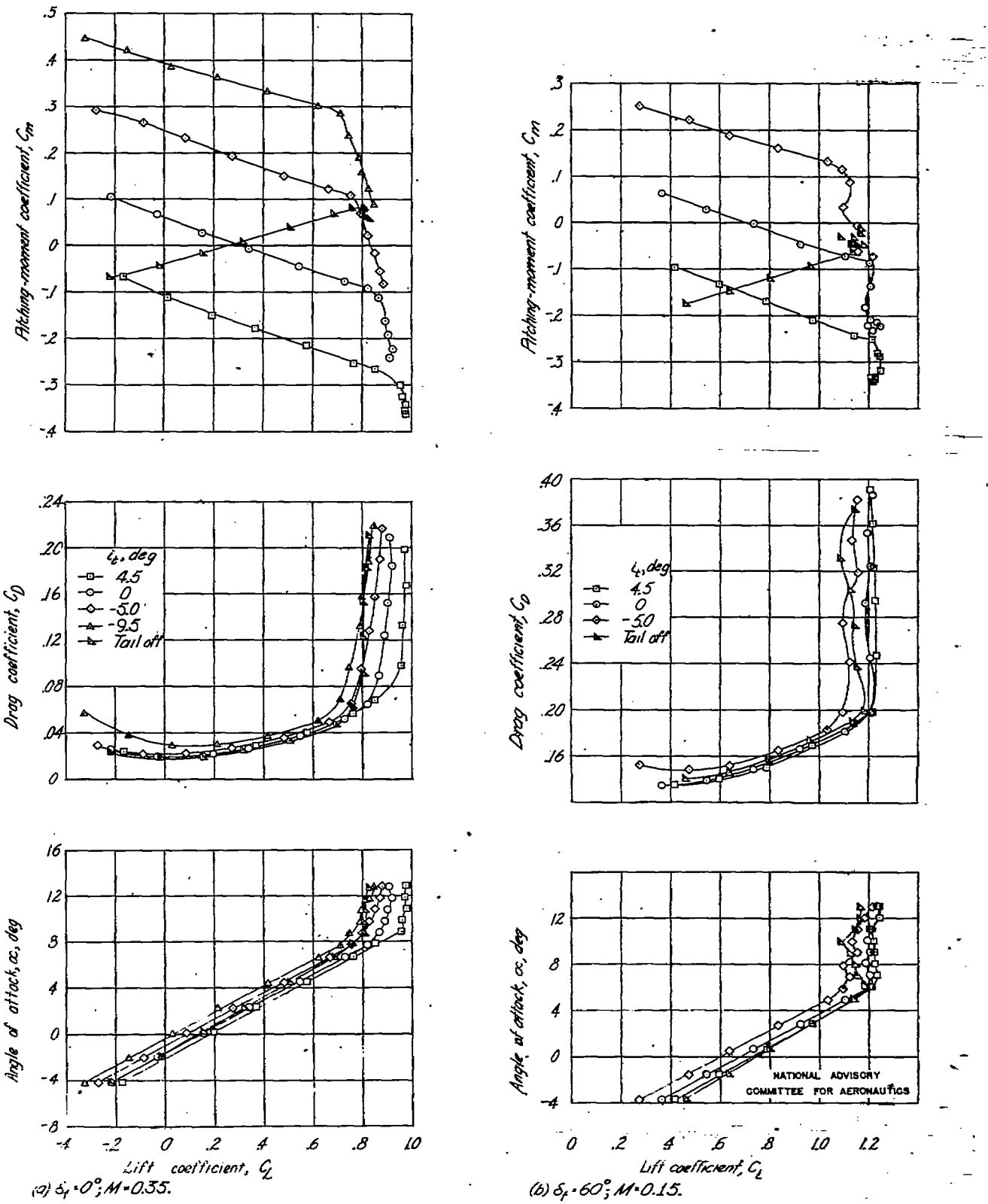

Figure 12.- Effect of stabilizer setting on the aerodynamic characteristics in pitch of the model with a 47° vee tail.

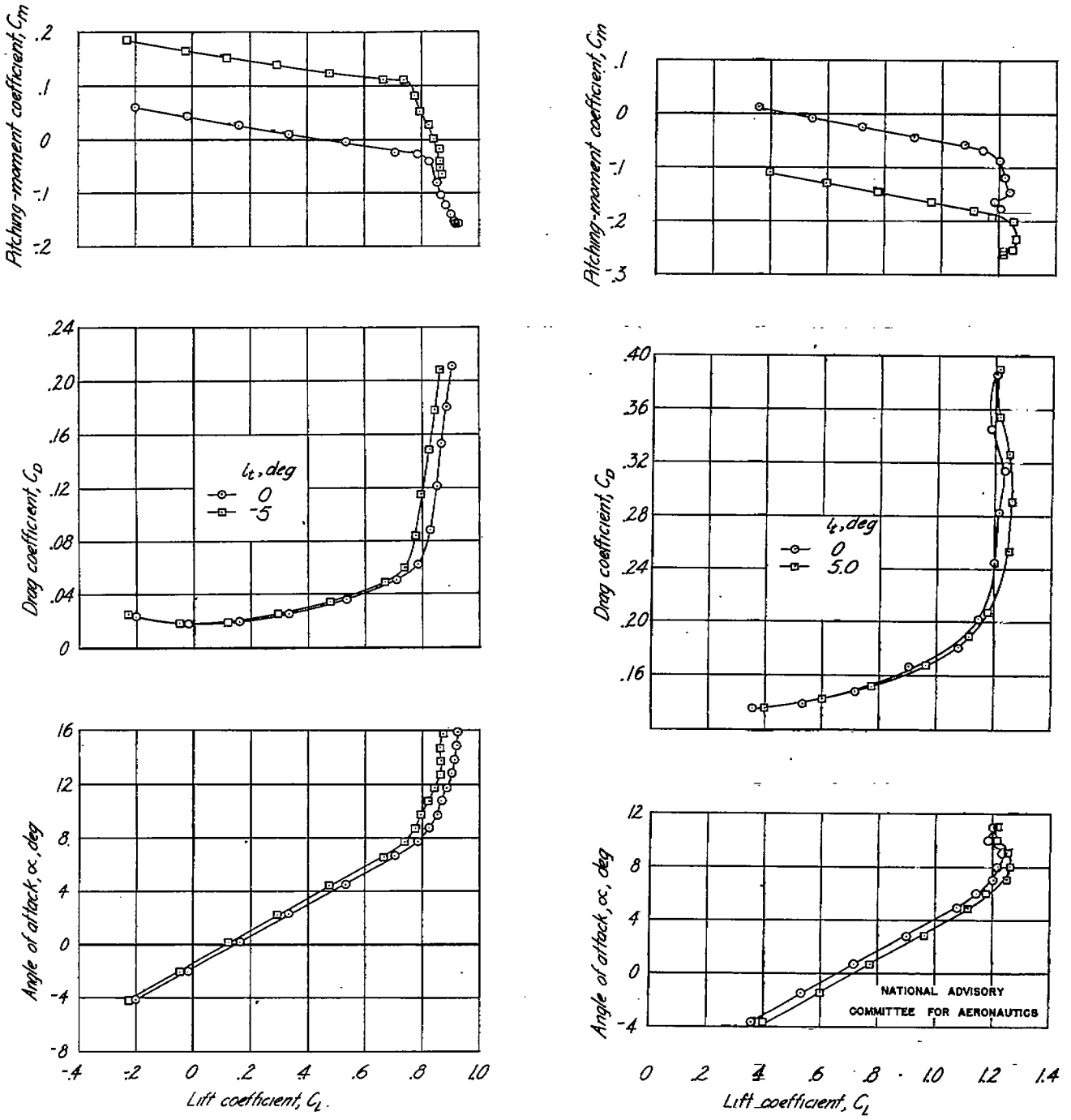

(a) $\delta_f = 0°$; $M = 0.35$.

(b) $\delta_f = 60°$; $M = 0.15$.

Figure 13.- Effect of stabilizer setting on the aerodynamic characteristics in pitch of the model with a 55° vee tail.

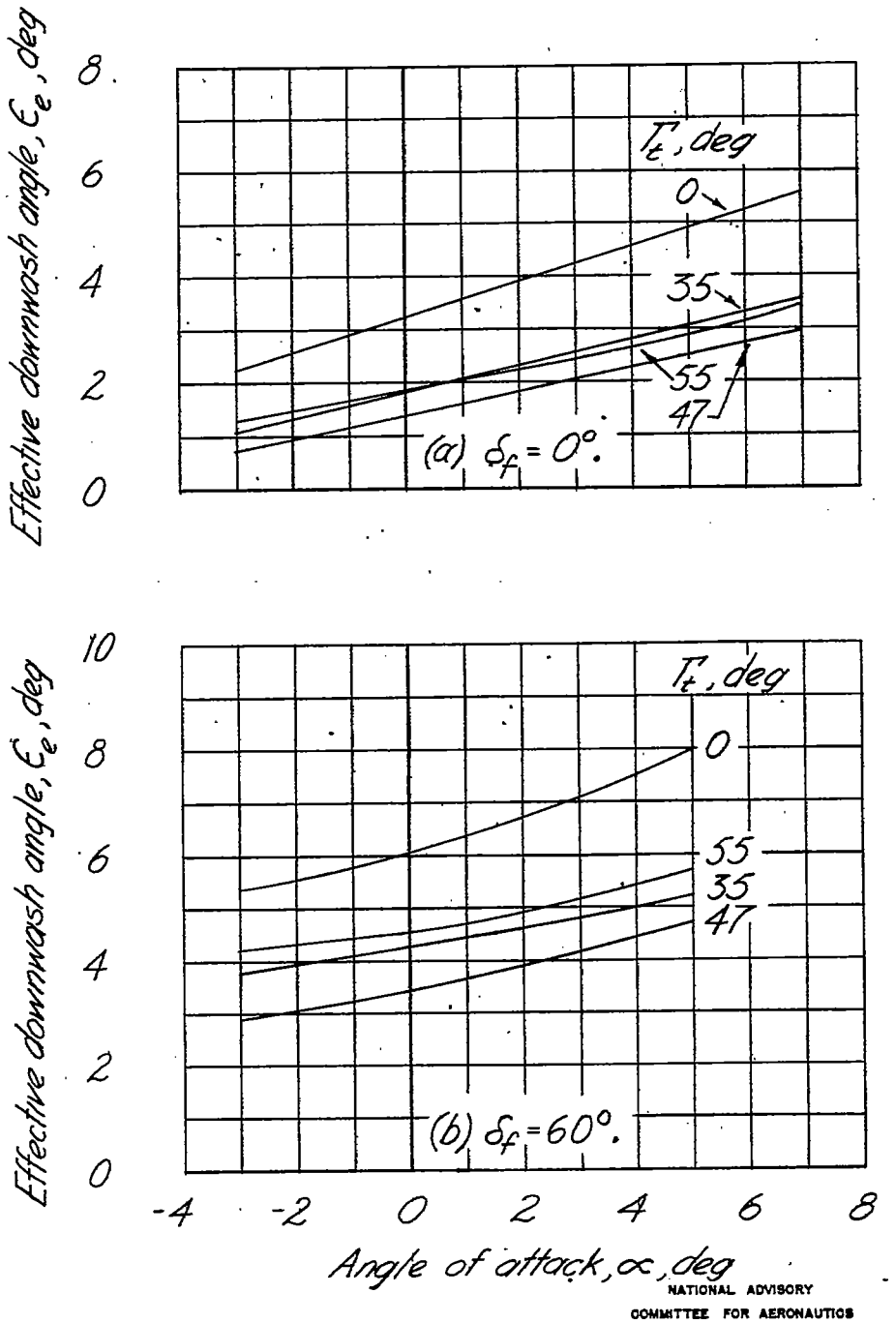

Figure 14.- Variation of effective downwash with angle of attack.

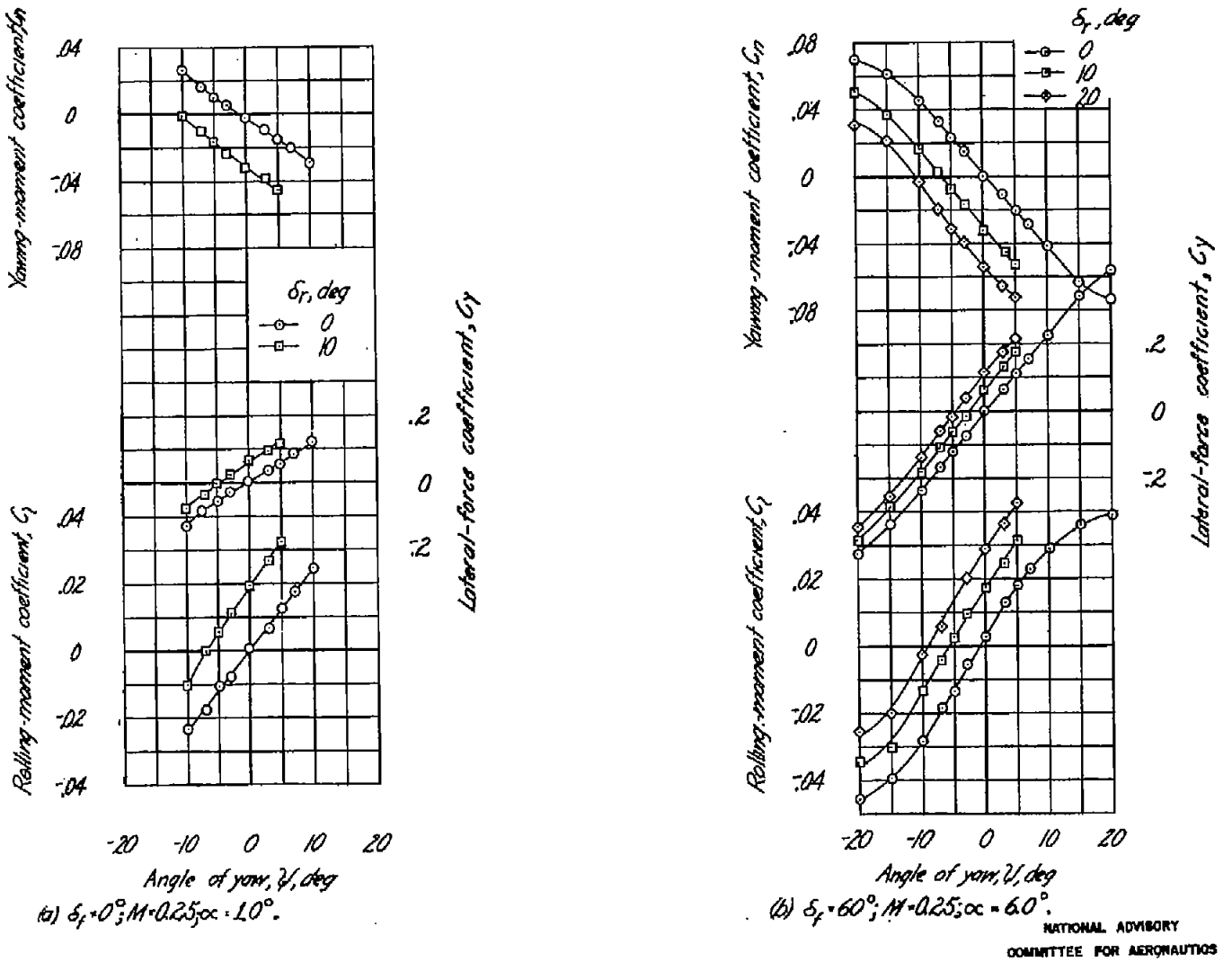

Figure 15.- Effect of rudder deflection on the aerodynamic characteristics in yaw of the model with the 35° vee tail. $\delta_e = 0°$; $i_t = 0°$.

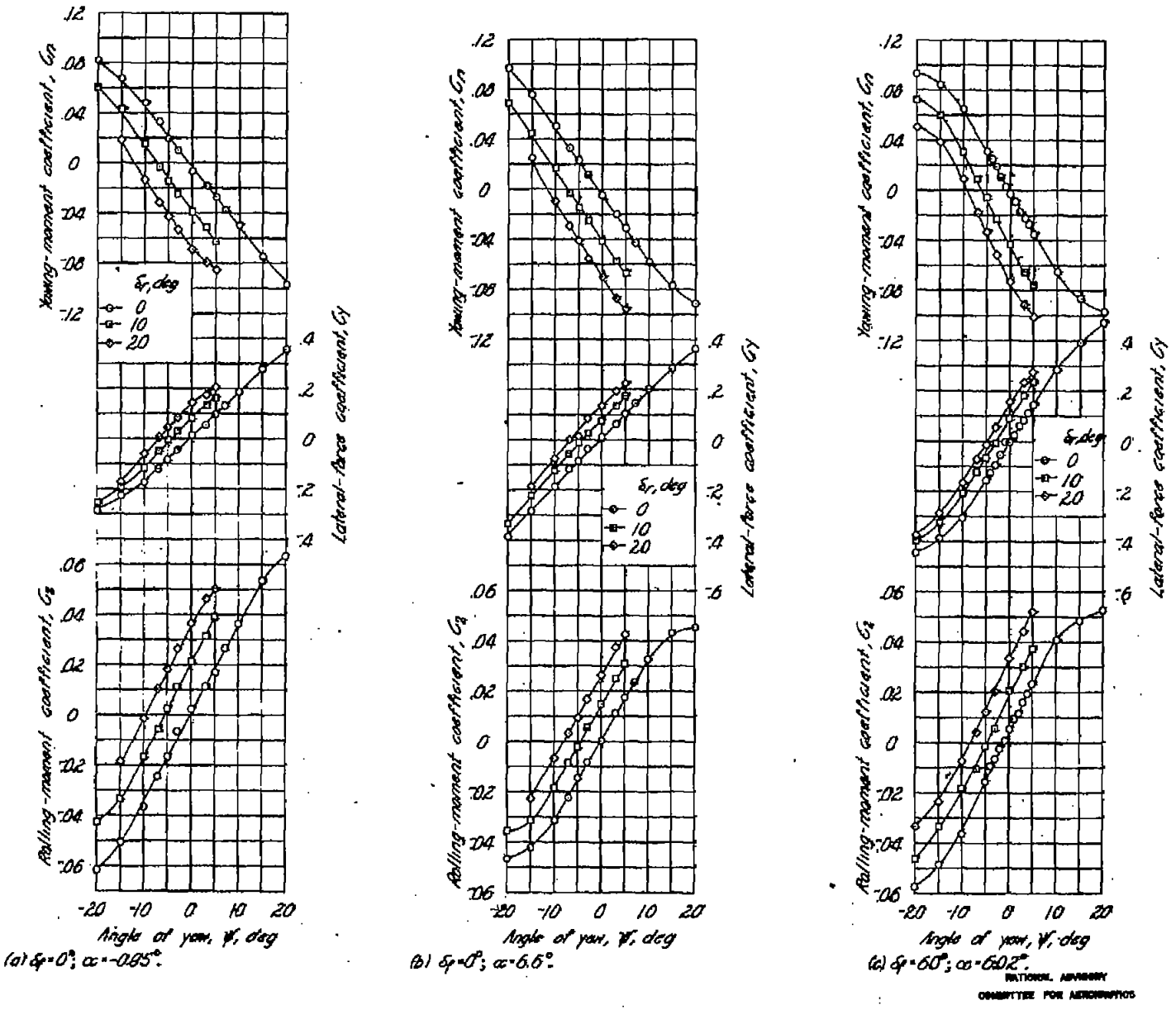

Figure 16.- Effect of rudder deflection in yaw of the model with the 47° vee tail.

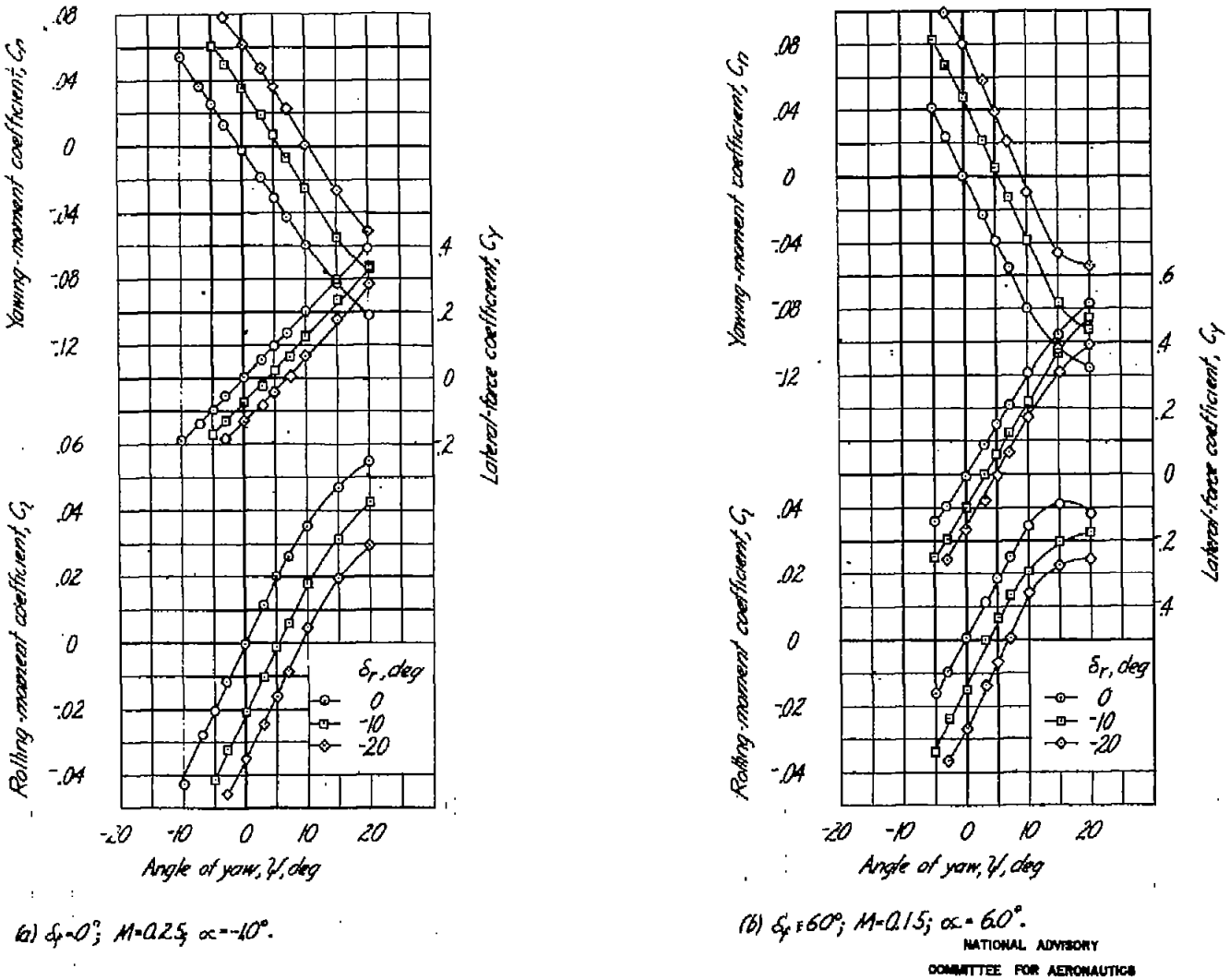

Figure 17.- Effect of rudder deflection on the aerodynamic characteristics in yaw of the model with the 55° vee tail. δ_e = 0°; i_t = 0°.

NATIONAL ADVISORY COMMITTEE FOR AERONAUTICS

TECHNICAL NOTE

No. 1478

WIND-TUNNEL INVESTIGATION OF THE STABILITY AND CONTROL CHARACTERISTICS OF A COMPLETE MODEL EQUIPPED WITH A VEE TAIL

By Edward C. Polhamus and Robert J. Moss

Langley Memorial Aeronautical Laboratory
Langley Field, Va.

Washington
November 1947

NATIONAL ADVISORY COMMITTEE FOR AERONAUTICS

TECHNICAL NOTE NO. 1478

WIND-TUNNEL INVESTIGATION OF THE STABILITY AND CONTROL CHARACTERISTICS OF A COMPLETE MODEL EQUIPPED WITH A VEE TAIL

By Edward C. Polhamus and Robert J. Moss

SUMMARY

A wind-tunnel investigation was conducted to determine the low-speed stability and control characteristics of a complete model equipped with a vee tail. Tail dihedral angles of 35°, 47°, and 55° were tested and the results compared with results of tests of a conventional-tail arrangement used with the same wing-fuselage combination. The area of the vee tail was slightly greater than that of the conventional-tail assembly (approx. 2 percent), and the vee tail was mounted on a small dorsal trunk (10 percent of vee-tail area). The total wetted area of the vee-tail assembly, therefore, was approximately 12 percent greater than that of the conventional-tail assembly. The aspect ratio of the vee tail was equal to that of the horizontal tail but greater than that of the vertical tail.

The 47° vee tail was the best of those tested when both longitudinal and lateral stability were concerned, and it contributed 40 percent more longitudinal and directional stability and 90 percent more dihedral effect than the conventional tail.

The increase in directional stability was due to the dorsal trunk and to the fact that the vee tail had a greater aspect ratio than the vertical tail.

The increase in longitudinal stability was caused by the increase in stabilizer effectiveness and the decrease in the rate of change of effective downwash with angle of attack due to the high tail position and the favorable effect of sidewash at the tail. A method of predicting the sidewash effect is presented in an appendix.

INTRODUCTION

Interest has been displayed in vee tails, particularly for high-speed aircraft, because of: (1) the possibility of a reduction in drag of the empennage due to an improved tail-fuselage juncture and due to a reduction in tail area and (2) the location of the tail out of the wing wake without encountering difficult structural problems. The isolated-tail theory (reference 1) indicates that an isolated vee-tail surface producing stability parameters equal to those produced by an isolated conventional-tail assembly (and having equal effective aspect ratios) must have an area equal to that of the conventional-tail assembly. When the vee tail is used with a wing-fuselage combination, additional factors such as the downwash and sidewash associated with the wing-fuselage vortex pattern must be considered. Inasmuch as the effects of these factors are difficult to evaluate theoretically, an experimental investigation was made of a vee tail used with a wing-fuselage combination. This vee tail had the same tail length and approximately the same total area as the sum of the horizontal and vertical tail surfaces of a conventional tail that was previously investigated with the same wing-fuselage combination. The vee tail, however, was mounted on a small dorsal trunk, the area of which was approximately 10 percent of the area of the vee tail. The effect of this dorsal trunk on lateral stability should be considered when comparing the vee and conventional tails. The aspect ratio of the vee tail was equal to that of the horizontal tail but was greater than that of the vertical tail.

The investigation included stability and control tests, with and without wing flaps, for tail dihedral angles of 35°, 47°, and 55°.

SYMBOLS

The system of axes used for the presentation of the data together with an indication of the sense of the positive forces and moments is presented in figure 1. All moments are presented about the center of gravity. Pertinent symbols are defined as follows:

C_L lift coefficient (Lift/qS)

C_D drag coefficient (Drag/qS)

C_m pitching-moment coefficient $\left(\frac{\text{Pitching moment}}{qS\bar{c}}\right)$

C_l rolling-moment coefficient $\left(\frac{\text{Rolling moment}}{qSb}\right)$

C_n yawing-moment coefficient $\left(\frac{\text{Yawing moment}}{qSb}\right)$

C_Y lateral-force coefficient $\left(\frac{\text{Lateral force}}{qS}\right)$

S wing area, square feet

b wing span, feet

$\bar{c}$ wing mean aerodynamic chord (M.A.C.), feet

q dynamic pressure, pounds per square foot $\left(\rho V^2/2\right)$

ρ mass density of air, slugs per cubic foot

V free-stream velocity, feet per second

M Mach number

α angle of attack of fuselage center line, degrees

ϵ angle of downwash, degrees

ϵ_e effective downwash (downwash that alone has same effect as downwash and sidewash)

i_t stabilizer setting (angle between line of intersection of tail panels and fuselage center line), degrees

ψ angle of yaw, degrees

δ control-surface deflection with reference to fixed surface and measured in plane normal to fixed surface, degrees

Γ_t tail dihedral angle with reference to horizontal, degrees

Subscripts:

t tail

e elevator

r rudder

f flap

m measured value

δ_e, i_t, δ_r, α, ψ denote partial derivative of a coefficient with respect to δ_e, i_t, δ_r, α, ψ, respectively; for example, $C_{m_{\delta_e}} = \frac{\partial C_m}{\partial \delta_e}$

MODEL AND APPARATUS

The model equipped with a 47° vee tail is shown mounted in the Langley 300 MPH 7- by 10-foot tunnel in figures 2 and 3 and a three-view drawing of the model as tested is presented in figure 4. Details of the vee-tail panel are presented in figure 5; details of the conventional-tail assembly are shown in figures 6 and 7.

The model was constructed of wood attached to metal reinforcing members with Cycleweld cement except for the all-metal control surfaces. The tail-control surfaces and wing flaps were 20-percent-chord plain flaps and the ailerons were 15-percent-chord plain flaps. All controls were flat-sided from the hinge line to the trailing edge and all control gaps were sealed.

Specific model configurations referred to herein are as follows:

(a) High-speed configuration
Flaps retracted
Landing gear retracted

(b) Landing configuration
Flaps deflected 60°
Landing gear extended

The tests were conducted in the Langley 300 MPH 7- by 10-foot tunnel, which is a closed rectangular tunnel with a contraction ratio of 14:1 and is powered by a 1600-horsepower synchronous motor.

TESTS

Test Conditions

Tests in the high-speed configuration were run at dynamic pressures of 88.5 and 165.2 pounds per square foot. Tests in the

landing configuration were run at a dynamic pressure of 33.5 pounds per square foot. The corresponding approximate values of Mach number and Reynolds number (based on a wing mean aerodynamic chord of 1.202 ft) were as follows:

Dynamic pressure (lb/sq ft)	Mach number	Reynolds number
33.5	0.15	1.28×10^6
88.5	.25	2.08×10^6
165.2	.35	2.82×10^6

The Reynolds number was computed using a turbulence factor of unity. The degree of turbulence of the tunnel is not known quantitatively but is believed to be small because of the high contraction ratio.

Corrections

All data have been corrected for tares caused by the model-support struts. Jet-boundary corrections were computed as follows (reference 2), where the subscript m refers to the measured values:

$$\alpha = \alpha_m + 0.88C_{L_m}$$

$$C_D = C_{D_m} + 0.0128C_{L_m}^2$$

$$C_m = C_{m_m} + 0.0222C_{L_m} \qquad \text{(for flaps undeflected)}$$

$$C_m = C_{m_m} + 0.0227C_{L_m} \qquad \text{(for flaps deflected)}$$

$$C_l = 0.98C_{l_m}$$

$$C_n = C_{n_m} - 0.0173C_{l_m}C_{L_m}$$

All force and moment coefficients were corrected for blocking by the method presented in reference 3. An increment in drag coefficient has been added in order to account for the horizontal buoyancy effected by the longitudinal static pressure gradient in the tunnel.

RESULTS AND DISCUSSION

An outline of the figures presenting the results is as follows:

Lift characteristics.- The lift characteristics of the model with the vee tail are presented in figures 8 to 13 and are summarized in the following table:

Γ_t (deg)	$C_{L_{max}}$ trimmed	C_{L_α}
$\delta_f = 0^\circ$		
35	0.76	0.085
47	.86	.088
55	.81	.085
$\delta_f = 60^\circ$		
35	1.19	.090
47	1.15	.086
55	1.18	.083

Horizontal tail characteristics.- Mean values describing the effectiveness of the elevator and stabilizer for the different dihedral angles are plotted against tail dihedral angle in figures 19 and 20, respectively. The values at $\Gamma_t = 0^\circ$ that are presented were

obtained by multiplying the values obtained with a conventional horizontal tail of the same aspect ratio (data obtained in the Langley 300 MPH 7- by 10-foot tunnel) on the same wing-fuselage combination by the ratio of tail areas. Also presented in these figures are the theoretical variations based on the isolated-tail theory of reference 1. The experimental and theoretical results are in fair agreement, but the general trend of the experimental results seems to indicate that there may be a slight increase in effectiveness at the higher dihedral angles over that predicted by the theory.

Downwash at the tail.- The average effective-downwash values for the various tail dihedral angles are presented in figure 14. These values were evaluated from tail-on and tail-off pitching moments; and, since the pitching moment contributed by a vee tail depends on sidewash as well as downwash, the effective downwash, rather than the actual downwash existing in the vertical plane, is obtained. The effective downwash is defined as the downwash that alone would produce the same pitching moment as that produced by the actual downwash and sidewash. A method of estimating the effect of sidewash on effective downwash and longitudinal stability is presented in the appendix.

Figure 21 shows the effect of tail dihedral angle on the rate of change of effective downwash angle with angle of attack. Two theoretical variations with dihedral angle are also included. One curve takes into account the change in tail height and was determined from the charts of reference 4 by assuming the tail height to be equal to the height of the tail mean aerodynamic chord. The other curve includes both the effect of tail height and the effect of sidewash (see appendix) and is in fair agreement with the experimental data.

Rudder effectiveness.- Values of the rudder-effectiveness parameter $C_{n_{\delta_r}}$ obtained from figures 15 to 17 are plotted against tail dihedral angle Γ_t in figure 22. The theoretical variation of $C_{n_{\delta_r}}$ with Γ_t, as estimated from the isolated-tail theory of reference 1, is also presented. The increase in effectiveness is probably due to the rudder induced load carried by the dorsal trunk. Also presented in figure 22 are the variations of $C_{l_{\delta_r}}$ and $C_{l_{\delta_r}}/C_{n_{\delta_r}}$ with Γ_t. The ratio of adverse rolling moments to favorable yawing moments produced by rudder deflection is greater for the vee tail than for the conventional tail.

Static longitudinal stability.- The neutral-point locations for both the cruising and landing configurations are presented in figure 23.

The tail-off neutral points and the assumed center-of-gravity position at 25 percent M.A.C. about which the moments were measured are also indicated. The curves indicate that the model with the vee tail has greater longitudinal stability than the model with the horizontal tail for the three tail dihedral angles tested. The 47° tail, which according to isolated-tail theory should contribute the same longitudinal stability as the horizontal tail tested, actually contributes 40 percent more longitudinal stability than the horizontal tail. The variation of $\left(C_{m_\alpha}\right)_t$ with Γ_t is presented in figure 24. For comparison, the horizontal-tail contribution $\left(\Gamma_t = 0°\right)$ was increased by the ratio of the vee-tail area to the horizontal-tail area. Also presented in this figure is the theoretical variation of $\left(C_{m_\alpha}\right)_t$ with Γ_t, and it can be seen that the decrease in longitudinal stability with dihedral angle is overestimated. The overestimated decrease in stability can be accounted for by the increase in stabilizer effectiveness and the decrease in the rate of change of effective downwash with angle of attack due to the increased tail height and the favorable effect of sidewash. A method of estimating this sidewash effect is presented in the appendix.

Static directional and lateral stability.- The static lateral-stability parameters determined from pitch tests at yaw angles of 5° and -5° for both the high-speed and the landing configurations are plotted against angle of attack in figure 18. In the high-speed configuration a large amount of directional and lateral stability exists for all three dihedral angles and the maximum stability would appear to occur at some angle between 47° and 55°. In the landing configuration the high static directional stability and the dihedral effect are indicated for angles of attack below 6°. Above 6° there is a slight loss of dihedral effect and a large loss in directional stability. It will be noted that the 47° vee tail, which is the best of those tested, contributed approximately 40 percent more longitudinal and directional stability and 90 percent more dihedral effect than the conventional tail. The increase in directional stability, however, is due to the fact that the aspect ratio of the vee tail is greater than that of the vertical tail and due to the dorsal trunk upon which the vee tail was mounted. The effect of this trunk can be seen in figure 25, which presents the actual and theoretical variations of the tail contribution to directional stability $\left(C_{n_\psi}\right)_t$ and to dihedral effect $\left(C_{l_\psi}\right)_t$ with tail dihedral angle. The reasons for the large contribution to directional stability of this small trunk (approx. 10 percent of the vee-tail area) are that the trunk increases the effective aspect ratio of the vee tail in yaw. Since tail effectiveness is proportional to $\sin^2\Gamma_t$, this trunk is more effective per unit area than the vee tail.

The high dihedral effect (equivalent to approx. 16.5° of wing geometric dihedral for the 47° tail) is due to the high geometric dihedral of the tail.

CONCLUSIONS

From low-speed wind-tunnel tests of a complete model equipped with a vee tail having tail dihedral angles of 35°, 47°, and 55° and from comparisons with tests of a conventional tail used with the same wing-fuselage combination, the following conclusions with regard to static stability and control were reached:

1. The 47° vee tail appeared to be the best of those tested when both longitudinal and lateral stability were concerned.

2. The 47° vee tail, the area of which was approximately the same (2 percent greater) as the conventional tail assembly but was mounted on a small dorsal trunk (10 percent of vee-tail area), contributed 40 percent more longitudinal and directional stability and 90 percent more dihedral effect than the conventional tail.

3. The increase in directional stability was due to the dorsal trunk and to the fact that the vee tail had a greater aspect ratio than the vertical tail.

4. The increase in longitudinal stability was caused by the increase in stabilizer effectiveness and the decrease in the rate of change of effective downwash with angle of attack due to the high tail position and the favorable effect of sidewash at the tail.

5. The measured variations of stabilizer and elevator effectiveness with tail dihedral angle agreed fairly well with the isolated-tail theory.

Langley Memorial Aeronautical Laboratory
National Advisory Committee for Aeronautics
Langley Field, Va., July 31, 1947

APPENDIX

METHOD OF ESTIMATING SIDEWASH EFFECT ON LONGITUDINAL STABILITY

Symbols

α	angle of attack of airplane in plane of symmetry
$(\alpha_N)_{tail}$	angle of attack of tail panel in plane normal to chord plane of tail surface
ϵ	induced angle (downwash) in plane of symmetry
ϵ_N	induced angle in plane normal to chord plane of tail surface
$(C_L)_{tail}$	lift coefficient of tail measured in plane of symmetry
$\left(C_{L_\alpha}\right)_N$	lift-curve slope of tail in plane normal to chord plane of tail surface
Γ_t	dihedral angle of tail surface
$(C_m)_{tail}$	airplane pitching moment due to tail lift
$\frac{b_t}{2}$	span of one vee-tail panel
$\bar{c}_w$	M.A.C. of wing
$\bar{c}_t$	M.A.C. of tail
c_t	local chord of tail
l_t	tail length measured from c.g. to $\bar{c}_t/4$
S_t	actual (not projected) area of tail
S_w	wing area
q	free-stream dynamic pressure
q_t	effective dynamic pressure at tail
w	total induced velocity in vertical plane $(w_T + w_B)$

w_T velocity in vertical plane induced by trailing vortices (downwash)

w_B velocity in vertical plane induced by bound vortex (downwash)

w_S velocity in plane normal to vertical plane induced by trailing vortices (sidewash)

w_N total induced velocity in plane normal to tail panel

w_{T_N} velocity in normal plane induced by trailing vortices

X tail length measured from $\bar{c}_w/4$ to $\bar{c}_t/4$

s wing vortex semispan

v tangential velocity of a vortex at Y for unit circulation

Y distance from vortex center to point in question

V velocity at tail parallel to X-axis

Method

When the longitudinal stability contributed by a vee tail is calculated, the effect of sidewash should be included. The following derivation of the longitudinal-stability equation includes this effect. The angle of attack in the plane normal to the tail panel is as follows (see fig. 26):

$$(\alpha_N)_{tail} = \alpha \cos \Gamma_t - \epsilon_N \tag{1}$$

and

$$(C_L)_{tail} = (C_{L_\alpha})_N (\alpha_N)_{tail} \cos \Gamma_t \tag{2}$$

By substituting equation (1) in equation (2)

$$(C_L)_{tail} = (C_{L_\alpha})_N \left(\alpha \cos \Gamma_t - \epsilon_N\right) \cos \Gamma_t \tag{3}$$

Now

$$\left(C_m\right)_{tail} = \left(C_L\right)_{tail} \frac{l_t}{\bar{c}_w} \frac{S_t}{S_w} \frac{q_t}{q} \tag{4}$$

and by substituting equation (3) in equation (4)

$$\left(C_m\right)_{tail} = \left(\alpha \cos \Gamma_t - \epsilon_N\right) \left(C_{L_\alpha}\right)_N \cos \Gamma_t \frac{l_t}{\bar{c}_w} \frac{S_t}{S_w} \frac{q_t}{q}$$

or

$$\left(C_{m_\alpha}\right)_{tail} = \left(\cos \Gamma - \frac{\partial \epsilon_N}{\partial \alpha}\right) \left(C_{L_\alpha}\right)_N \cos \Gamma_t \frac{l_t}{\bar{c}_w} \frac{S_t}{S_w} \frac{q_t}{q} \tag{5}$$

Since all available theoretical and experimental induced angles are presented as downwash angles, ϵ, equation (5) will be revised by replacing $\frac{\partial \epsilon_N}{\partial \alpha}$ with $\frac{\partial \epsilon}{\partial \alpha}$ and a correction factor. Since $\epsilon = \frac{w}{V}$ and $\epsilon_N = \frac{w_N}{V}$,

$$\frac{\partial \epsilon_N}{\partial \alpha} = \frac{\partial \epsilon}{\partial \alpha} \frac{w_N}{w} \tag{6}$$

By substituting equation (6) in equation (5)

$$\left(C_{m_\alpha}\right)_{tail} = \left(\cos \Gamma_t - \frac{\partial \epsilon}{\partial \alpha} \frac{w_N}{w}\right) \left(C_{L_\alpha}\right)_N \cos \Gamma_t \frac{l_t}{\bar{c}_w} \frac{S_t}{S_w} \frac{q_t}{q} \tag{7}$$

A more convenient form of equation (7) is

$$\left(C_{m_\alpha}\right)_{tail} = \left(1 - \frac{\partial \epsilon}{\partial \alpha} \frac{w_N}{w \cos \Gamma_t}\right) \left(C_{L_\alpha}\right)_N \cos^2 \Gamma_t \frac{l_t}{\bar{c}_w} \frac{S_t}{S_w} \frac{q_t}{q} \tag{8}$$

Values of $\frac{\partial \epsilon}{\partial \alpha}$ may be obtained from the charts of reference 4 by use of a tail height equal to the height of the M.A.C. of the tail. Values of $\frac{w_N}{w \cos \Gamma_t}$ may be obtained as follows:

$$\frac{w_N}{w \cos \Gamma_t} = \frac{w_B \cos \Gamma_t}{w \cos \Gamma_t} + \frac{w_{T_N}}{w \cos \Gamma_t}$$

and

$$\frac{w_N}{w \cos \Gamma_t} = \frac{w_B}{w} + \frac{w_{T_N}}{w_T \cos \Gamma_t} \frac{w_T}{w}$$

or

$$\frac{w_N}{w \cos \Gamma_t} = \frac{w_B}{w} + \frac{w_{T_N}}{w_T \cos \Gamma_t} \left(1 - \frac{w_B}{w}\right) \tag{9}$$

An approximate value $\frac{w_B}{w}$ may be obtained from the following equation which was derived from the equation for downwash due to the bound and trailing vortices given in reference 5:

$$\frac{w_B}{w} = \frac{s^2}{s^2 + X^2 + X\sqrt{X^2 + s^2}} \tag{10}$$

Equation (10) is for a point midway between the two trailing vortices in the plane of the horseshoe vortex but is sufficiently accurate for these calculations.

The factor $\frac{w_{T_N}}{w_T \cos \Gamma_t}$ (equation (9)) may be determined graphically as follows: By assuming a horseshoe vortex of span equal to 90 percent of the wing span (see fig. 27), the induced velocities due to the trailing vortices in the normal and vertical planes are obtained at various spanwise stations of the tail. Inasmuch as only velocity ratios are desired, the tangential velocity v of the vortex at the first spanwise point investigated may be drawn to any convenient length.

At any other point the velocity may then be easily drawn since it is inversely proportional to the distance Y from the vortex center to the point in question. At each spanwise station the induced velocities w_{T_N} and $w_T \cos \Gamma_t$ due to both trailing vortices are obtained and then the factor $\frac{w_{T_N}}{w_T \cos \Gamma_t}$ is weighted according to the local chord and integrated over the span in order to obtain an average value to substitute in equation (9). This procedure need be done for only one panel since it will be the same for both.

From figure 27 it can be seen that $\frac{w_{T_N}}{w_T \cos \Gamma_t}$ is less than unity and that the reduction is due to the sidewash w_S.

REFERENCES

1. Purser, Paul E., and Campbell, John P.: Experimental Verification of a Simplified Vee-Tail Theory and Analysis of Available Data on Complete Models with Vee Tails. NACA ACR No. L5A03, 1945.

2. Gillis, Clarence L., Polhamus, Edward C., and Gray, Joseph L., Jr.: Charts for Determining Jet-Boundary Corrections for Complete Models in 7- by 10-Foot Closed Rectangular Wind Tunnels. NACA ARR No. L5G31, 1945.

3. Thom, A.: Blockage Corrections in a Closed High-Speed Tunnel. R. & M. No. 2033, British A.R.C., 1943.

4. Silverstein, Abe, and Katzoff, S.: Design Charts for Predicting Downwash Angles and Wake Characteristics behind Plain and Flapped Wings. NACA Rep. No. 648, 1939.

5. von Kármán, Th., and Burgers, J. M.: General Aerodynamic Theory - Perfect Fluids. Mathematical Foundation of the Theory of Wings with Finite Span. Vol. II of Aerodynamic Theory, div. E, ch. III, W. F. Durand, ed., Julius Springer (Berlin), 1935, p. 142. (Reprint of 1943.)

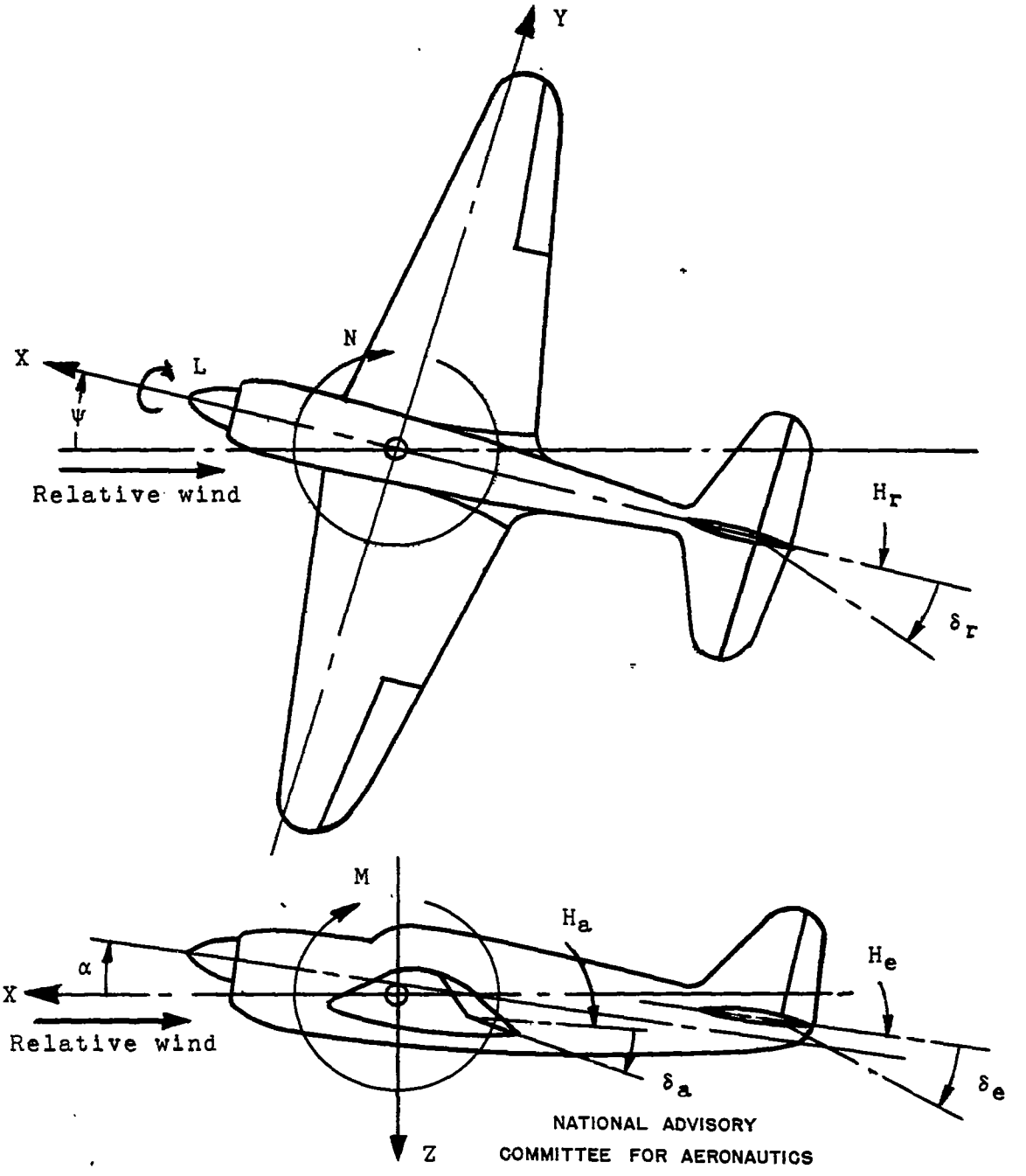

Figure 1.- System of axes and control-surface hinge moments and deflections. Positive values of forces, moments, and angles are indicated by arrows. Positive values of tab hinge moments and deflections are in the same directions as the positive values for the control surfaces to which the tabs are attached.

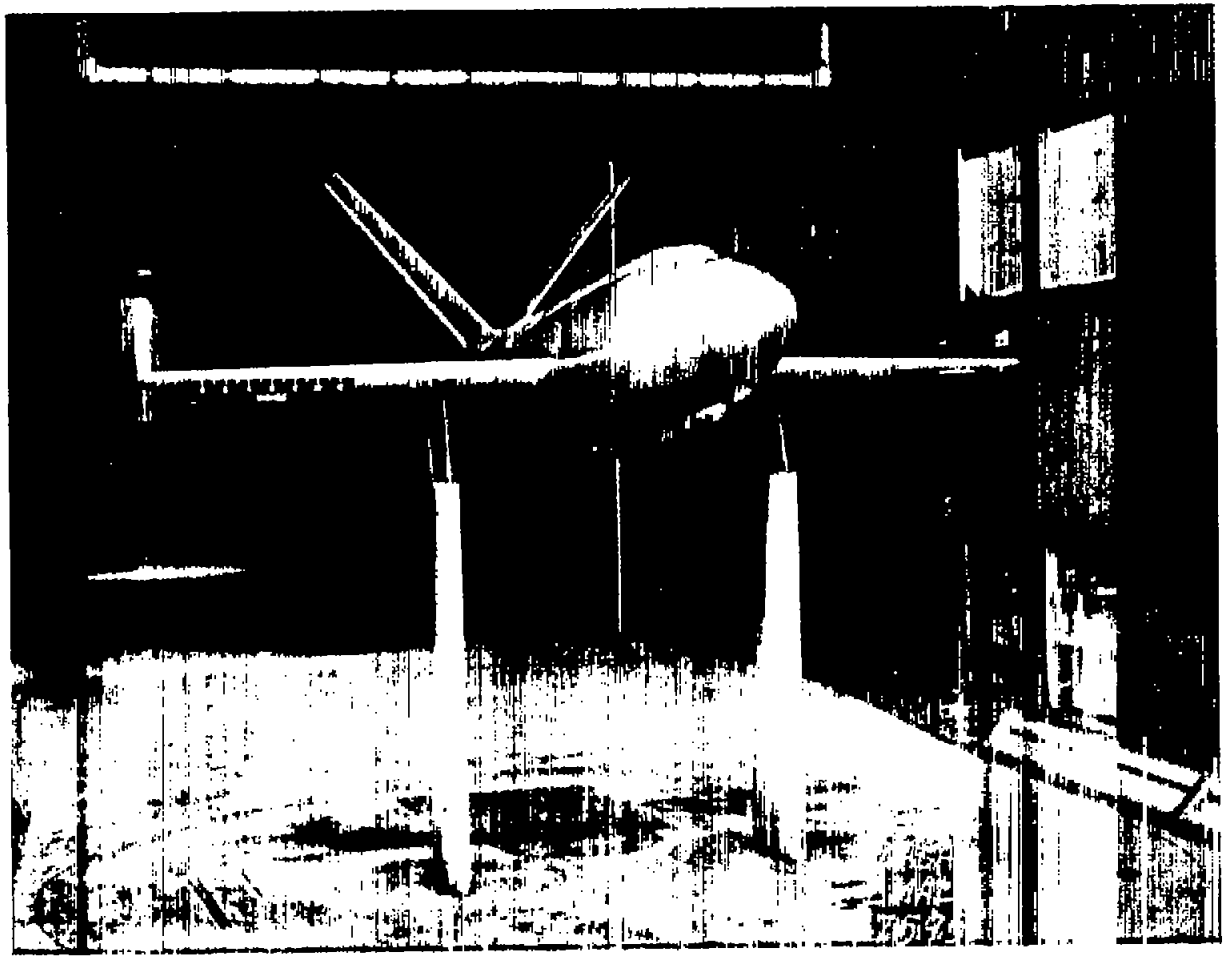

Figure 2.- Front view of model mounted in the Langley 300 MPH 7- by 10-foot tunnel.

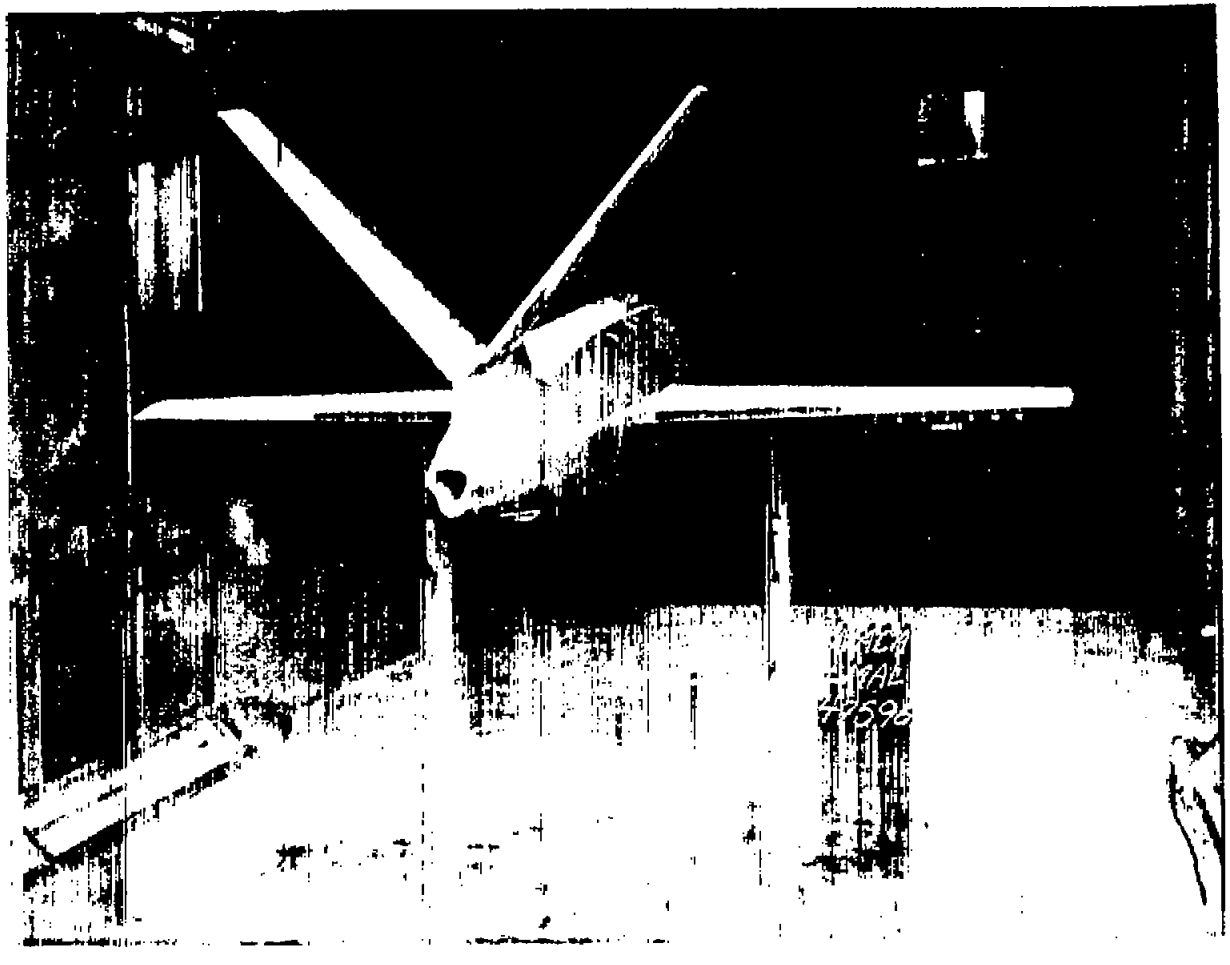

Figure 3.- Rear view of model mounted in the Langley 300 MPH 7- by 10-foot tunnel.

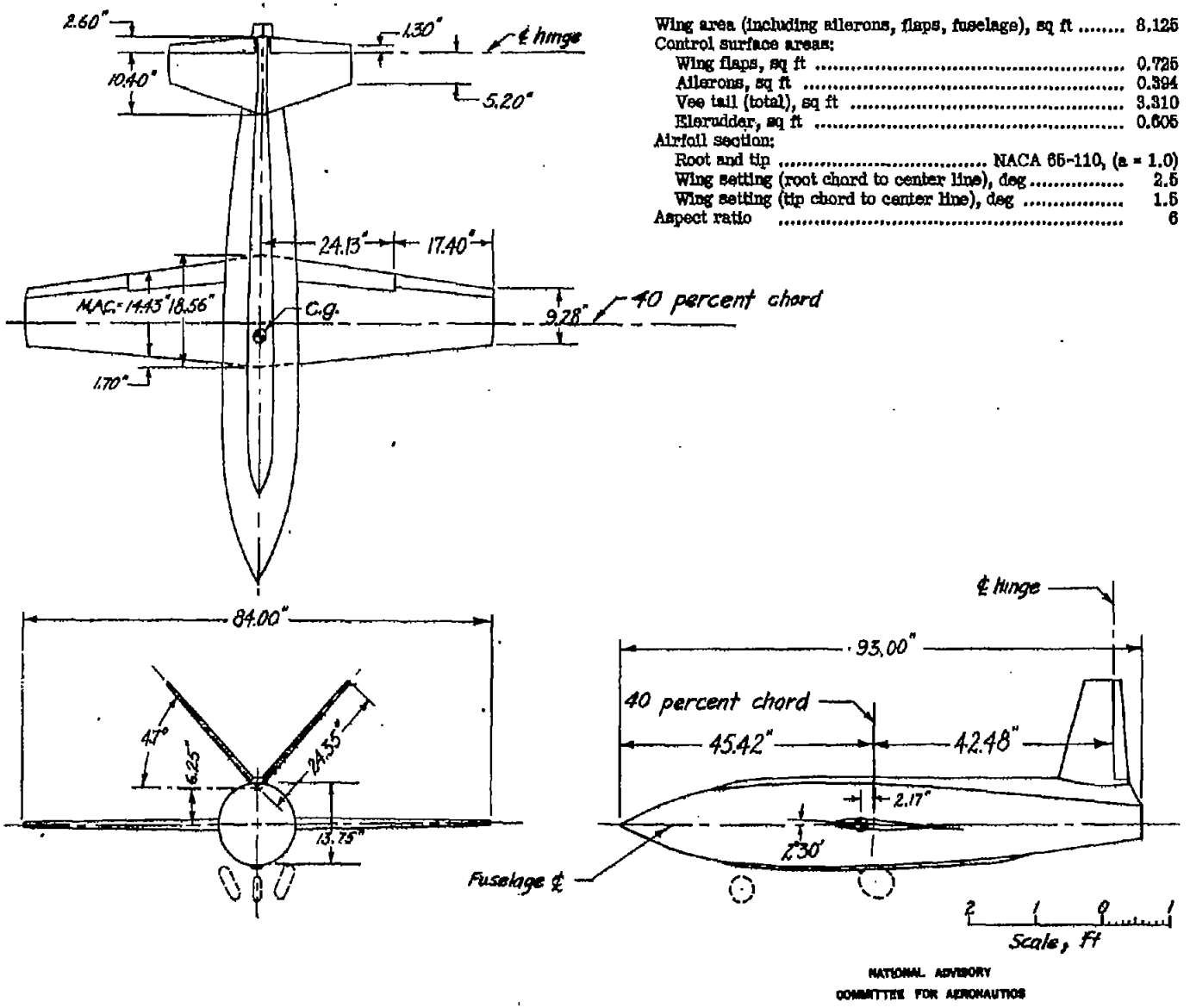

Wing area (including ailerons, flaps, fuselage), sq ft	8.125
Control surface areas:	
Wing flaps, sq ft	0.725
Ailerons, sq ft	0.394
Vee tail (total), sq ft	3.310
Elerudder, sq ft	0.605
Airfoil section:	
Root and tip	NACA 65-110, (a = 1.0)
Wing setting (root chord to center line), deg	2.5
Wing setting (tip chord to center line), deg	1.5
Aspect ratio	6

Figure 4.- Three-view drawing of the model.

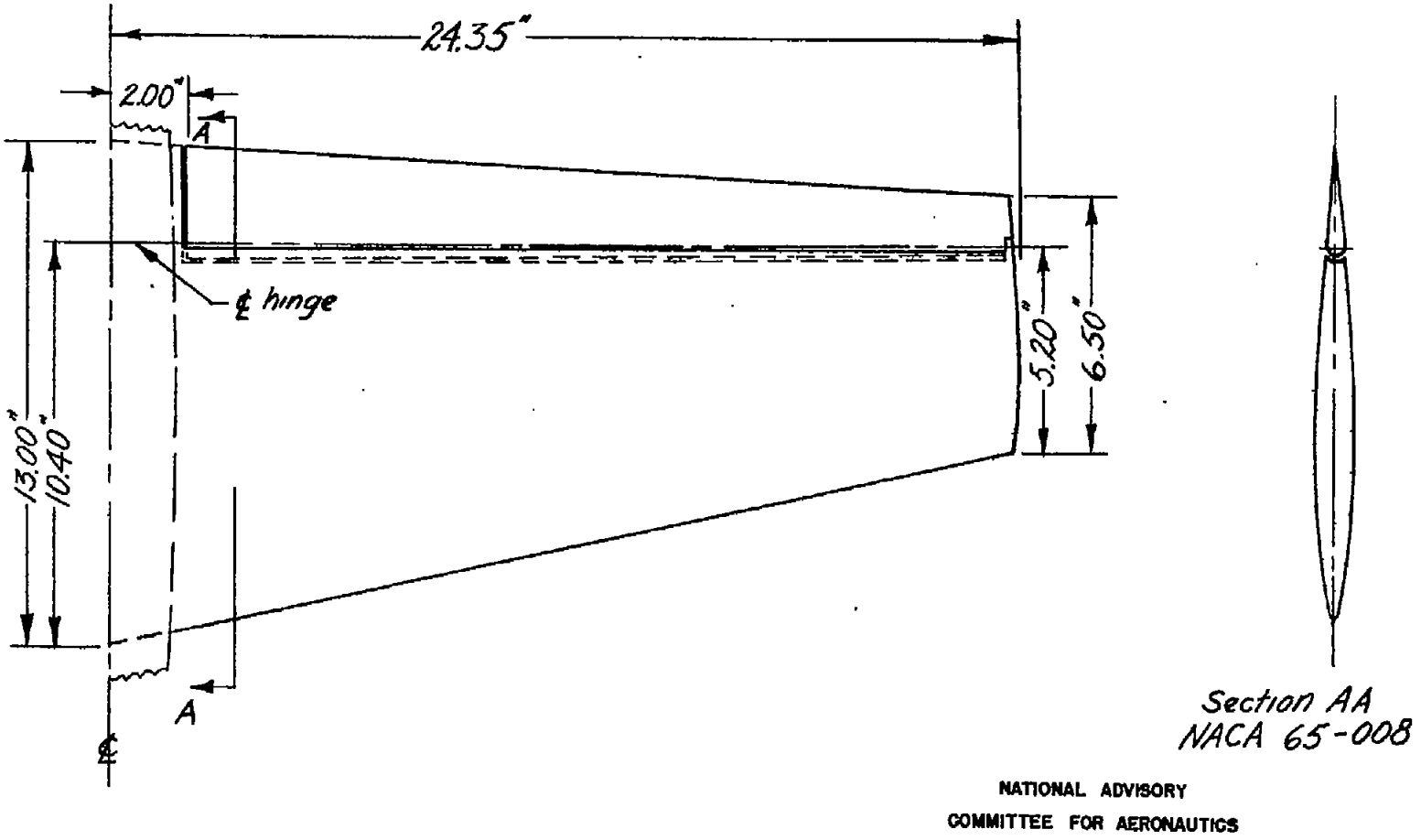

Figure 5.- Vee-tail panel. Area (total, not including trunk), 3.31 square feet; area (dorsal trunk), 0.32 square feet; aspect ratio, 5.0.

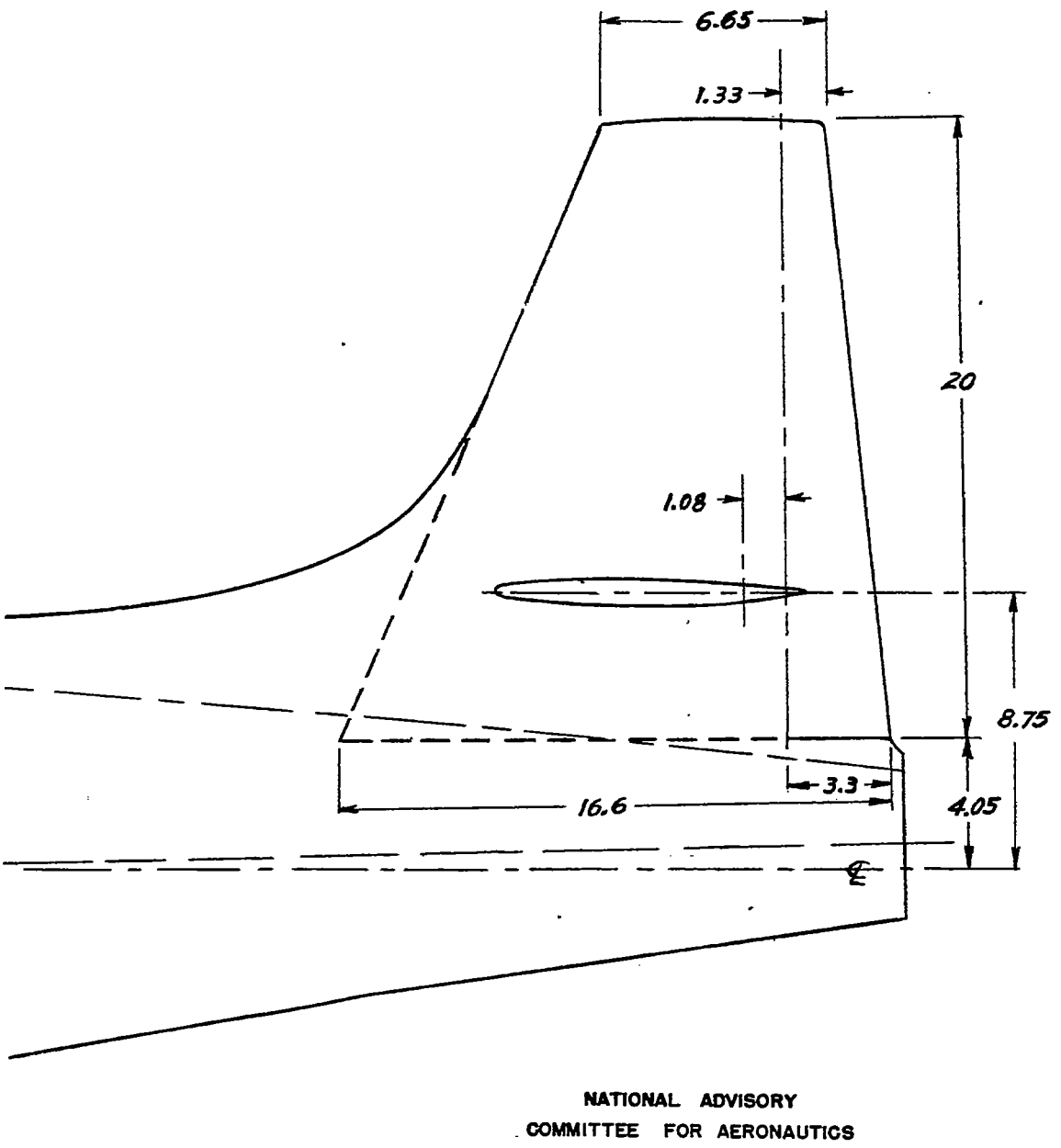

Figure 6.- Vertical tail. Area (total), 1.60 square feet; aspect ratio, 1.74.

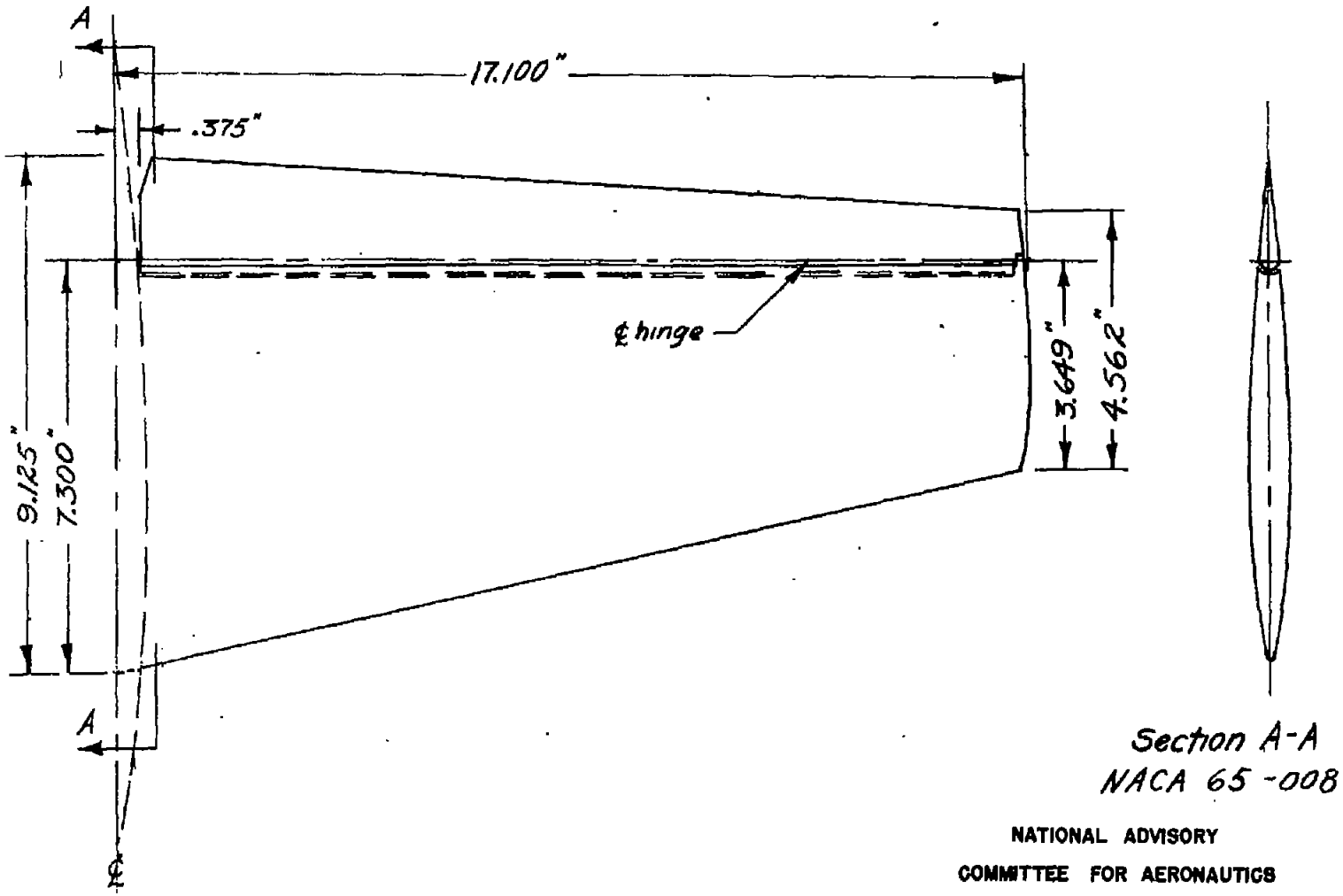

Figure 7.- Horizontal tail. Area (total), 1.625 square feet; aspect ratio, 5.0; trailing edge angle, 10°.

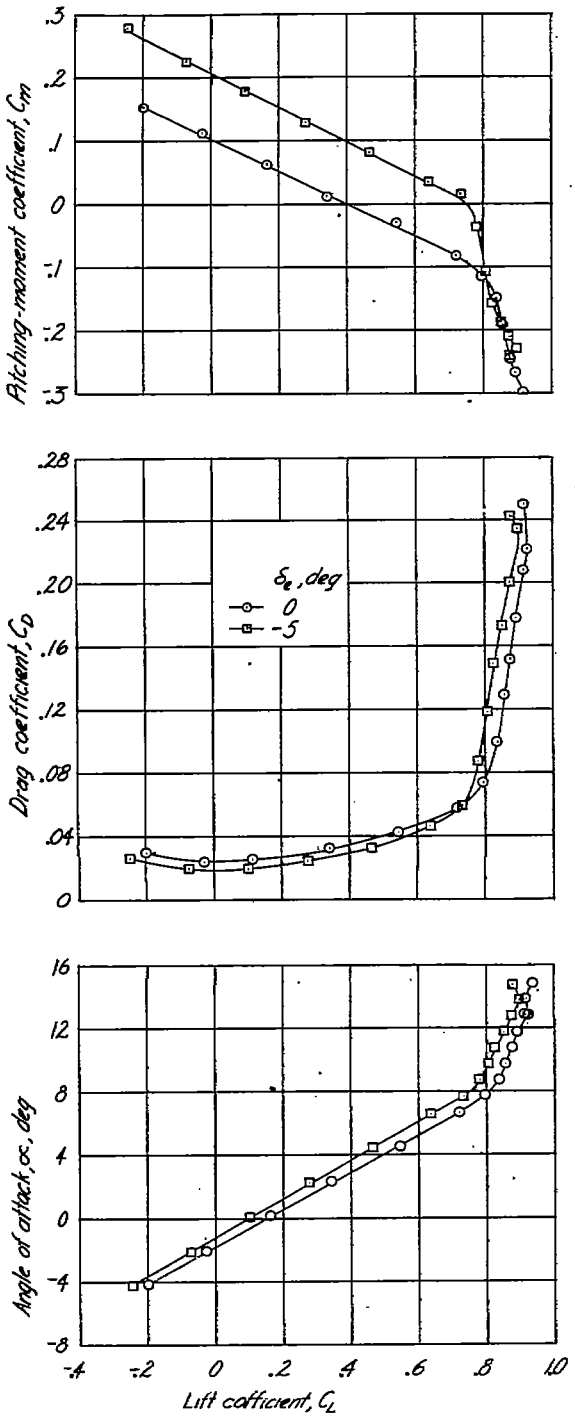

(a) $\delta_f = 0°$; $M = 0.35$.

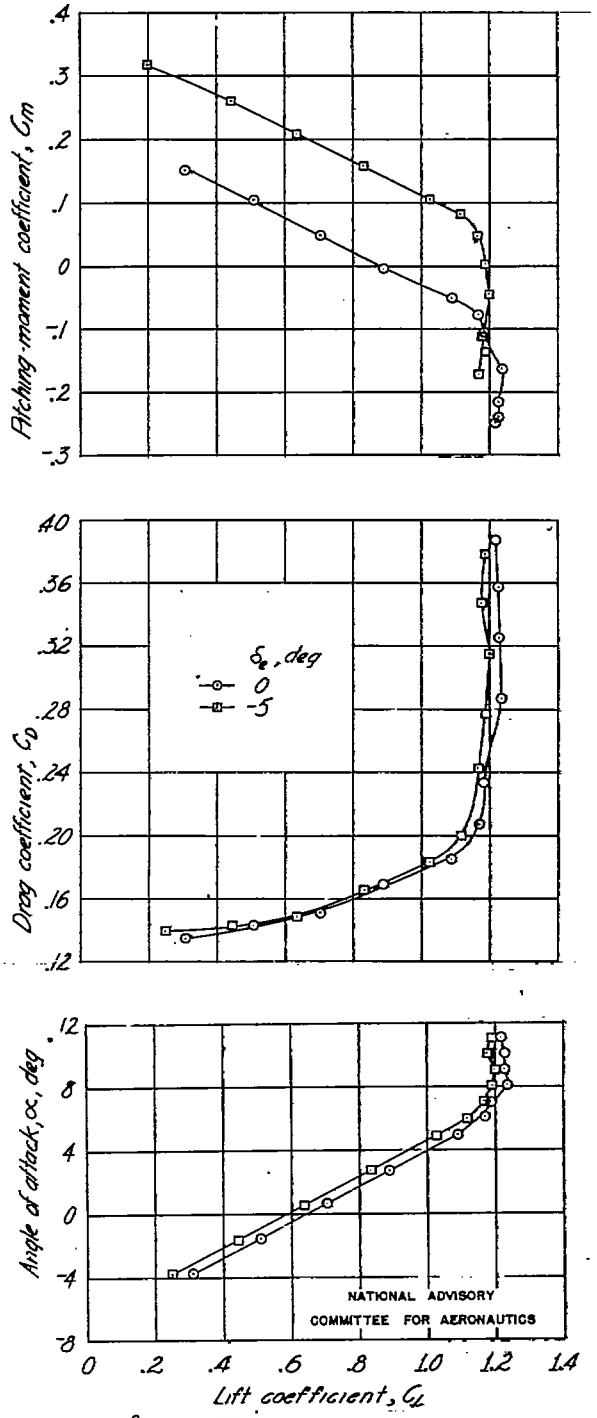

(b) $\delta_f = 60°$; $M = 0.15$.

Figure 8.- Effect of elevator deflection on the aerodynamic characteristics in pitch of the model with a 35° vee tail.

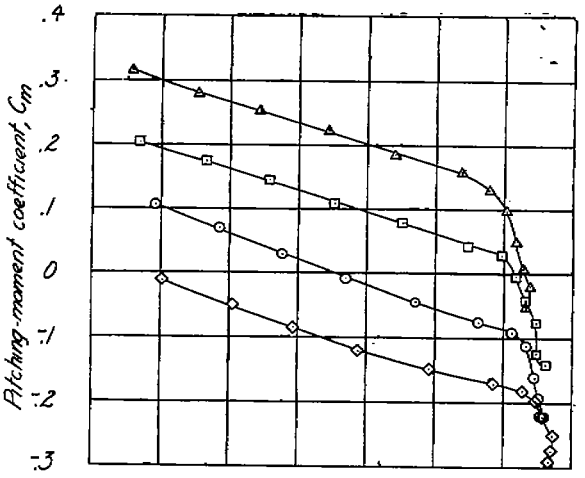

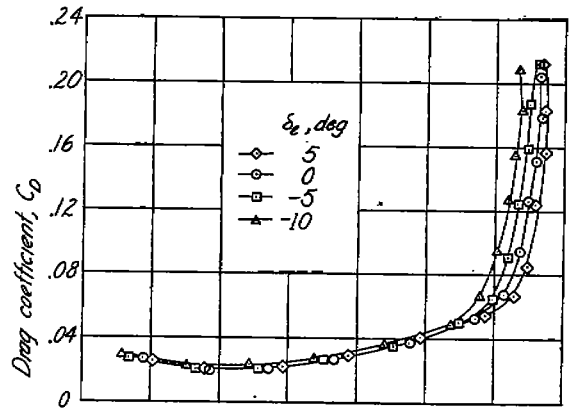

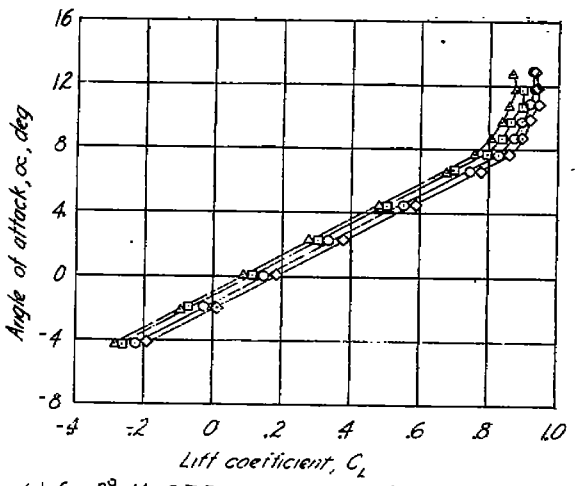

(a) $\delta_f = 0°$; $M = 0.35$.

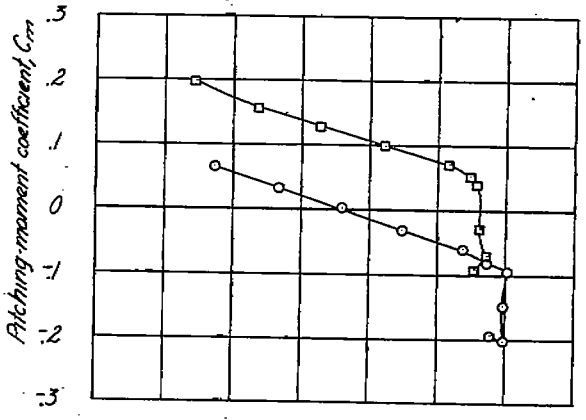

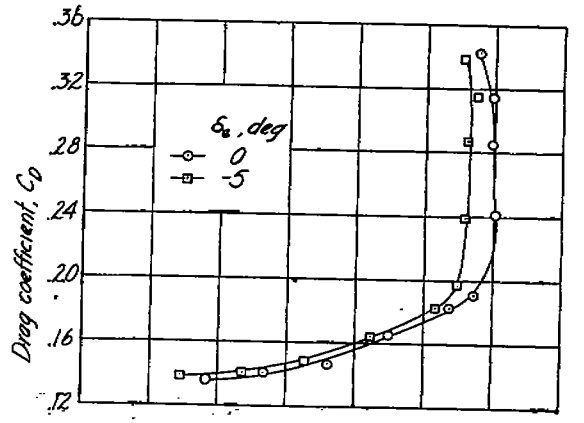

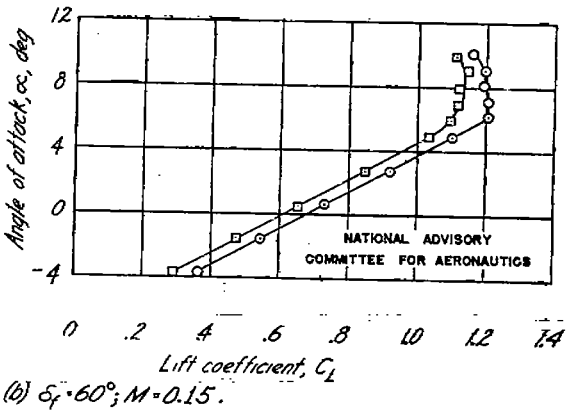

(b) $\delta_f = 60°$; $M = 0.15$.

Figure 9.- Effect of elevator deflection on the aerodynamic characteristics in pitch of the model with a 47° vee tail.

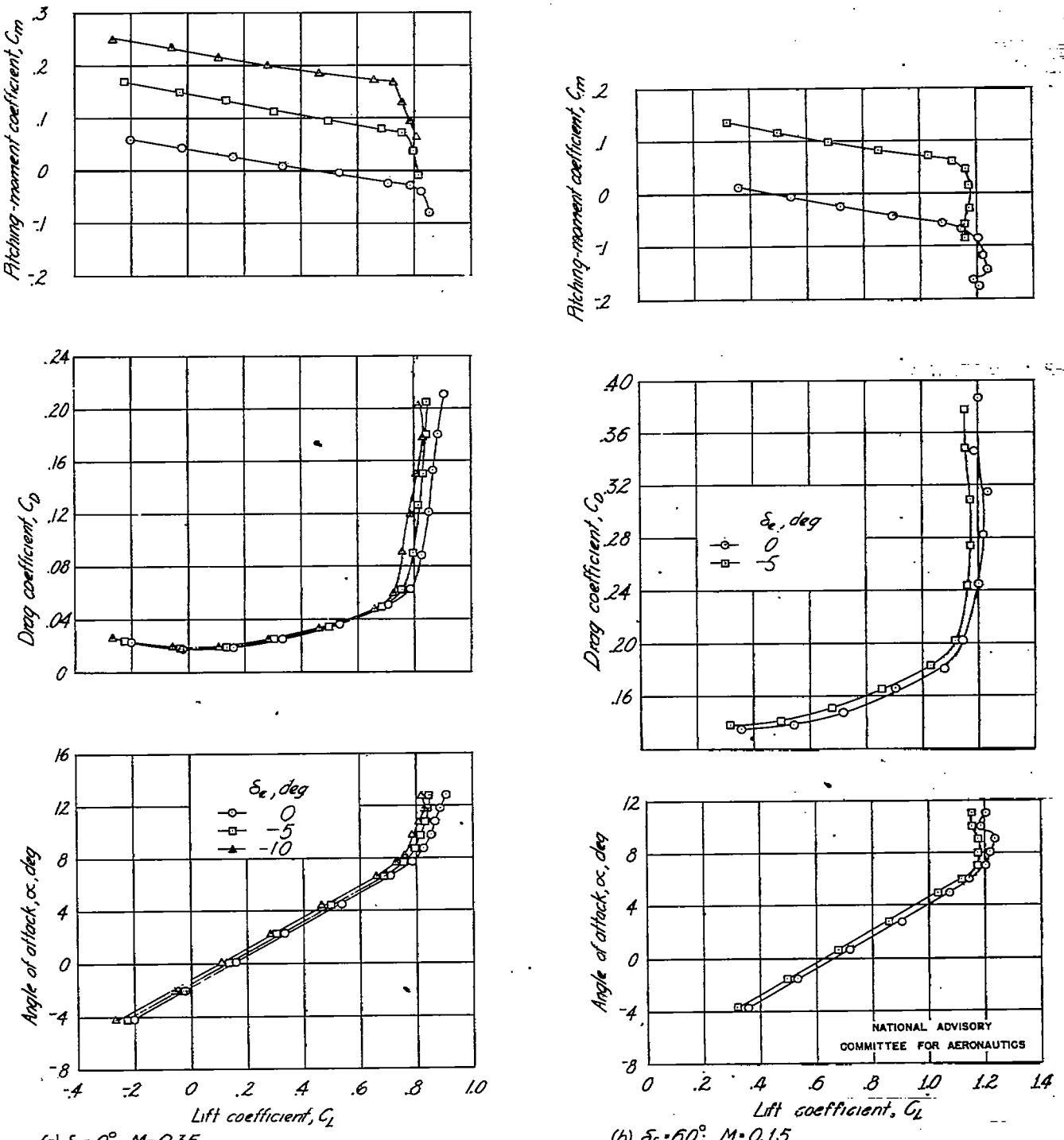

Figure 10.- Effect of elevator deflection on the aerodynamic characteristics in pitch of the model with a 55° vee tail.

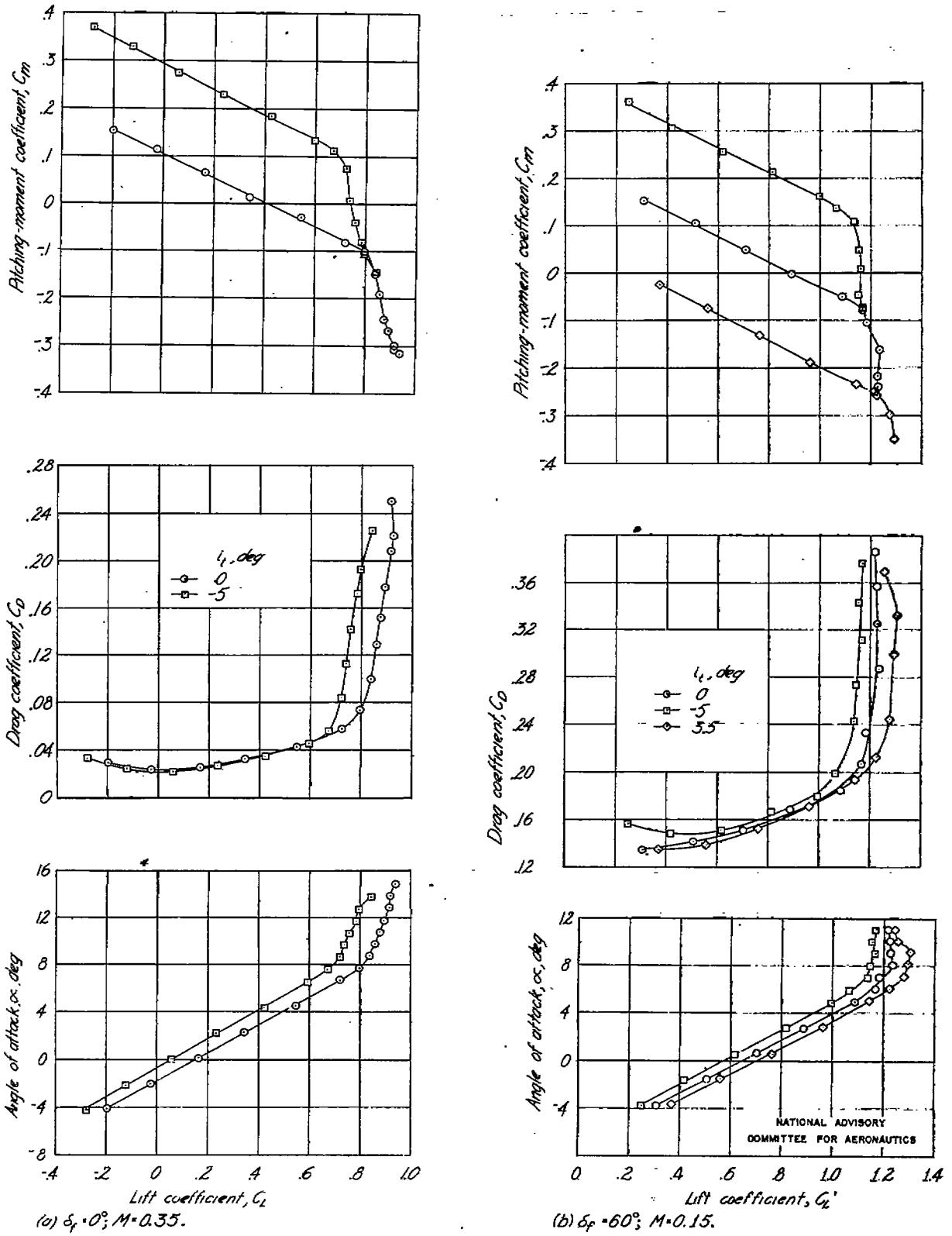

Figure 11.- Effect of stabilizer setting on the aerodynamic characteristics in pitch of the model with a 35° vee tail.

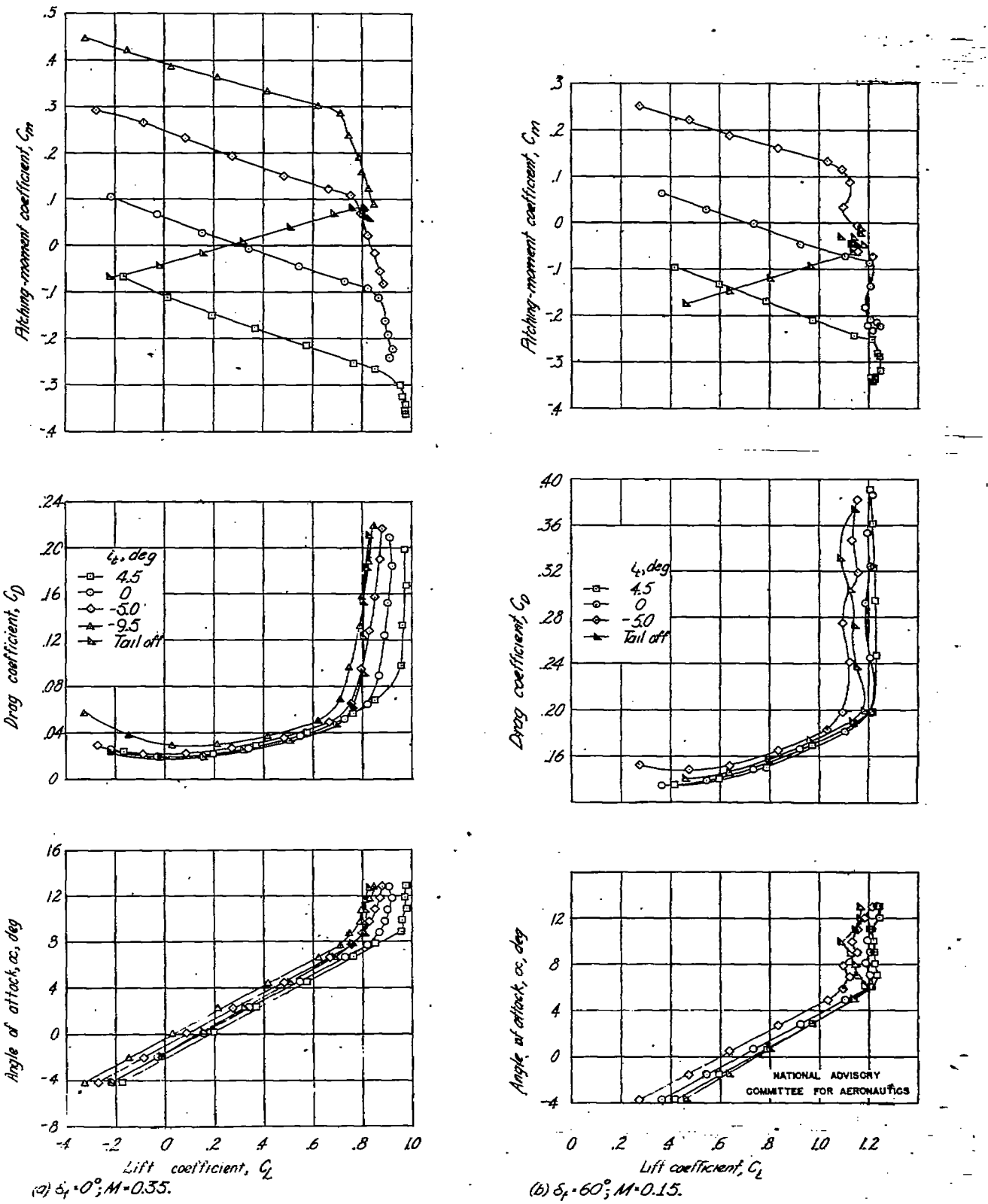

Figure 12.- Effect of stabilizer setting on the aerodynamic characteristics in pitch of the model with a 47° vee tail.

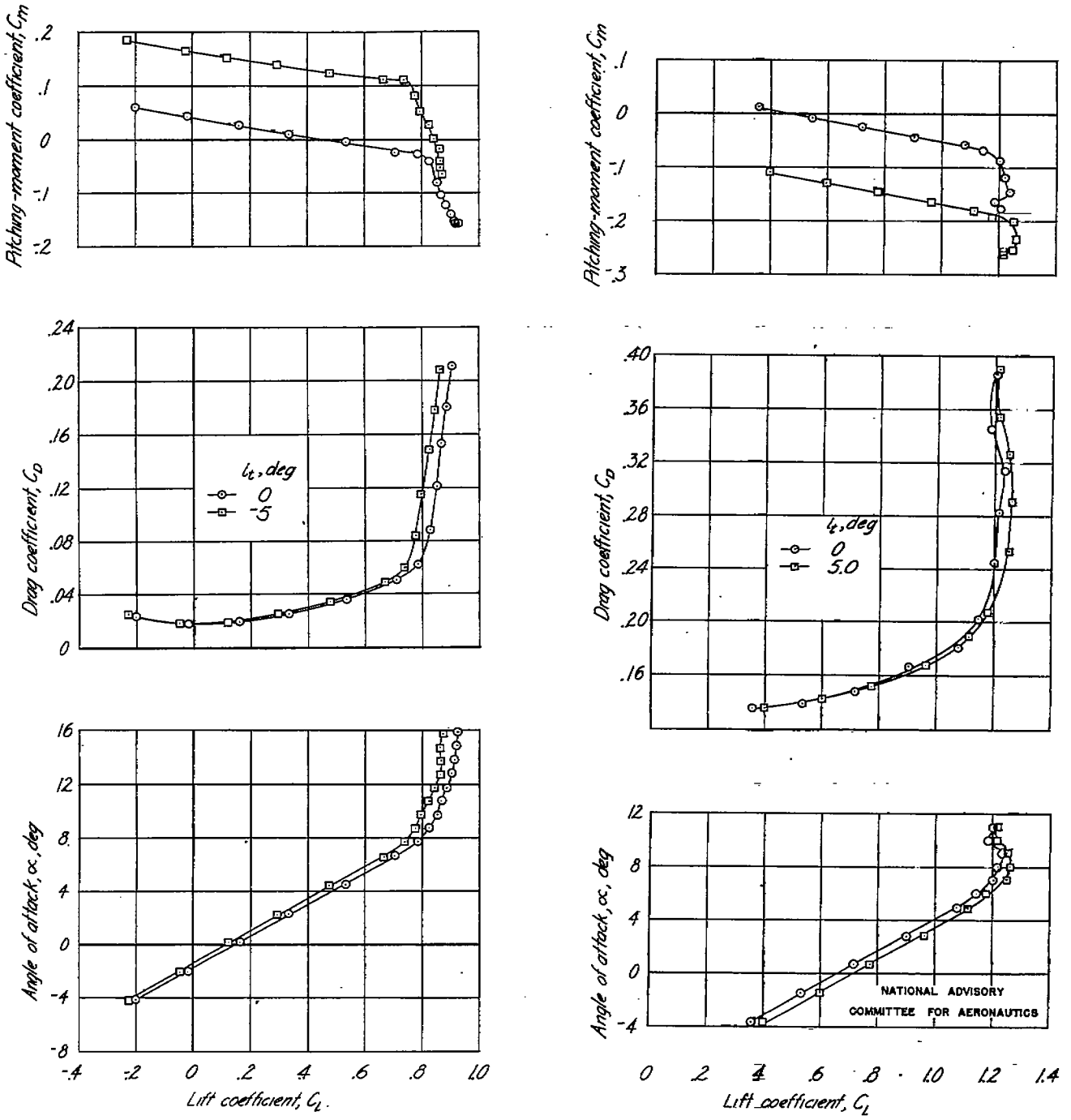

(a) $\delta_f = 0°$; $M = 0.35$.

(b) $\delta_f = 60°$; $M = 0.15$.

Figure 13.- Effect of stabilizer setting on the aerodynamic characteristics in pitch of the model with a 55° vee tail.

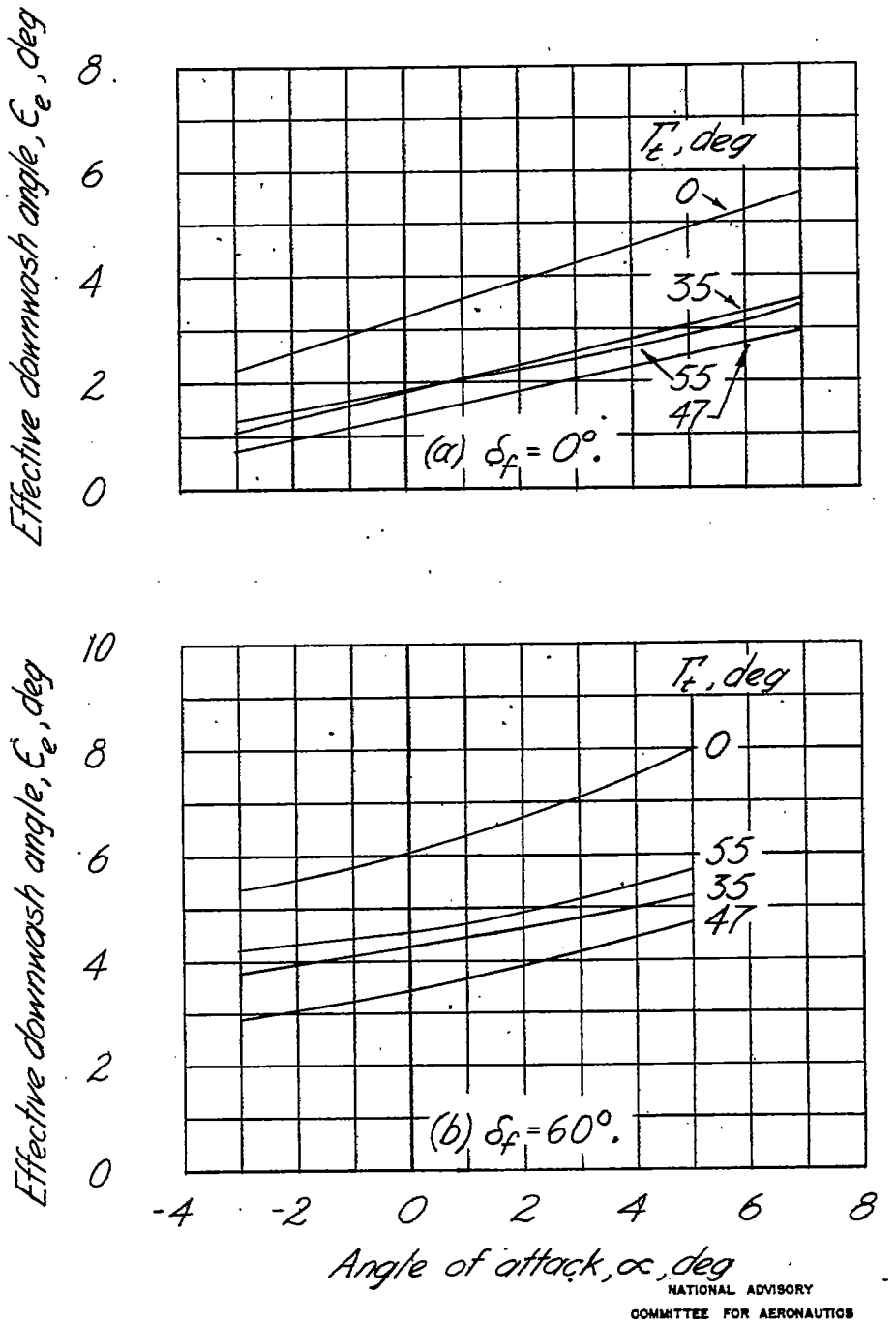

Figure 14.- Variation of effective downwash with angle of attack.

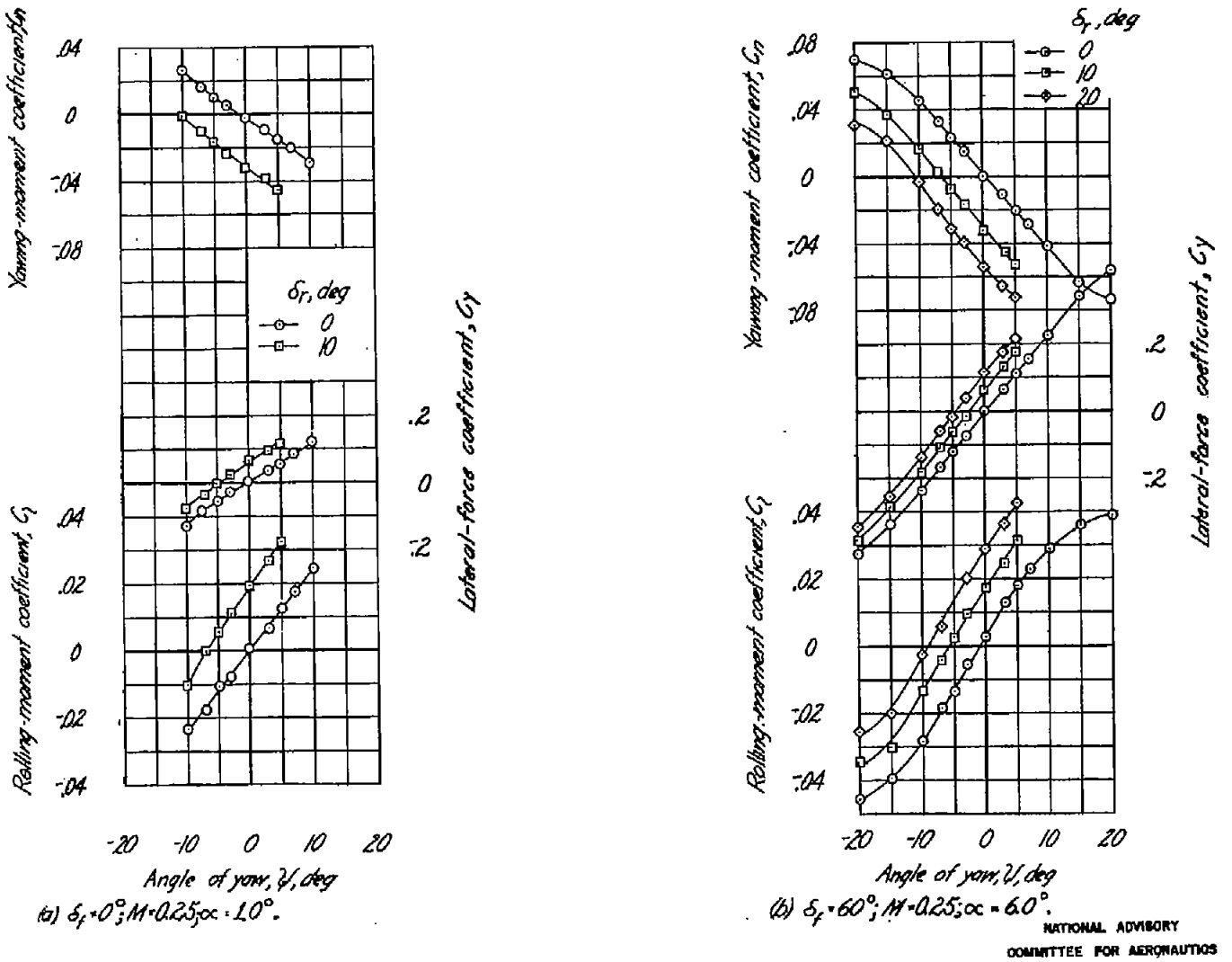

Figure 15.- Effect of rudder deflection on the aerodynamic characteristics in yaw of the model with the 35° vee tail. $\delta_e = 0°$; $i_t = 0°$.

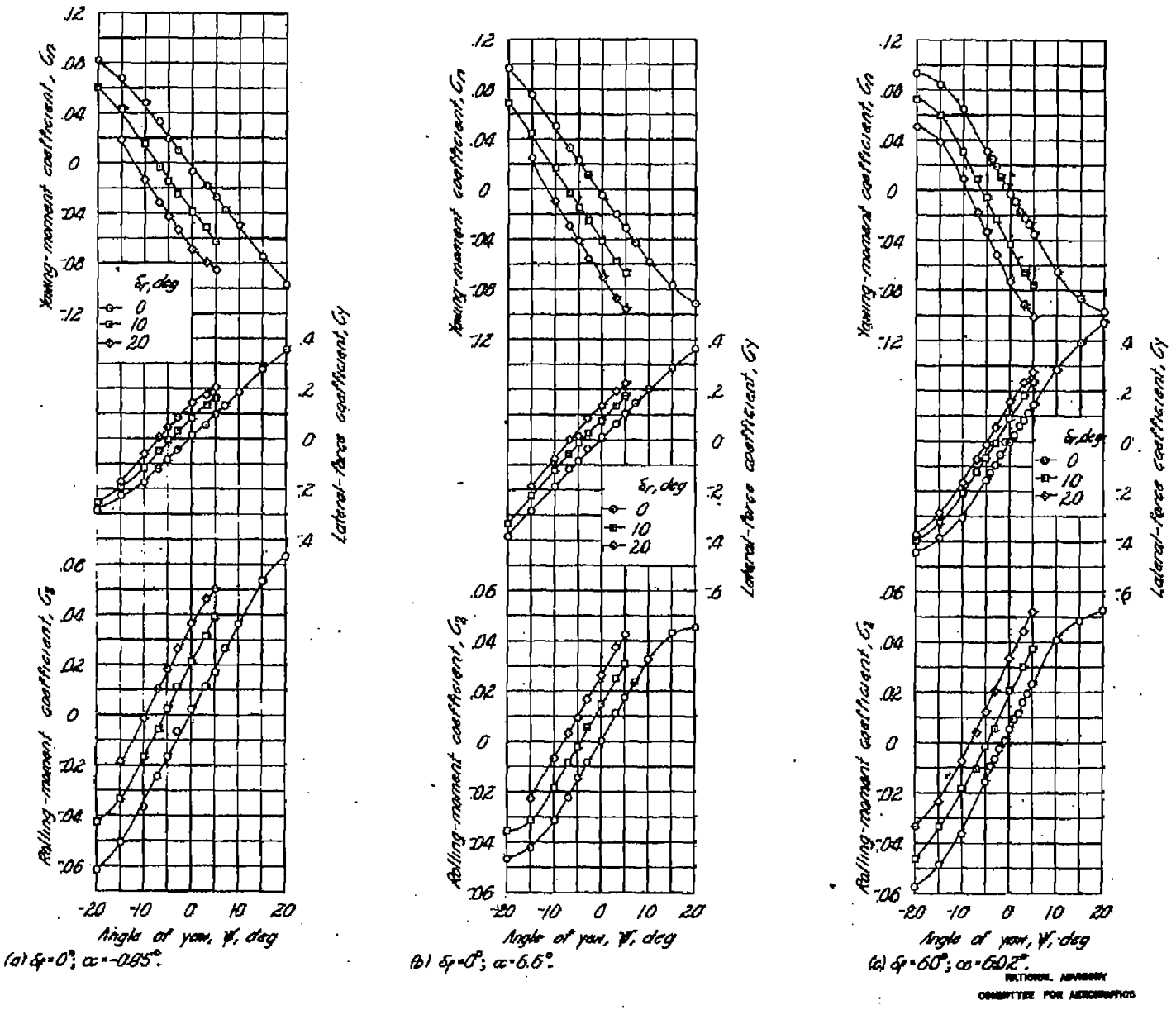

Figure 16.- Effect of rudder deflection in yaw of the model with the 47° vee tail.

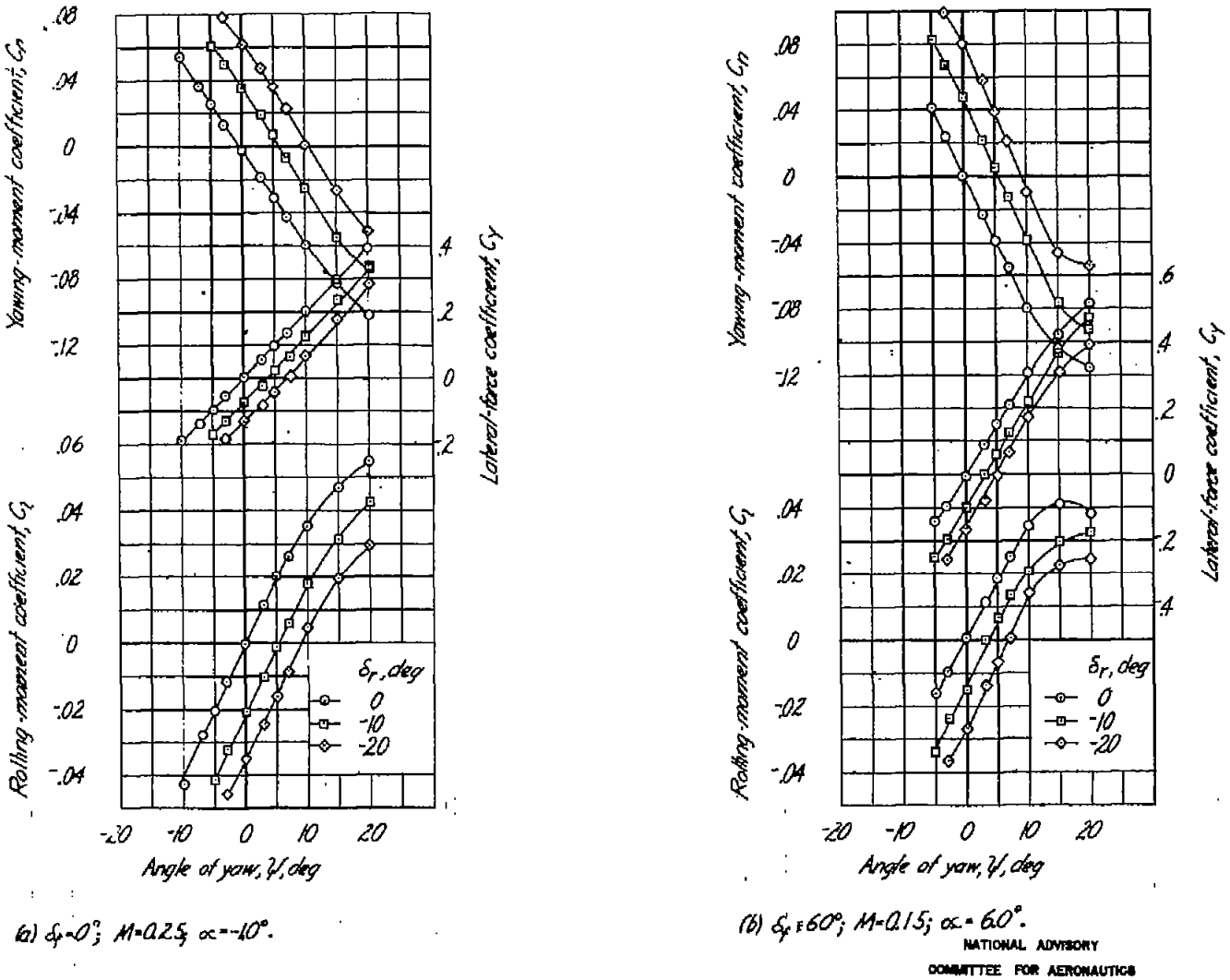

Figure 17.- Effect of rudder deflection on the aerodynamic characteristics in yaw of the model with the 55° vee tail. δ_e = 0°; i_t = 0°.

NATIONAL ADVISORY COMMITTEE FOR AERONAUTICS

TECHNICAL NOTE

No. 1478

WIND-TUNNEL INVESTIGATION OF THE STABILITY AND CONTROL CHARACTERISTICS OF A COMPLETE MODEL EQUIPPED WITH A VEE TAIL

By Edward C. Polhamus and Robert J. Moss

Langley Memorial Aeronautical Laboratory
Langley Field, Va.

Washington
November 1947

NATIONAL ADVISORY COMMITTEE FOR AERONAUTICS

TECHNICAL NOTE NO. 1478

WIND-TUNNEL INVESTIGATION OF THE STABILITY AND CONTROL CHARACTERISTICS OF A COMPLETE MODEL EQUIPPED WITH A VEE TAIL

By Edward C. Polhamus and Robert J. Moss

SUMMARY

A wind-tunnel investigation was conducted to determine the low-speed stability and control characteristics of a complete model equipped with a vee tail. Tail dihedral angles of 35°, 47°, and 55° were tested and the results compared with results of tests of a conventional-tail arrangement used with the same wing-fuselage combination. The area of the vee tail was slightly greater than that of the conventional-tail assembly (approx. 2 percent), and the vee tail was mounted on a small dorsal trunk (10 percent of vee-tail area). The total wetted area of the vee-tail assembly, therefore, was approximately 12 percent greater than that of the conventional-tail assembly. The aspect ratio of the vee tail was equal to that of the horizontal tail but greater than that of the vertical tail.

The 47° vee tail was the best of those tested when both longitudinal and lateral stability were concerned, and it contributed 40 percent more longitudinal and directional stability and 90 percent more dihedral effect than the conventional tail.

The increase in directional stability was due to the dorsal trunk and to the fact that the vee tail had a greater aspect ratio than the vertical tail.

The increase in longitudinal stability was caused by the increase in stabilizer effectiveness and the decrease in the rate of change of effective downwash with angle of attack due to the high tail position and the favorable effect of sidewash at the tail. A method of predicting the sidewash effect is presented in an appendix.

INTRODUCTION

Interest has been displayed in vee tails, particularly for high-speed aircraft, because of: (1) the possibility of a reduction in drag of the empennage due to an improved tail-fuselage juncture and due to a reduction in tail area and (2) the location of the tail out of the wing wake without encountering difficult structural problems. The isolated-tail theory (reference 1) indicates that an isolated vee-tail surface producing stability parameters equal to those produced by an isolated conventional-tail assembly (and having equal effective aspect ratios) must have an area equal to that of the conventional-tail assembly. When the vee tail is used with a wing-fuselage combination, additional factors such as the downwash and sidewash associated with the wing-fuselage vortex pattern must be considered. Inasmuch as the effects of these factors are difficult to evaluate theoretically, an experimental investigation was made of a vee tail used with a wing-fuselage combination. This vee tail had the same tail length and approximately the same total area as the sum of the horizontal and vertical tail surfaces of a conventional tail that was previously investigated with the same wing-fuselage combination. The vee tail, however, was mounted on a small dorsal trunk, the area of which was approximately 10 percent of the area of the vee tail. The effect of this dorsal trunk on lateral stability should be considered when comparing the vee and conventional tails. The aspect ratio of the vee tail was equal to that of the horizontal tail but was greater than that of the vertical tail.

The investigation included stability and control tests, with and without wing flaps, for tail dihedral angles of 35°, 47°, and 55°.

SYMBOLS

The system of axes used for the presentation of the data together with an indication of the sense of the positive forces and moments is presented in figure 1. All moments are presented about the center of gravity. Pertinent symbols are defined as follows:

C_L lift coefficient (Lift/qS)

C_D drag coefficient (Drag/qS)

C_m pitching-moment coefficient $\left(\frac{\text{Pitching moment}}{qS\bar{c}}\right)$

C_l rolling-moment coefficient $\left(\frac{\text{Rolling moment}}{qSb}\right)$

C_n yawing-moment coefficient $\left(\frac{\text{Yawing moment}}{qSb}\right)$

C_Y lateral-force coefficient $\left(\frac{\text{Lateral force}}{qS}\right)$

S wing area, square feet

b wing span, feet

$\bar{c}$ wing mean aerodynamic chord (M.A.C.), feet

q dynamic pressure, pounds per square foot $\left(\rho V^2/2\right)$

ρ mass density of air, slugs per cubic foot

V free-stream velocity, feet per second

M Mach number

α angle of attack of fuselage center line, degrees

ϵ angle of downwash, degrees

ϵ_e effective downwash (downwash that alone has same effect as downwash and sidewash)

i_t stabilizer setting (angle between line of intersection of tail panels and fuselage center line), degrees

ψ angle of yaw, degrees

δ control-surface deflection with reference to fixed surface and measured in plane normal to fixed surface, degrees

Γ_t tail dihedral angle with reference to horizontal, degrees

Subscripts:

t tail

e elevator

r rudder

f flap

m measured value

δ_e, i_t, δ_r, α, ψ denote partial derivative of a coefficient with respect to δ_e, i_t, δ_r, α, ψ, respectively; for example, $C_{m_{\delta_e}} = \frac{\partial C_m}{\partial \delta_e}$

MODEL AND APPARATUS

The model equipped with a 47° vee tail is shown mounted in the Langley 300 MPH 7- by 10-foot tunnel in figures 2 and 3 and a three-view drawing of the model as tested is presented in figure 4. Details of the vee-tail panel are presented in figure 5; details of the conventional-tail assembly are shown in figures 6 and 7.

The model was constructed of wood attached to metal reinforcing members with Cycleweld cement except for the all-metal control surfaces. The tail-control surfaces and wing flaps were 20-percent-chord plain flaps and the ailerons were 15-percent-chord plain flaps. All controls were flat-sided from the hinge line to the trailing edge and all control gaps were sealed.

Specific model configurations referred to herein are as follows:

(a) High-speed configuration
Flaps retracted
Landing gear retracted

(b) Landing configuration
Flaps deflected 60°
Landing gear extended

The tests were conducted in the Langley 300 MPH 7- by 10-foot tunnel, which is a closed rectangular tunnel with a contraction ratio of 14:1 and is powered by a 1600-horsepower synchronous motor.

TESTS

Test Conditions

Tests in the high-speed configuration were run at dynamic pressures of 88.5 and 165.2 pounds per square foot. Tests in the

landing configuration were run at a dynamic pressure of 33.5 pounds per square foot. The corresponding approximate values of Mach number and Reynolds number (based on a wing mean aerodynamic chord of 1.202 ft) were as follows:

Dynamic pressure (lb/sq ft)	Mach number	Reynolds number
33.5	0.15	1.28×10^6
88.5	.25	2.08×10^6
165.2	.35	2.82×10^6

The Reynolds number was computed using a turbulence factor of unity. The degree of turbulence of the tunnel is not known quantitatively but is believed to be small because of the high contraction ratio.

Corrections

All data have been corrected for tares caused by the model-support struts. Jet-boundary corrections were computed as follows (reference 2), where the subscript m refers to the measured values:

$$\alpha = \alpha_m + 0.88C_{L_m}$$

$$C_D = C_{D_m} + 0.0128C_{L_m}^2$$

$$C_m = C_{m_m} + 0.0222C_{L_m} \qquad \text{(for flaps undeflected)}$$

$$C_m = C_{m_m} + 0.0227C_{L_m} \qquad \text{(for flaps deflected)}$$

$$C_l = 0.98C_{l_m}$$

$$C_n = C_{n_m} - 0.0173C_{l_m}C_{L_m}$$

All force and moment coefficients were corrected for blocking by the method presented in reference 3. An increment in drag coefficient has been added in order to account for the horizontal buoyancy effected by the longitudinal static pressure gradient in the tunnel.

RESULTS AND DISCUSSION

An outline of the figures presenting the results is as follows:

Lift characteristics.- The lift characteristics of the model with the vee tail are presented in figures 8 to 13 and are summarized in the following table:

Γ_t (deg)	$C_{L_{max}}$ trimmed	C_{L_α}
$\delta_f = 0^\circ$		
35	0.76	0.085
47	.86	.088
55	.81	.085
$\delta_f = 60^\circ$		
35	1.19	.090
47	1.15	.086
55	1.18	.083

Horizontal tail characteristics.- Mean values describing the effectiveness of the elevator and stabilizer for the different dihedral angles are plotted against tail dihedral angle in figures 19 and 20, respectively. The values at $\Gamma_t = 0^\circ$ that are presented were

obtained by multiplying the values obtained with a conventional horizontal tail of the same aspect ratio (data obtained in the Langley 300 MPH 7- by 10-foot tunnel) on the same wing-fuselage combination by the ratio of tail areas. Also presented in these figures are the theoretical variations based on the isolated-tail theory of reference 1. The experimental and theoretical results are in fair agreement, but the general trend of the experimental results seems to indicate that there may be a slight increase in effectiveness at the higher dihedral angles over that predicted by the theory.

Downwash at the tail.- The average effective-downwash values for the various tail dihedral angles are presented in figure 14. These values were evaluated from tail-on and tail-off pitching moments; and, since the pitching moment contributed by a vee tail depends on sidewash as well as downwash, the effective downwash, rather than the actual downwash existing in the vertical plane, is obtained. The effective downwash is defined as the downwash that alone would produce the same pitching moment as that produced by the actual downwash and sidewash. A method of estimating the effect of sidewash on effective downwash and longitudinal stability is presented in the appendix.

Figure 21 shows the effect of tail dihedral angle on the rate of change of effective downwash angle with angle of attack. Two theoretical variations with dihedral angle are also included. One curve takes into account the change in tail height and was determined from the charts of reference 4 by assuming the tail height to be equal to the height of the tail mean aerodynamic chord. The other curve includes both the effect of tail height and the effect of sidewash (see appendix) and is in fair agreement with the experimental data.

Rudder effectiveness.- Values of the rudder-effectiveness parameter $C_{n_{\delta_r}}$ obtained from figures 15 to 17 are plotted against tail dihedral angle Γ_t in figure 22. The theoretical variation of $C_{n_{\delta_r}}$ with Γ_t, as estimated from the isolated-tail theory of reference 1, is also presented. The increase in effectiveness is probably due to the rudder induced load carried by the dorsal trunk. Also presented in figure 22 are the variations of $C_{l_{\delta_r}}$ and $C_{l_{\delta_r}}/C_{n_{\delta_r}}$ with Γ_t. The ratio of adverse rolling moments to favorable yawing moments produced by rudder deflection is greater for the vee tail than for the conventional tail.

Static longitudinal stability.- The neutral-point locations for both the cruising and landing configurations are presented in figure 23.

The tail-off neutral points and the assumed center-of-gravity position at 25 percent M.A.C. about which the moments were measured are also indicated. The curves indicate that the model with the vee tail has greater longitudinal stability than the model with the horizontal tail for the three tail dihedral angles tested. The 47° tail, which according to isolated-tail theory should contribute the same longitudinal stability as the horizontal tail tested, actually contributes 40 percent more longitudinal stability than the horizontal tail. The variation of $\left(C_{m_\alpha}\right)_t$ with Γ_t is presented in figure 24. For comparison, the horizontal-tail contribution $\left(\Gamma_t = 0°\right)$ was increased by the ratio of the vee-tail area to the horizontal-tail area. Also presented in this figure is the theoretical variation of $\left(C_{m_\alpha}\right)_t$ with Γ_t, and it can be seen that the decrease in longitudinal stability with dihedral angle is overestimated. The overestimated decrease in stability can be accounted for by the increase in stabilizer effectiveness and the decrease in the rate of change of effective downwash with angle of attack due to the increased tail height and the favorable effect of sidewash. A method of estimating this sidewash effect is presented in the appendix.

Static directional and lateral stability.- The static lateral-stability parameters determined from pitch tests at yaw angles of 5° and -5° for both the high-speed and the landing configurations are plotted against angle of attack in figure 18. In the high-speed configuration a large amount of directional and lateral stability exists for all three dihedral angles and the maximum stability would appear to occur at some angle between 47° and 55°. In the landing configuration the high static directional stability and the dihedral effect are indicated for angles of attack below 6°. Above 6° there is a slight loss of dihedral effect and a large loss in directional stability. It will be noted that the 47° vee tail, which is the best of those tested, contributed approximately 40 percent more longitudinal and directional stability and 90 percent more dihedral effect than the conventional tail. The increase in directional stability, however, is due to the fact that the aspect ratio of the vee tail is greater than that of the vertical tail and due to the dorsal trunk upon which the vee tail was mounted. The effect of this trunk can be seen in figure 25, which presents the actual and theoretical variations of the tail contribution to directional stability $\left(C_{n_\psi}\right)_t$ and to dihedral effect $\left(C_{l_\psi}\right)_t$ with tail dihedral angle. The reasons for the large contribution to directional stability of this small trunk (approx. 10 percent of the vee-tail area) are that the trunk increases the effective aspect ratio of the vee tail in yaw. Since tail effectiveness is proportional to $\sin^2\Gamma_t$, this trunk is more effective per unit area than the vee tail.

The high dihedral effect (equivalent to approx. 16.5° of wing geometric dihedral for the 47° tail) is due to the high geometric dihedral of the tail.

CONCLUSIONS

From low-speed wind-tunnel tests of a complete model equipped with a vee tail having tail dihedral angles of 35°, 47°, and 55° and from comparisons with tests of a conventional tail used with the same wing-fuselage combination, the following conclusions with regard to static stability and control were reached:

1. The 47° vee tail appeared to be the best of those tested when both longitudinal and lateral stability were concerned.

2. The 47° vee tail, the area of which was approximately the same (2 percent greater) as the conventional tail assembly but was mounted on a small dorsal trunk (10 percent of vee-tail area), contributed 40 percent more longitudinal and directional stability and 90 percent more dihedral effect than the conventional tail.

3. The increase in directional stability was due to the dorsal trunk and to the fact that the vee tail had a greater aspect ratio than the vertical tail.

4. The increase in longitudinal stability was caused by the increase in stabilizer effectiveness and the decrease in the rate of change of effective downwash with angle of attack due to the high tail position and the favorable effect of sidewash at the tail.

5. The measured variations of stabilizer and elevator effectiveness with tail dihedral angle agreed fairly well with the isolated-tail theory.

Langley Memorial Aeronautical Laboratory
National Advisory Committee for Aeronautics
Langley Field, Va., July 31, 1947

APPENDIX

METHOD OF ESTIMATING SIDEWASH EFFECT ON LONGITUDINAL STABILITY

Symbols

α	angle of attack of airplane in plane of symmetry
$(\alpha_N)_{tail}$	angle of attack of tail panel in plane normal to chord plane of tail surface
ϵ	induced angle (downwash) in plane of symmetry
ϵ_N	induced angle in plane normal to chord plane of tail surface
$(C_L)_{tail}$	lift coefficient of tail measured in plane of symmetry
$\left(C_{L_\alpha}\right)_N$	lift-curve slope of tail in plane normal to chord plane of tail surface
Γ_t	dihedral angle of tail surface
$(C_m)_{tail}$	airplane pitching moment due to tail lift
$\frac{b_t}{2}$	span of one vee-tail panel
$\bar{c}_w$	M.A.C. of wing
$\bar{c}_t$	M.A.C. of tail
c_t	local chord of tail
l_t	tail length measured from c.g. to $\bar{c}_t/4$
S_t	actual (not projected) area of tail
S_w	wing area
q	free-stream dynamic pressure
q_t	effective dynamic pressure at tail
w	total induced velocity in vertical plane $(w_T + w_B)$

w_T velocity in vertical plane induced by trailing vortices (downwash)

w_B velocity in vertical plane induced by bound vortex (downwash)

w_S velocity in plane normal to vertical plane induced by trailing vortices (sidewash)

w_N total induced velocity in plane normal to tail panel

w_{T_N} velocity in normal plane induced by trailing vortices

X tail length measured from $\bar{c}_w/4$ to $\bar{c}_t/4$

s wing vortex semispan

v tangential velocity of a vortex at Y for unit circulation

Y distance from vortex center to point in question

V velocity at tail parallel to X-axis

Method

When the longitudinal stability contributed by a vee tail is calculated, the effect of sidewash should be included. The following derivation of the longitudinal-stability equation includes this effect. The angle of attack in the plane normal to the tail panel is as follows (see fig. 26):

$$(\alpha_N)_{tail} = \alpha \cos \Gamma_t - \epsilon_N \tag{1}$$

and

$$(C_L)_{tail} = (C_{L_\alpha})_N (\alpha_N)_{tail} \cos \Gamma_t \tag{2}$$

By substituting equation (1) in equation (2)

$$(C_L)_{tail} = (C_{L_\alpha})_N \left(\alpha \cos \Gamma_t - \epsilon_N\right) \cos \Gamma_t \tag{3}$$

Now

$$\left(C_m\right)_{tail} = \left(C_L\right)_{tail} \frac{l_t}{\bar{c}_w} \frac{S_t}{S_w} \frac{q_t}{q} \tag{4}$$

and by substituting equation (3) in equation (4)

$$\left(C_m\right)_{tail} = \left(\alpha \cos \Gamma_t - \epsilon_N\right) \left(C_{L_\alpha}\right)_N \cos \Gamma_t \frac{l_t}{\bar{c}_w} \frac{S_t}{S_w} \frac{q_t}{q}$$

or

$$\left(C_{m_\alpha}\right)_{tail} = \left(\cos \Gamma - \frac{\partial \epsilon_N}{\partial \alpha}\right) \left(C_{L_\alpha}\right)_N \cos \Gamma_t \frac{l_t}{\bar{c}_w} \frac{S_t}{S_w} \frac{q_t}{q} \tag{5}$$

Since all available theoretical and experimental induced angles are presented as downwash angles, ϵ, equation (5) will be revised by replacing $\frac{\partial \epsilon_N}{\partial \alpha}$ with $\frac{\partial \epsilon}{\partial \alpha}$ and a correction factor. Since $\epsilon = \frac{w}{V}$ and $\epsilon_N = \frac{w_N}{V}$,

$$\frac{\partial \epsilon_N}{\partial \alpha} = \frac{\partial \epsilon}{\partial \alpha} \frac{w_N}{w} \tag{6}$$

By substituting equation (6) in equation (5)

$$\left(C_{m_\alpha}\right)_{tail} = \left(\cos \Gamma_t - \frac{\partial \epsilon}{\partial \alpha} \frac{w_N}{w}\right) \left(C_{L_\alpha}\right)_N \cos \Gamma_t \frac{l_t}{\bar{c}_w} \frac{S_t}{S_w} \frac{q_t}{q} \tag{7}$$

A more convenient form of equation (7) is

$$\left(C_{m_\alpha}\right)_{tail} = \left(1 - \frac{\partial \epsilon}{\partial \alpha} \frac{w_N}{w \cos \Gamma_t}\right) \left(C_{L_\alpha}\right)_N \cos^2 \Gamma_t \frac{l_t}{\bar{c}_w} \frac{S_t}{S_w} \frac{q_t}{q} \tag{8}$$

Values of $\frac{\partial \epsilon}{\partial \alpha}$ may be obtained from the charts of reference 4 by use of a tail height equal to the height of the M.A.C. of the tail. Values of $\frac{w_N}{w \cos \Gamma_t}$ may be obtained as follows:

$$\frac{w_N}{w \cos \Gamma_t} = \frac{w_B \cos \Gamma_t}{w \cos \Gamma_t} + \frac{w_{T_N}}{w \cos \Gamma_t}$$

and

$$\frac{w_N}{w \cos \Gamma_t} = \frac{w_B}{w} + \frac{w_{T_N}}{w_T \cos \Gamma_t} \frac{w_T}{w}$$

or

$$\frac{w_N}{w \cos \Gamma_t} = \frac{w_B}{w} + \frac{w_{T_N}}{w_T \cos \Gamma_t} \left(1 - \frac{w_B}{w}\right) \tag{9}$$

An approximate value $\frac{w_B}{w}$ may be obtained from the following equation which was derived from the equation for downwash due to the bound and trailing vortices given in reference 5:

$$\frac{w_B}{w} = \frac{s^2}{s^2 + X^2 + X\sqrt{X^2 + s^2}} \tag{10}$$

Equation (10) is for a point midway between the two trailing vortices in the plane of the horseshoe vortex but is sufficiently accurate for these calculations.

The factor $\frac{w_{T_N}}{w_T \cos \Gamma_t}$ (equation (9)) may be determined graphically as follows: By assuming a horseshoe vortex of span equal to 90 percent of the wing span (see fig. 27), the induced velocities due to the trailing vortices in the normal and vertical planes are obtained at various spanwise stations of the tail. Inasmuch as only velocity ratios are desired, the tangential velocity v of the vortex at the first spanwise point investigated may be drawn to any convenient length.

At any other point the velocity may then be easily drawn since it is inversely proportional to the distance Y from the vortex center to the point in question. At each spanwise station the induced velocities w_{T_N} and $w_T \cos \Gamma_t$ due to both trailing vortices are obtained and then the factor $\frac{w_{T_N}}{w_T \cos \Gamma_t}$ is weighted according to the local chord and integrated over the span in order to obtain an average value to substitute in equation (9). This procedure need be done for only one panel since it will be the same for both.

From figure 27 it can be seen that $\frac{w_{T_N}}{w_T \cos \Gamma_t}$ is less than unity and that the reduction is due to the sidewash w_S.

REFERENCES

1. Purser, Paul E., and Campbell, John P.: Experimental Verification of a Simplified Vee-Tail Theory and Analysis of Available Data on Complete Models with Vee Tails. NACA ACR No. L5A03, 1945.

2. Gillis, Clarence L., Polhamus, Edward C., and Gray, Joseph L., Jr.: Charts for Determining Jet-Boundary Corrections for Complete Models in 7- by 10-Foot Closed Rectangular Wind Tunnels. NACA ARR No. L5G31, 1945.

3. Thom, A.: Blockage Corrections in a Closed High-Speed Tunnel. R. & M. No. 2033, British A.R.C., 1943.

4. Silverstein, Abe, and Katzoff, S.: Design Charts for Predicting Downwash Angles and Wake Characteristics behind Plain and Flapped Wings. NACA Rep. No. 648, 1939.

5. von Kármán, Th., and Burgers, J. M.: General Aerodynamic Theory - Perfect Fluids. Mathematical Foundation of the Theory of Wings with Finite Span. Vol. II of Aerodynamic Theory, div. E, ch. III, W. F. Durand, ed., Julius Springer (Berlin), 1935, p. 142. (Reprint of 1943.)

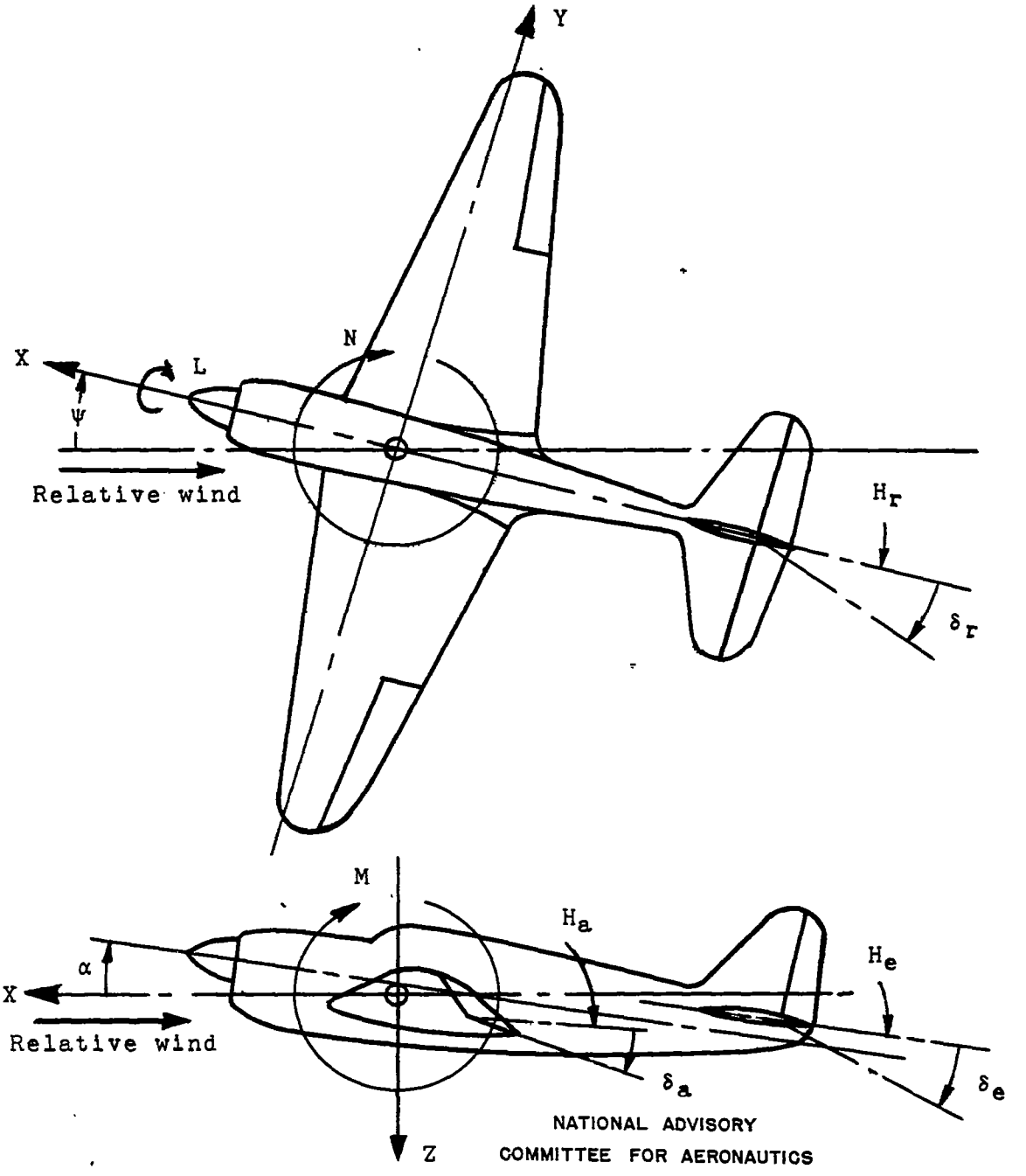

Figure 1.- System of axes and control-surface hinge moments and deflections. Positive values of forces, moments, and angles are indicated by arrows. Positive values of tab hinge moments and deflections are in the same directions as the positive values for the control surfaces to which the tabs are attached.

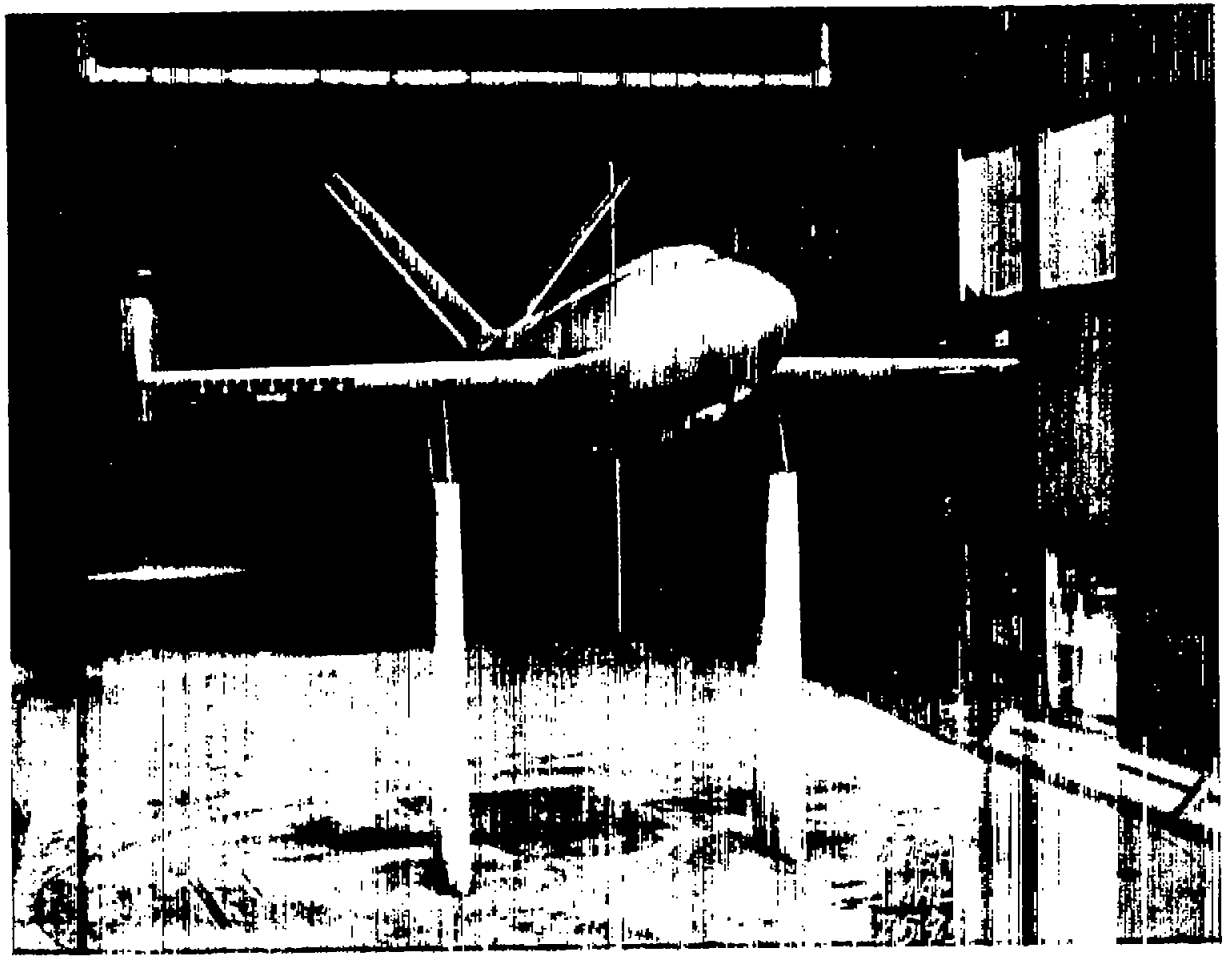

Figure 2.- Front view of model mounted in the Langley 300 MPH 7- by 10-foot tunnel.

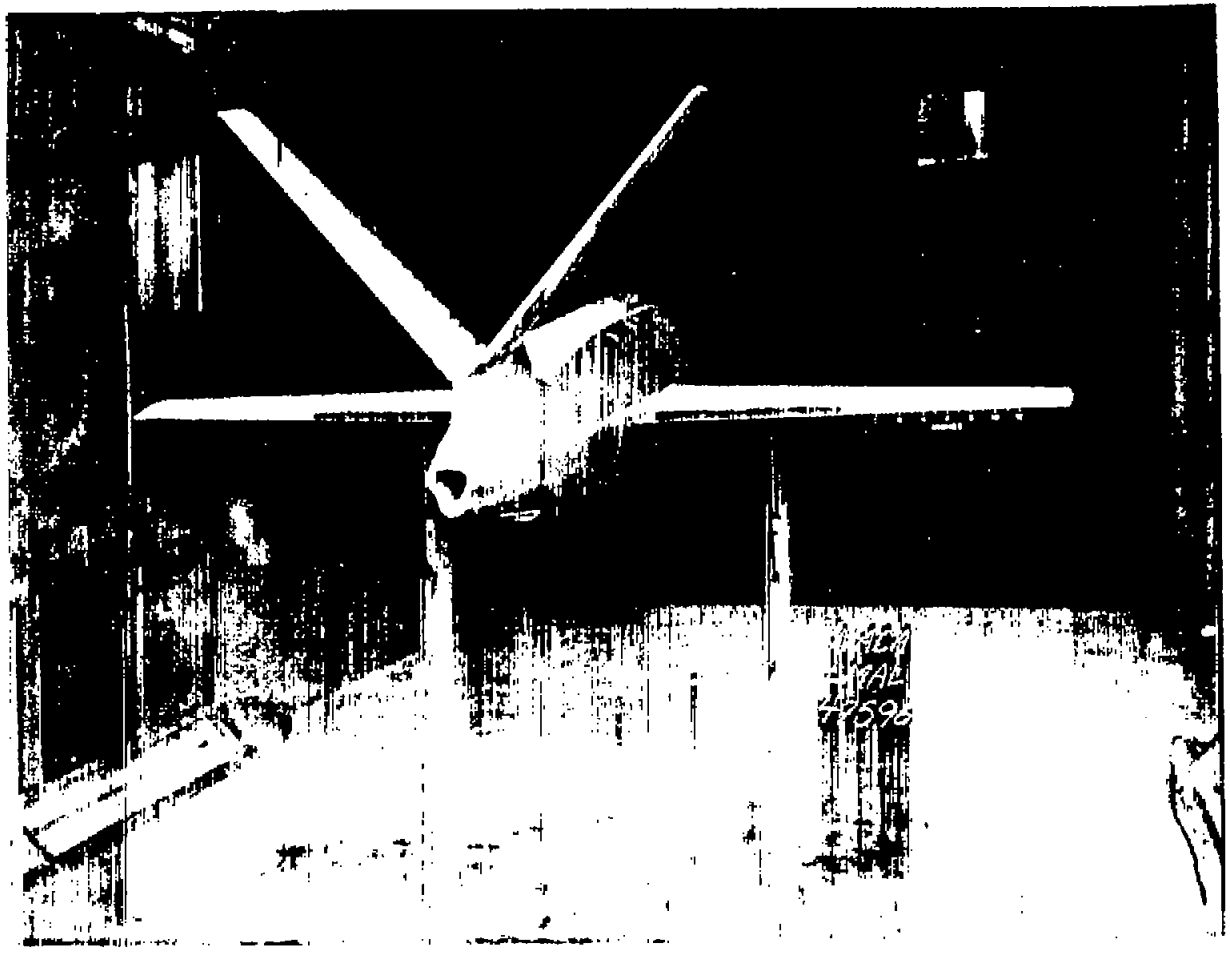

Figure 3.- Rear view of model mounted in the Langley 300 MPH 7- by 10-foot tunnel.

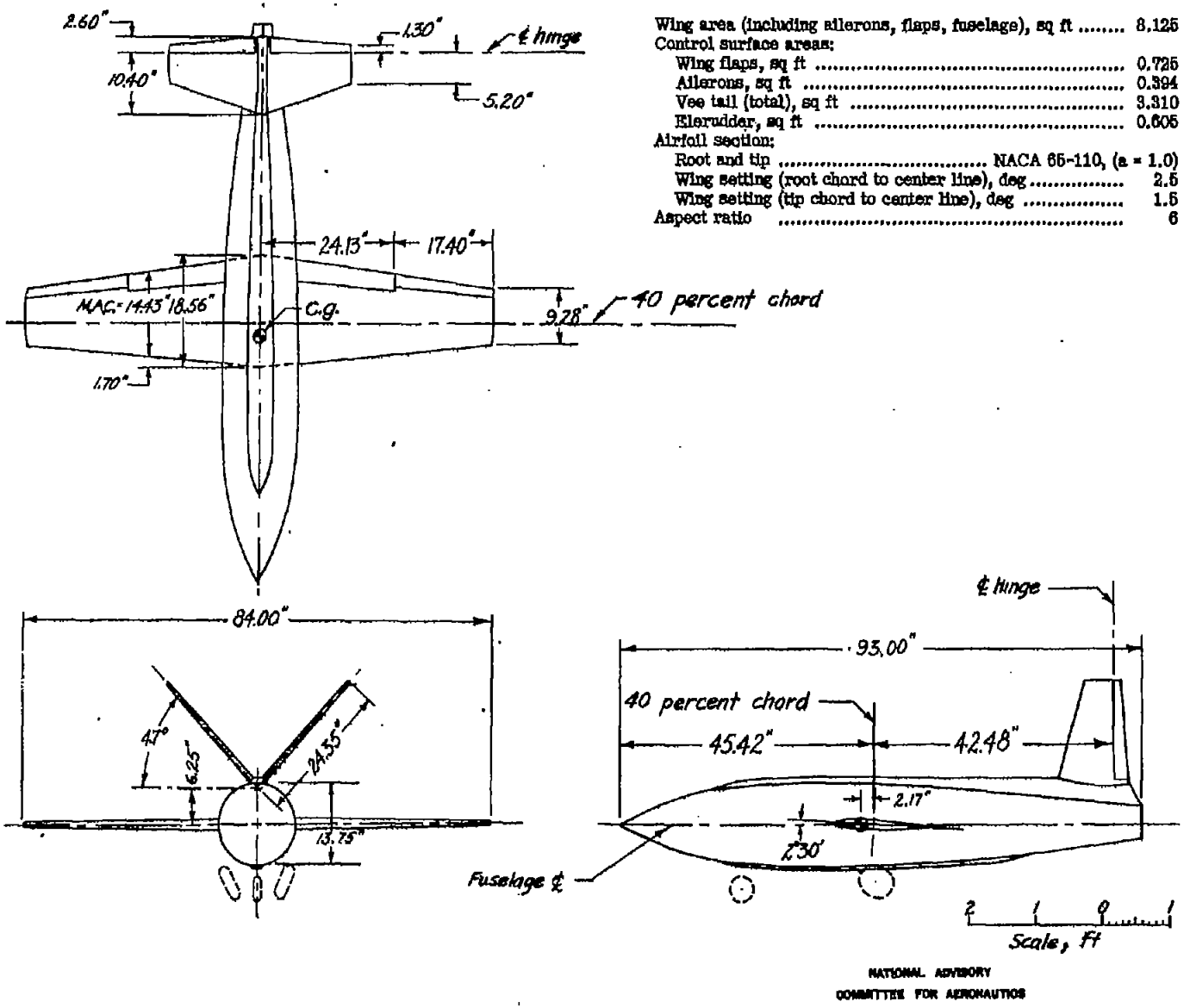

Wing area (including ailerons, flaps, fuselage), sq ft	8.125
Control surface areas:	
Wing flaps, sq ft	0.725
Ailerons, sq ft	0.394
Vee tail (total), sq ft	3.310
Elerudder, sq ft	0.605
Airfoil section:	
Root and tip	NACA 65-110, (a = 1.0)
Wing setting (root chord to center line), deg	2.5
Wing setting (tip chord to center line), deg	1.5
Aspect ratio	6

Figure 4.- Three-view drawing of the model.

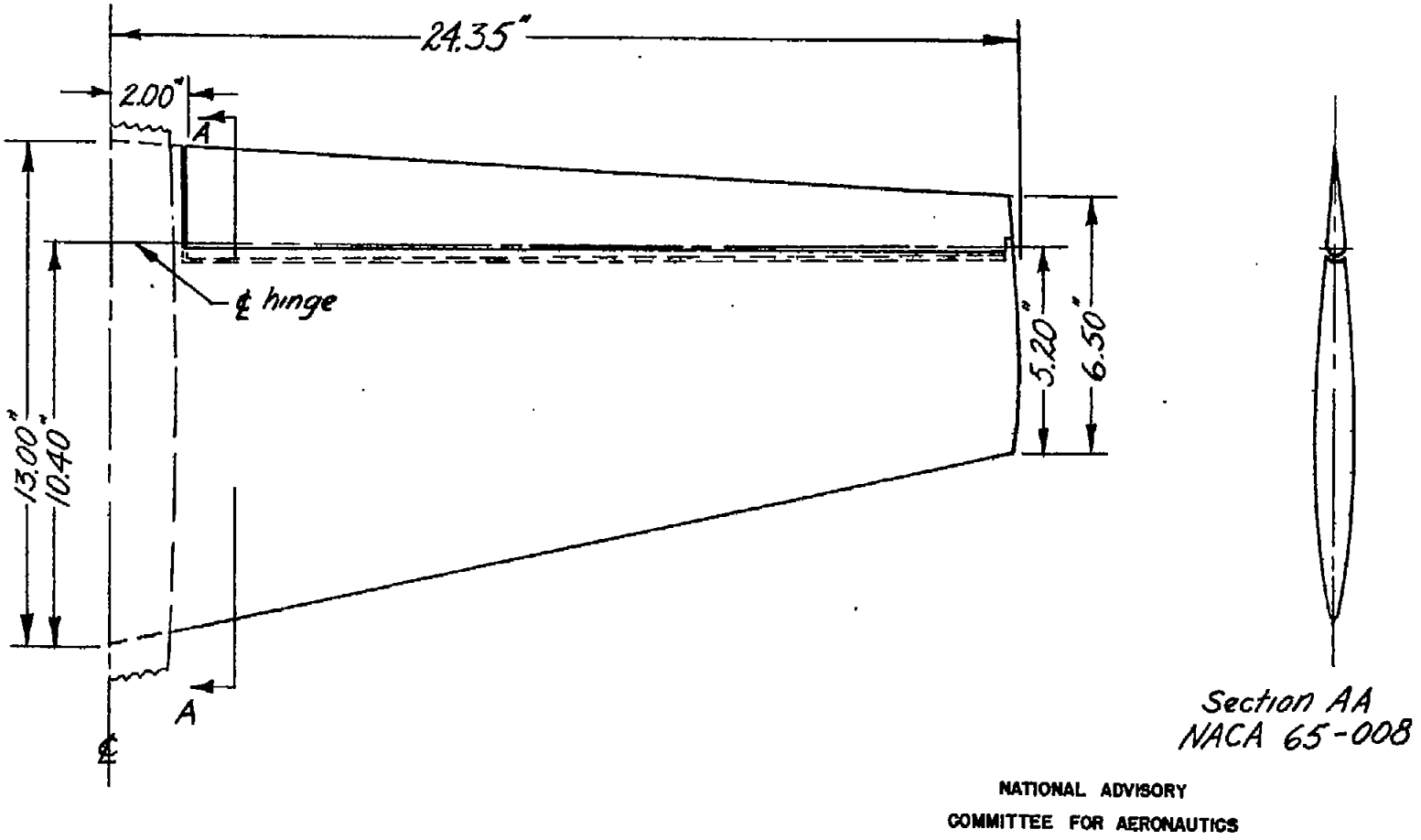

Figure 5.- Vee-tail panel. Area (total, not including trunk), 3.31 square feet; area (dorsal trunk), 0.32 square feet; aspect ratio, 5.0.

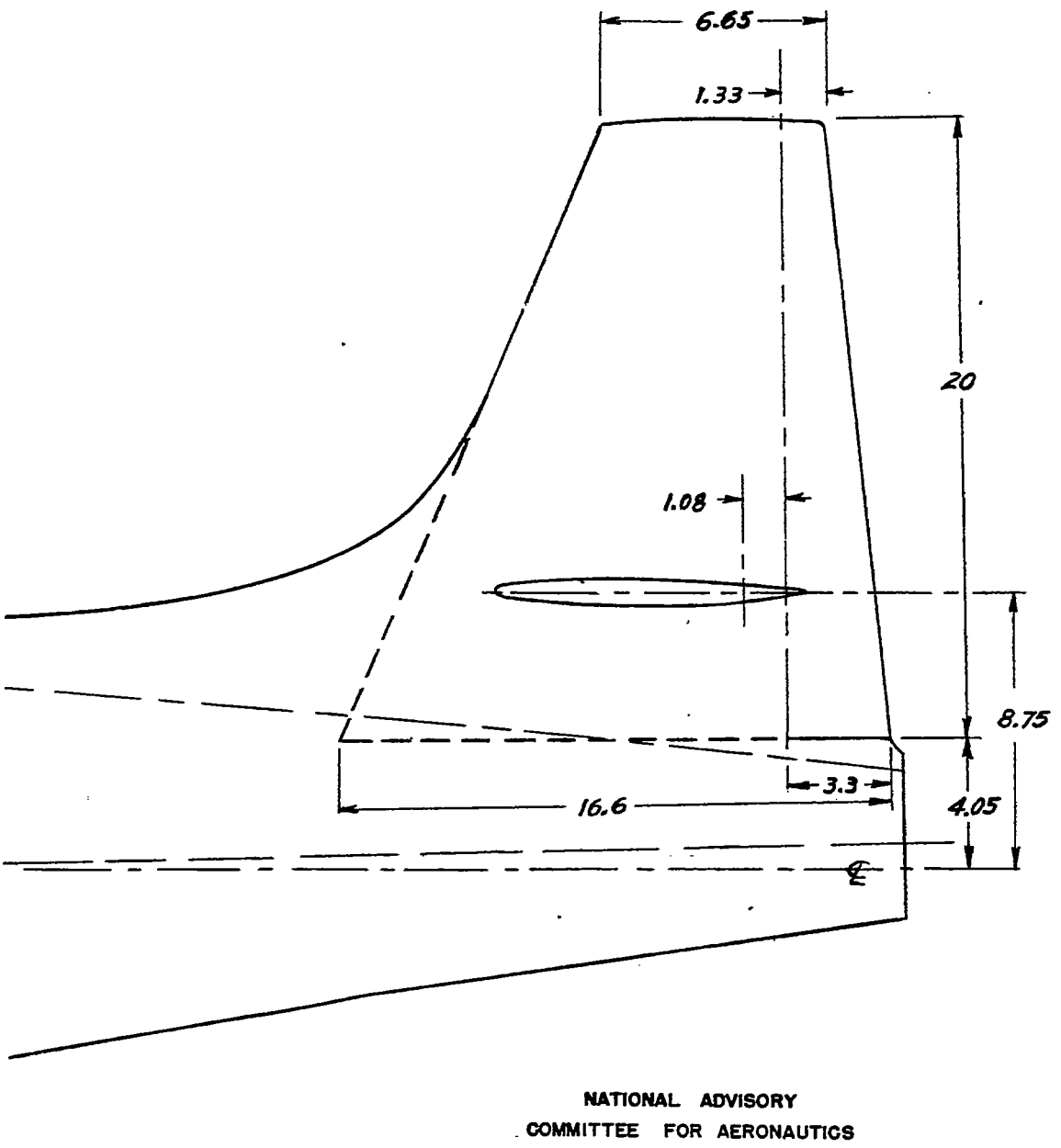

Figure 6.- Vertical tail. Area (total), 1.60 square feet; aspect ratio, 1.74.

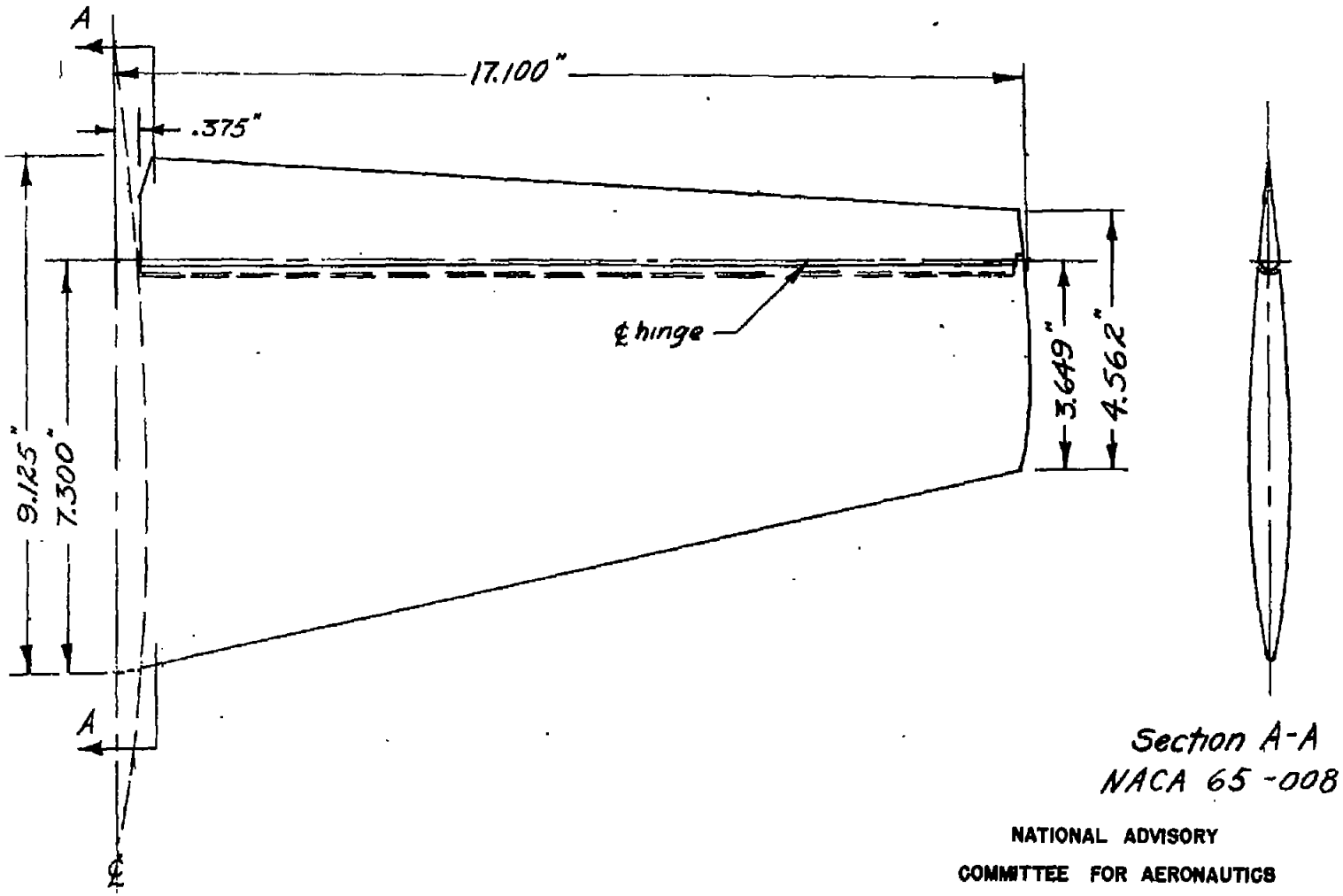

Figure 7.- Horizontal tail. Area (total), 1.625 square feet; aspect ratio, 5.0; trailing edge angle, 10°.

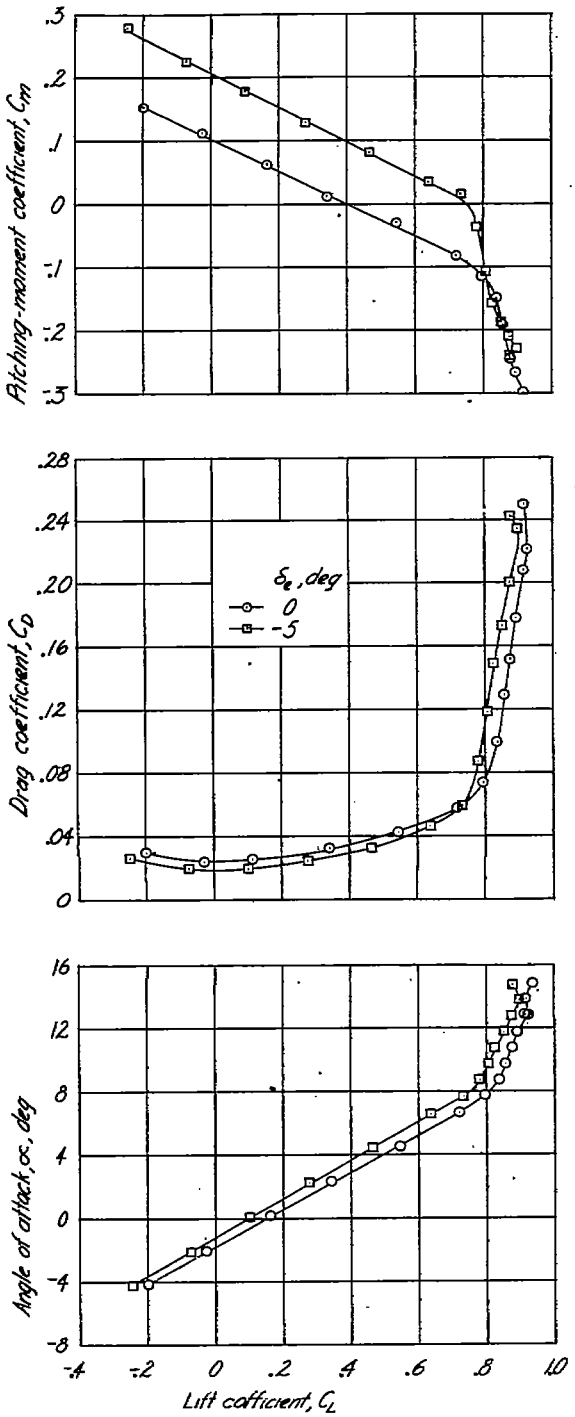

(a) $\delta_f = 0°$; $M = 0.35$.

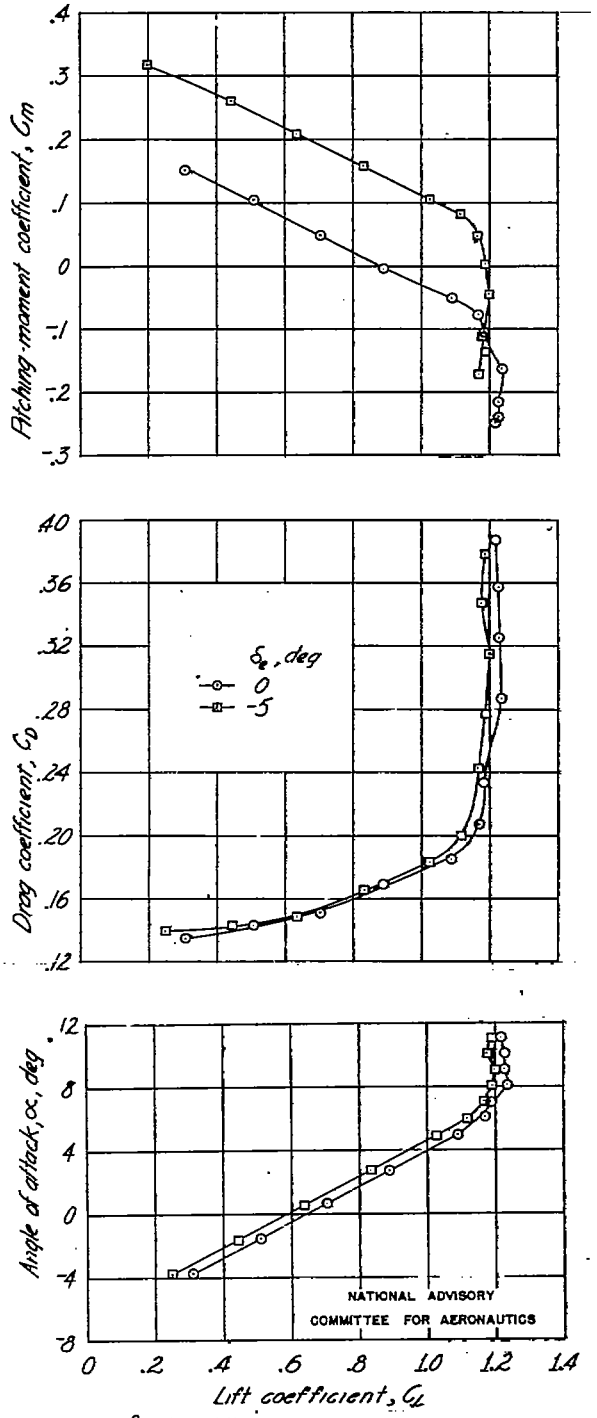

(b) $\delta_f = 60°$; $M = 0.15$.

Figure 8.- Effect of elevator deflection on the aerodynamic characteristics in pitch of the model with a 35° vee tail.

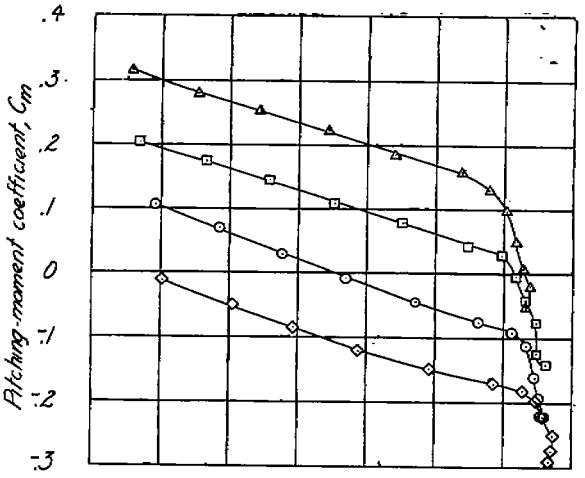

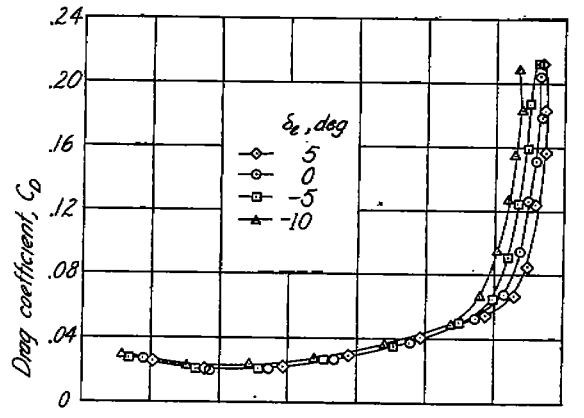

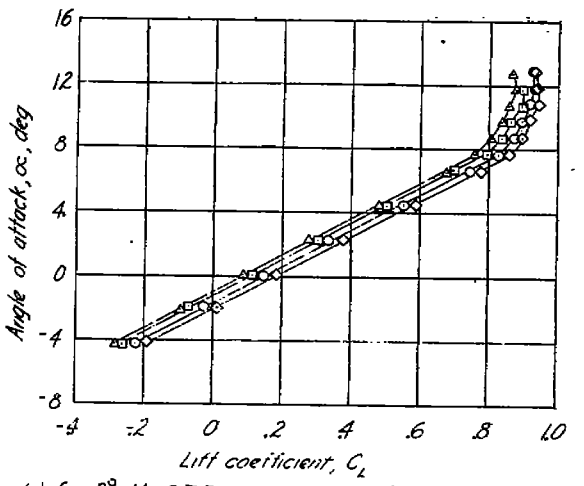

(a) $\delta_f = 0°$; $M = 0.35$.

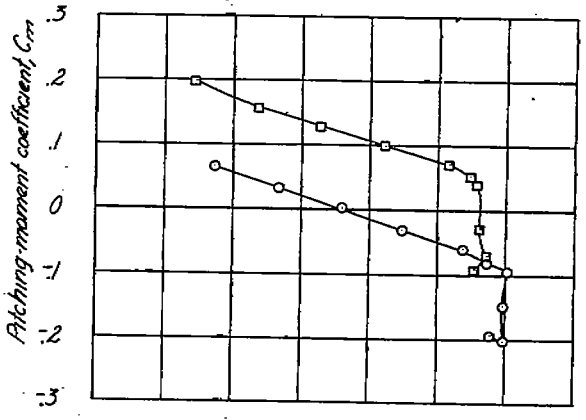

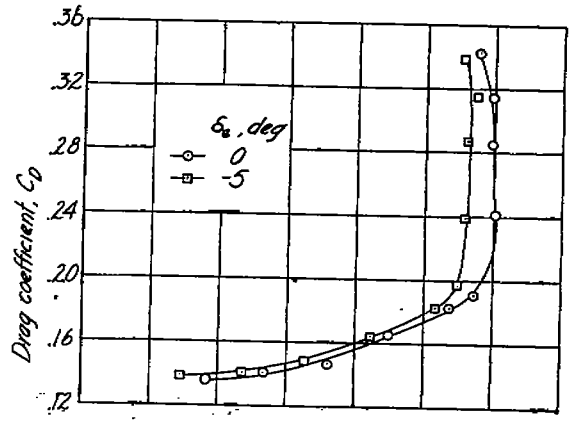

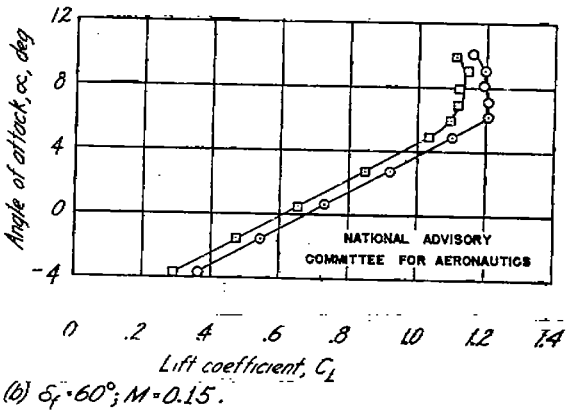

(b) $\delta_f = 60°$; $M = 0.15$.

Figure 9.- Effect of elevator deflection on the aerodynamic characteristics in pitch of the model with a 47° vee tail.

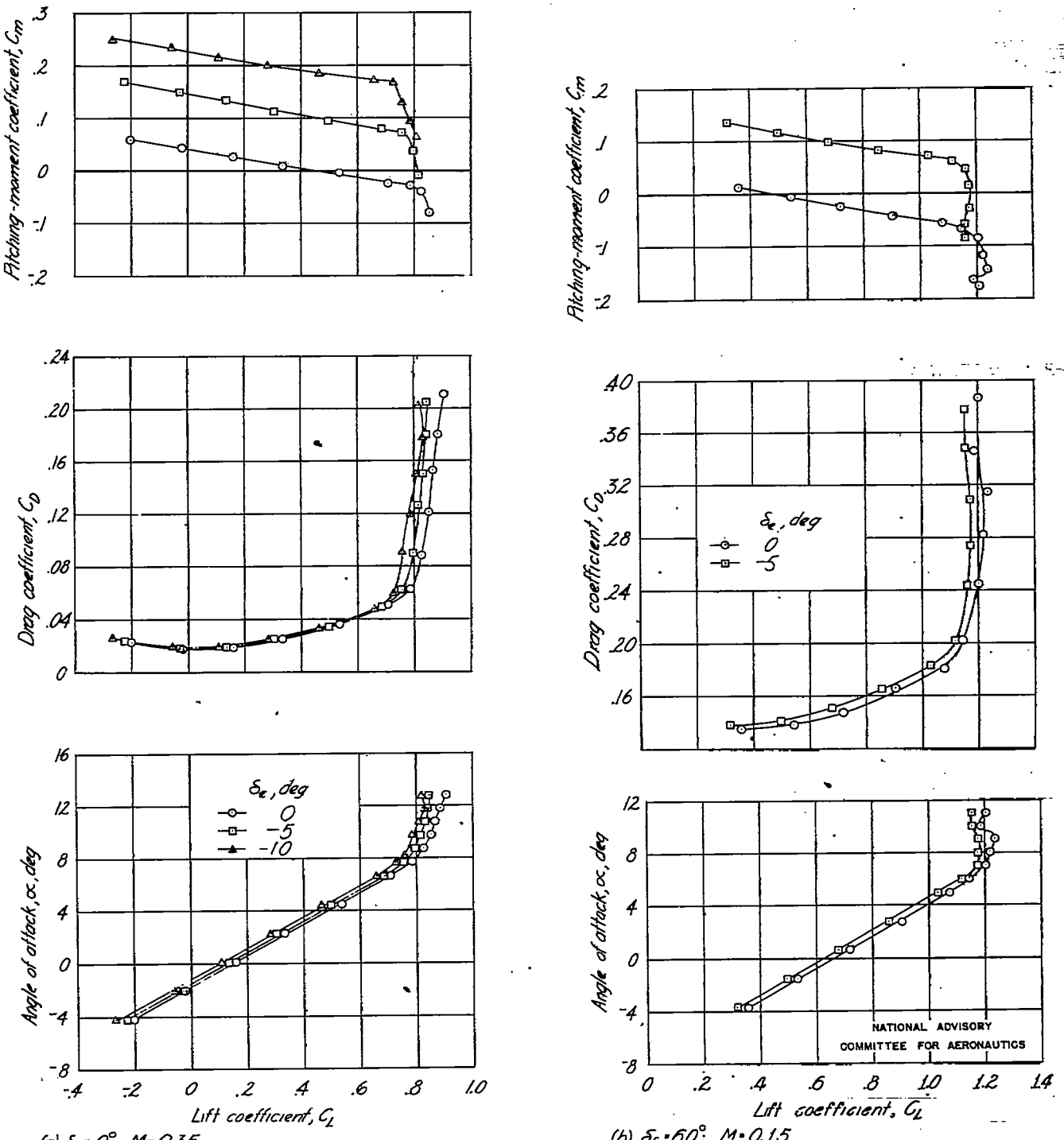

Figure 10.- Effect of elevator deflection on the aerodynamic characteristics in pitch of the model with a 55° vee tail.

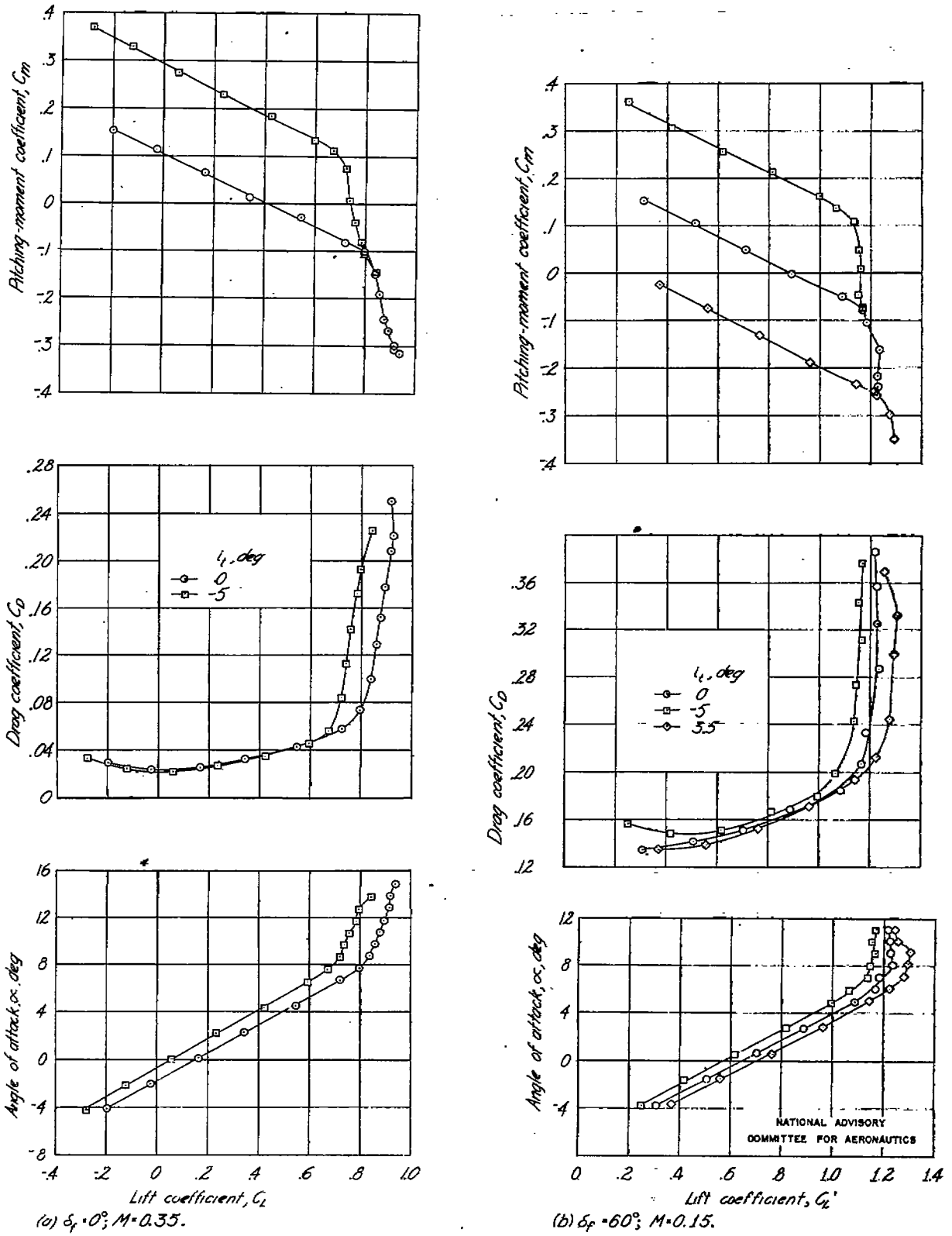

Figure 11.- Effect of stabilizer setting on the aerodynamic characteristics in pitch of the model with a 35° vee tail.

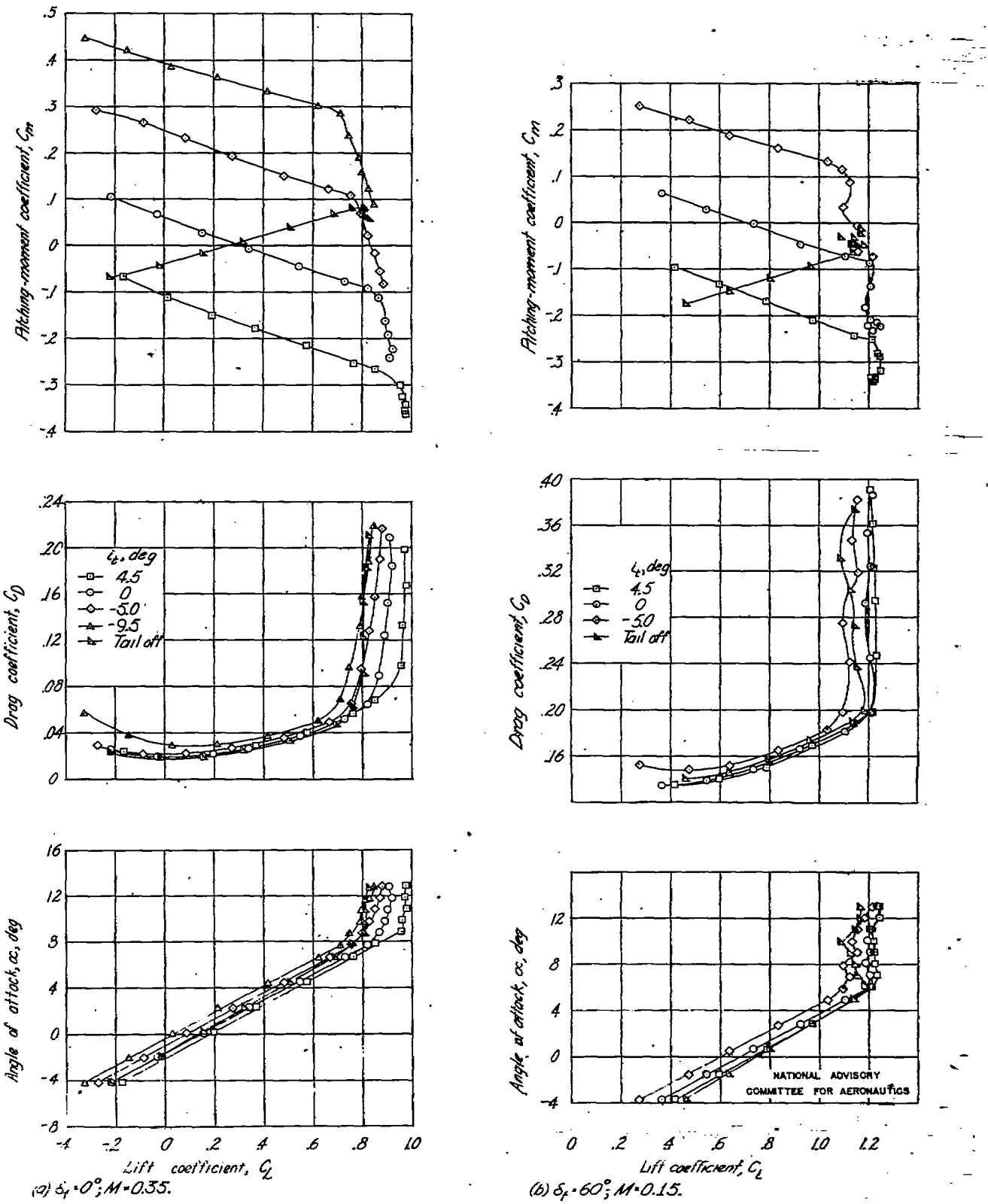

Figure 12.- Effect of stabilizer setting on the aerodynamic characteristics in pitch of the model with a 47° vee tail.

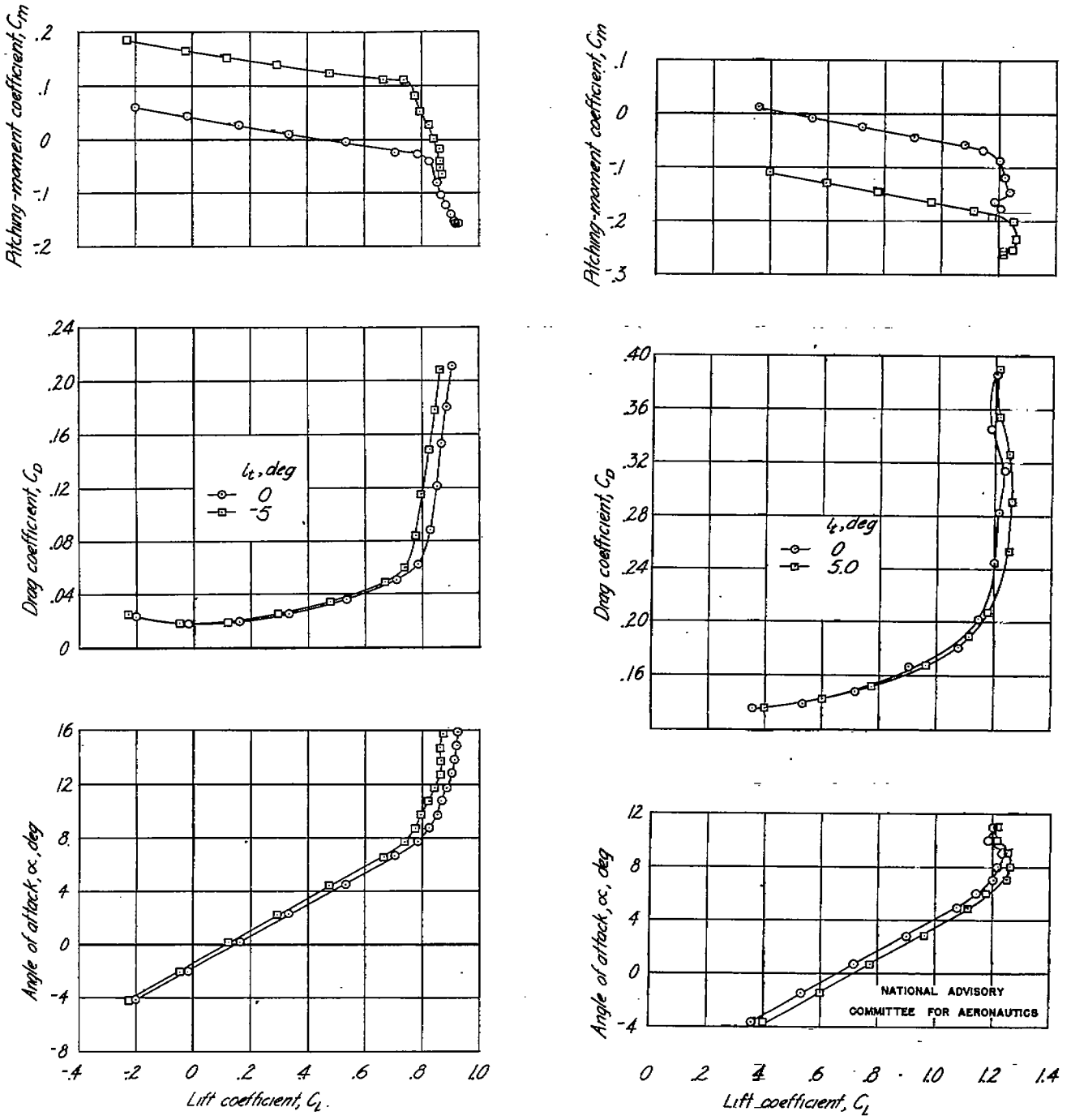

(a) $\delta_f = 0°$; $M = 0.35$.

(b) $\delta_f = 60°$; $M = 0.15$.

Figure 13.- Effect of stabilizer setting on the aerodynamic characteristics in pitch of the model with a 55° vee tail.

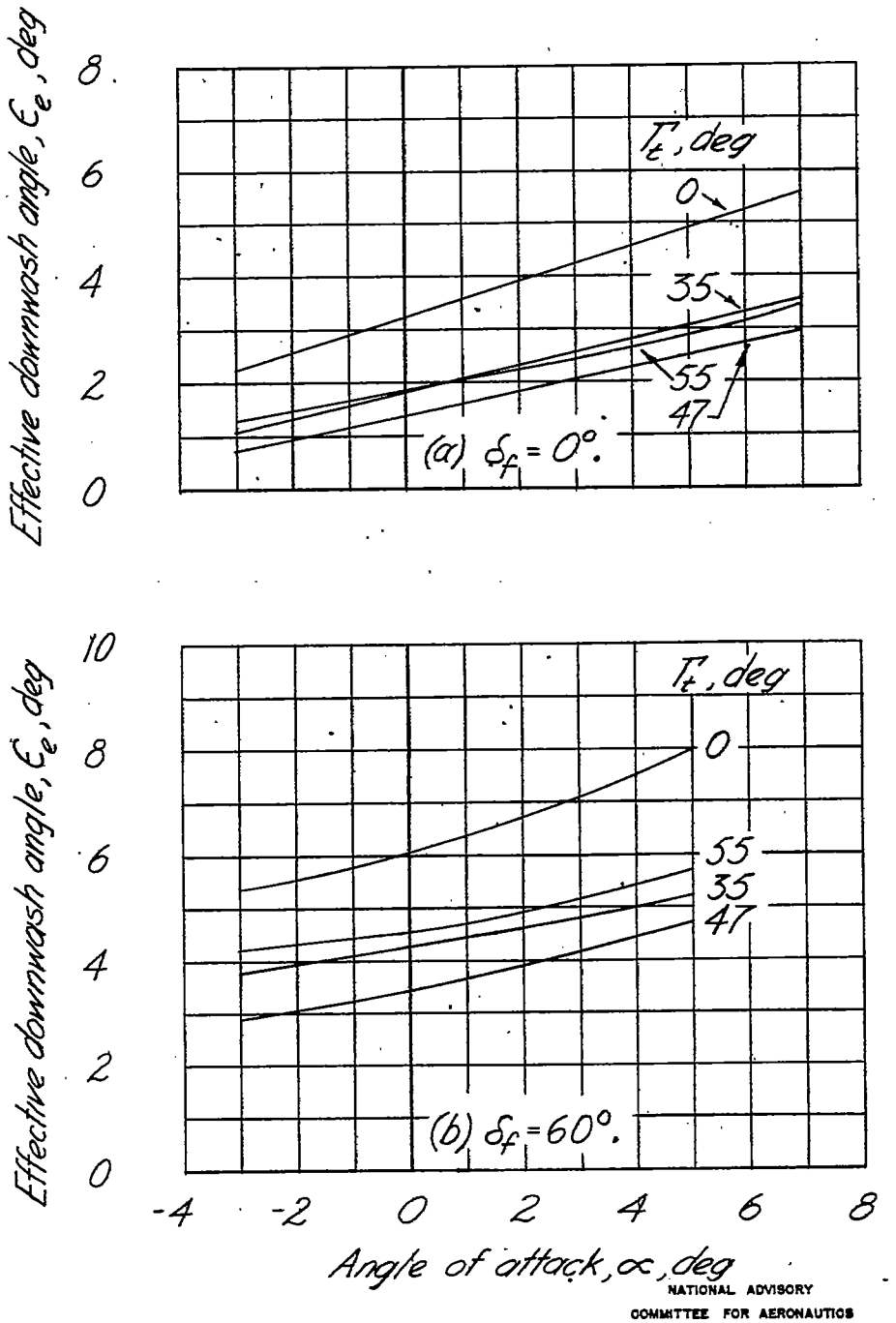

Figure 14.- Variation of effective downwash with angle of attack.

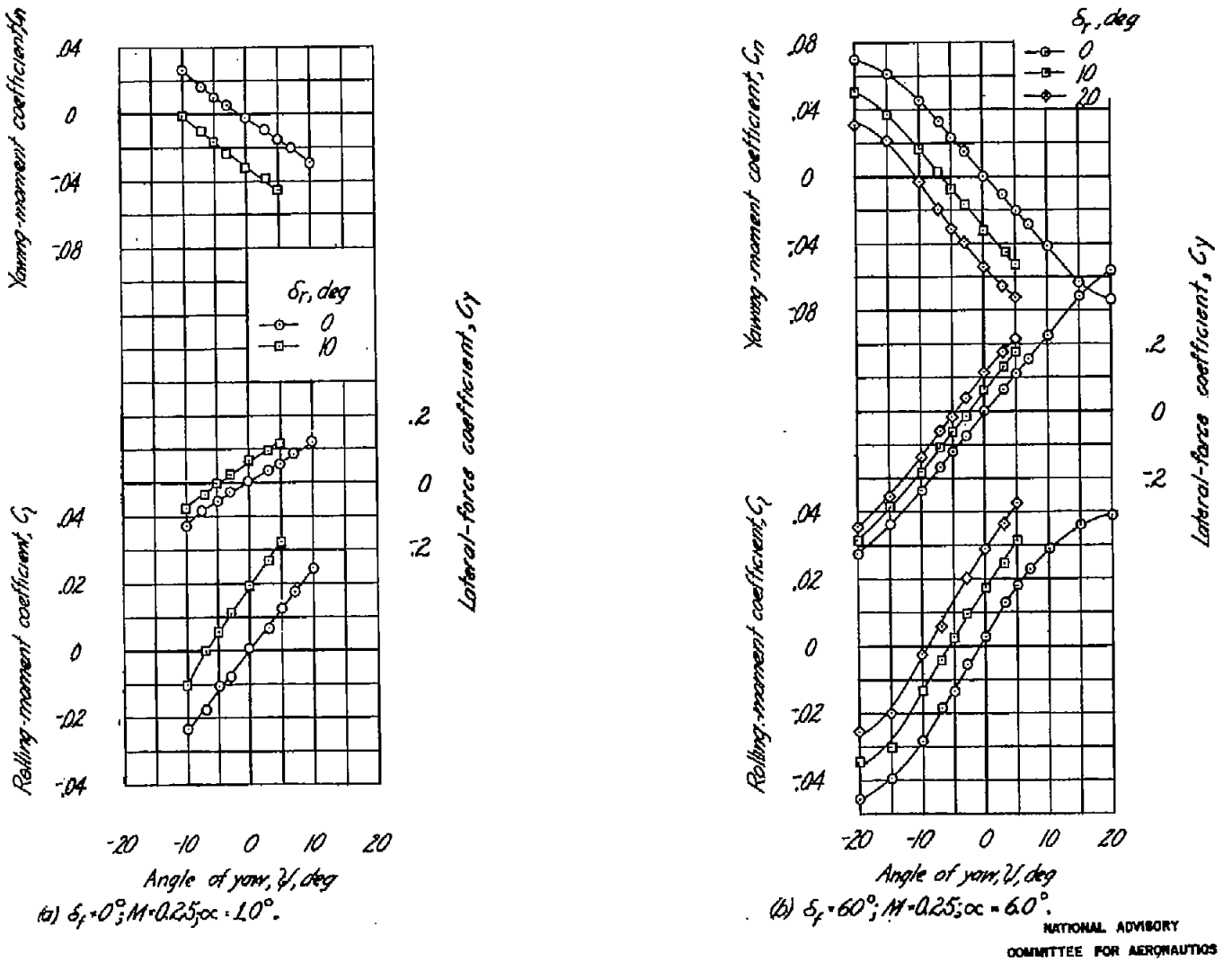

Figure 15.- Effect of rudder deflection on the aerodynamic characteristics in yaw of the model with the 35° vee tail. $\delta_e = 0°$; $i_t = 0°$.

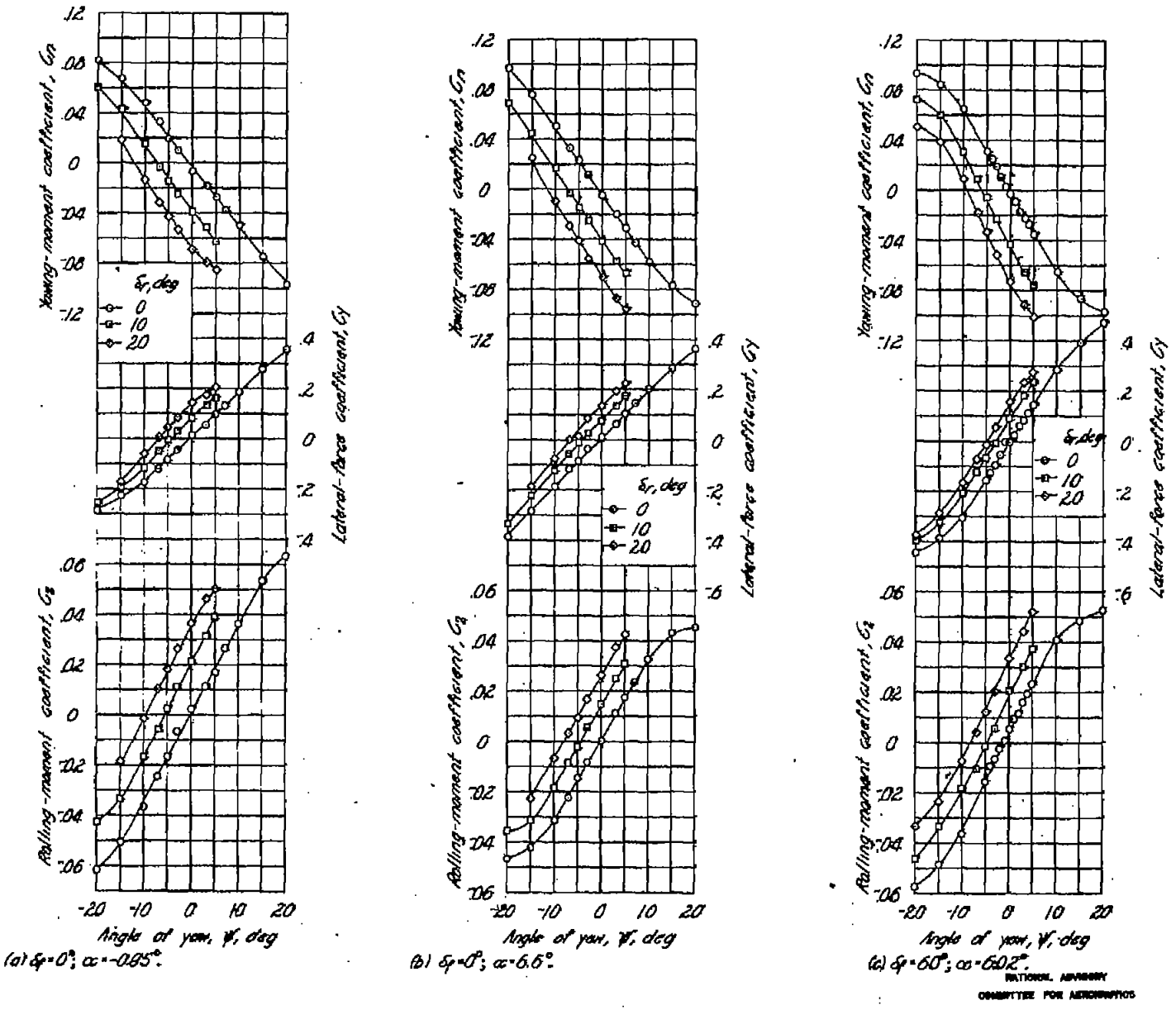

Figure 16.- Effect of rudder deflection in yaw of the model with the 47° vee tail.

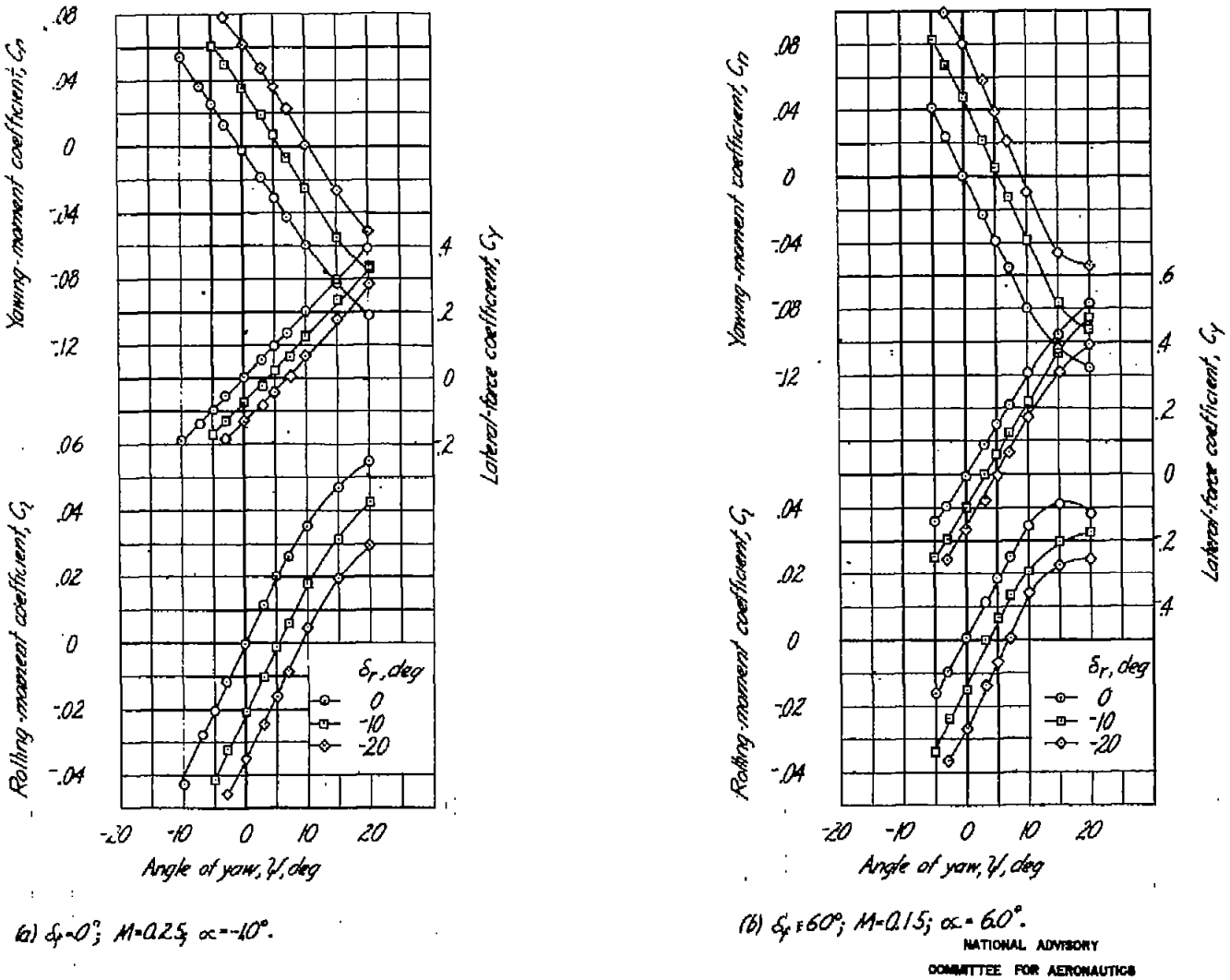

Figure 17.- Effect of rudder deflection on the aerodynamic characteristics in yaw of the model with the 55° vee tail. δ_e = 0°; i_t = 0°.

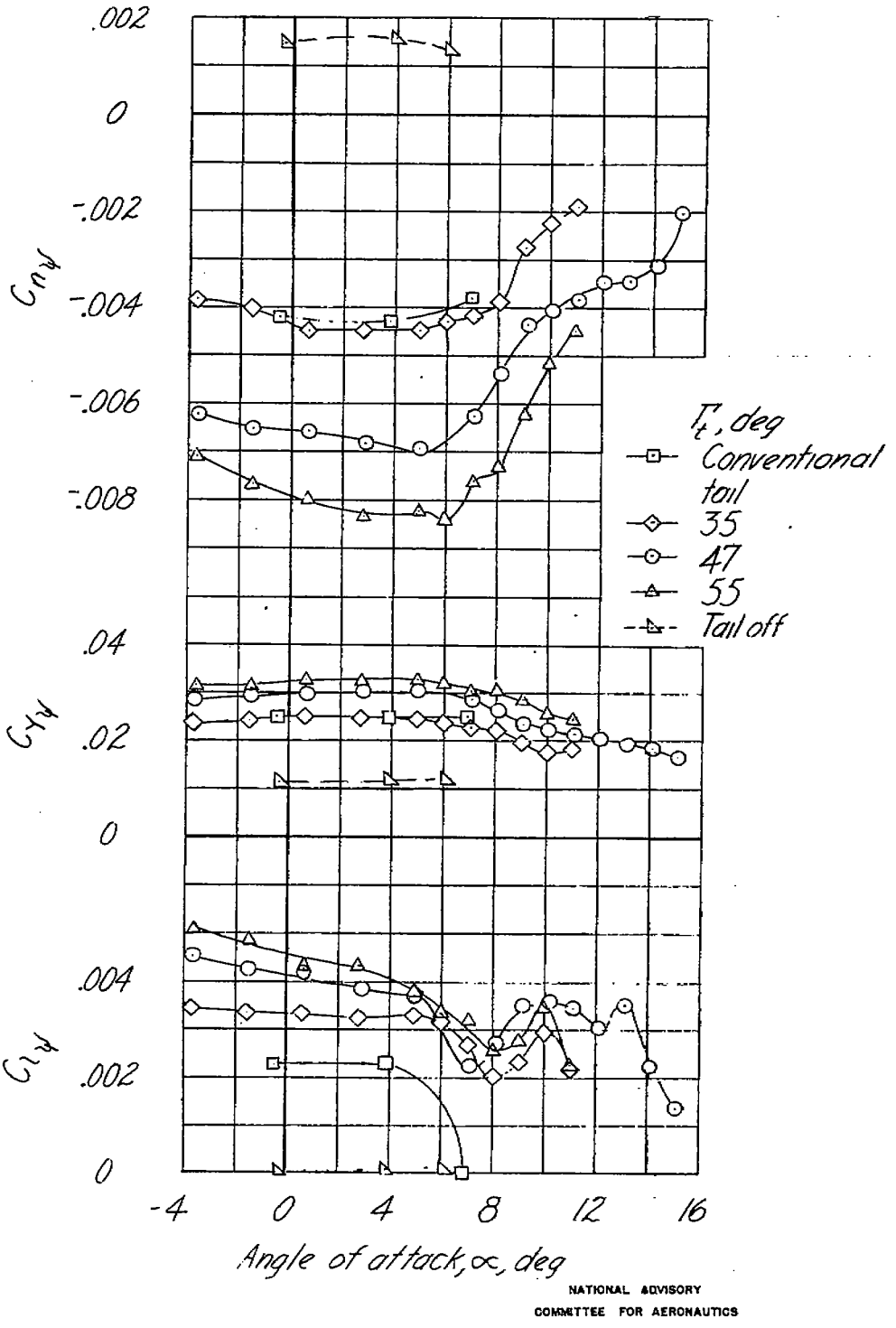

(b) $\delta_f = 60^\circ$; landing gear extended.

Figure 18.- Concluded.

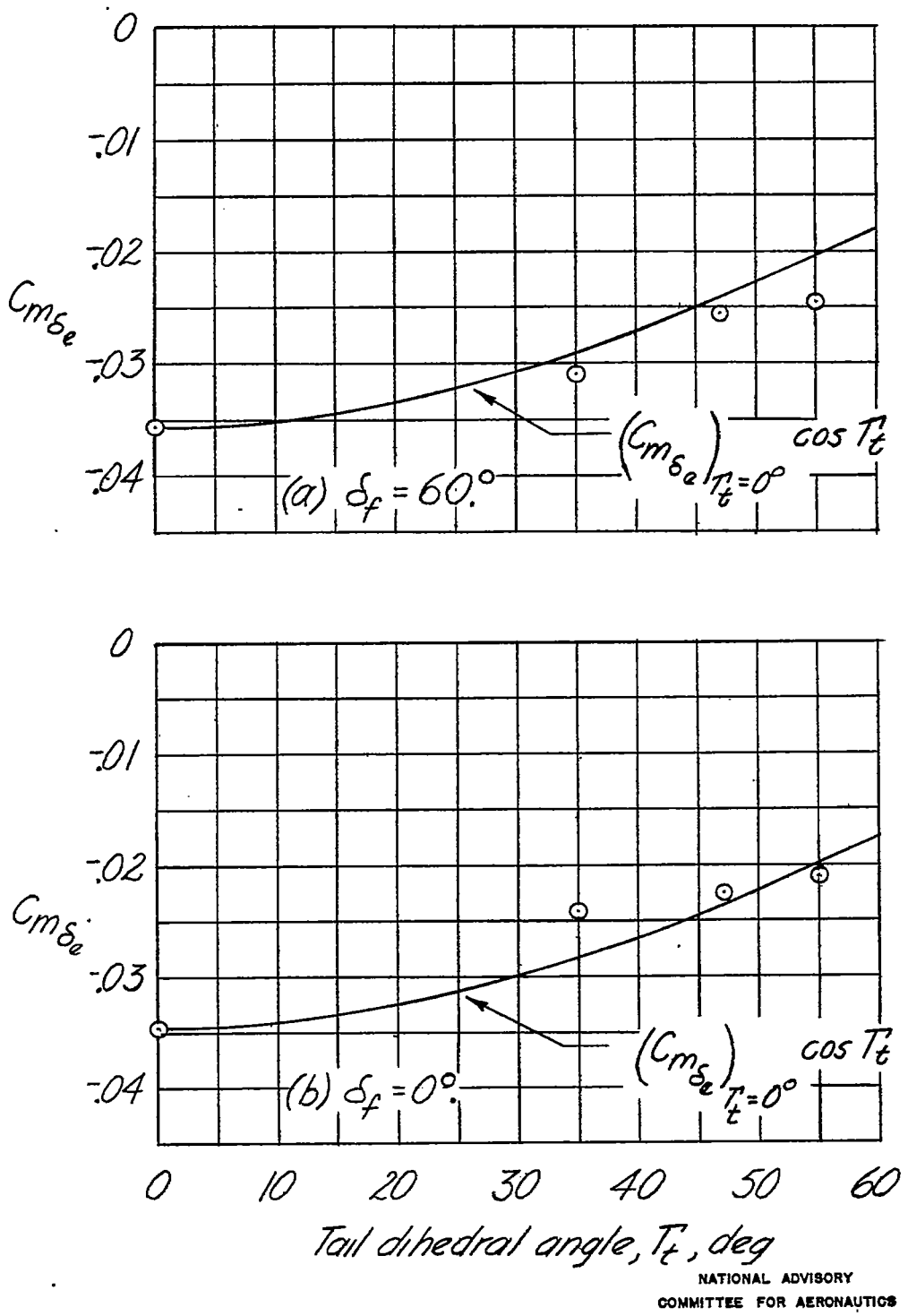

Figure 19.- Variation of elevator effectiveness with tail dihedral angle.

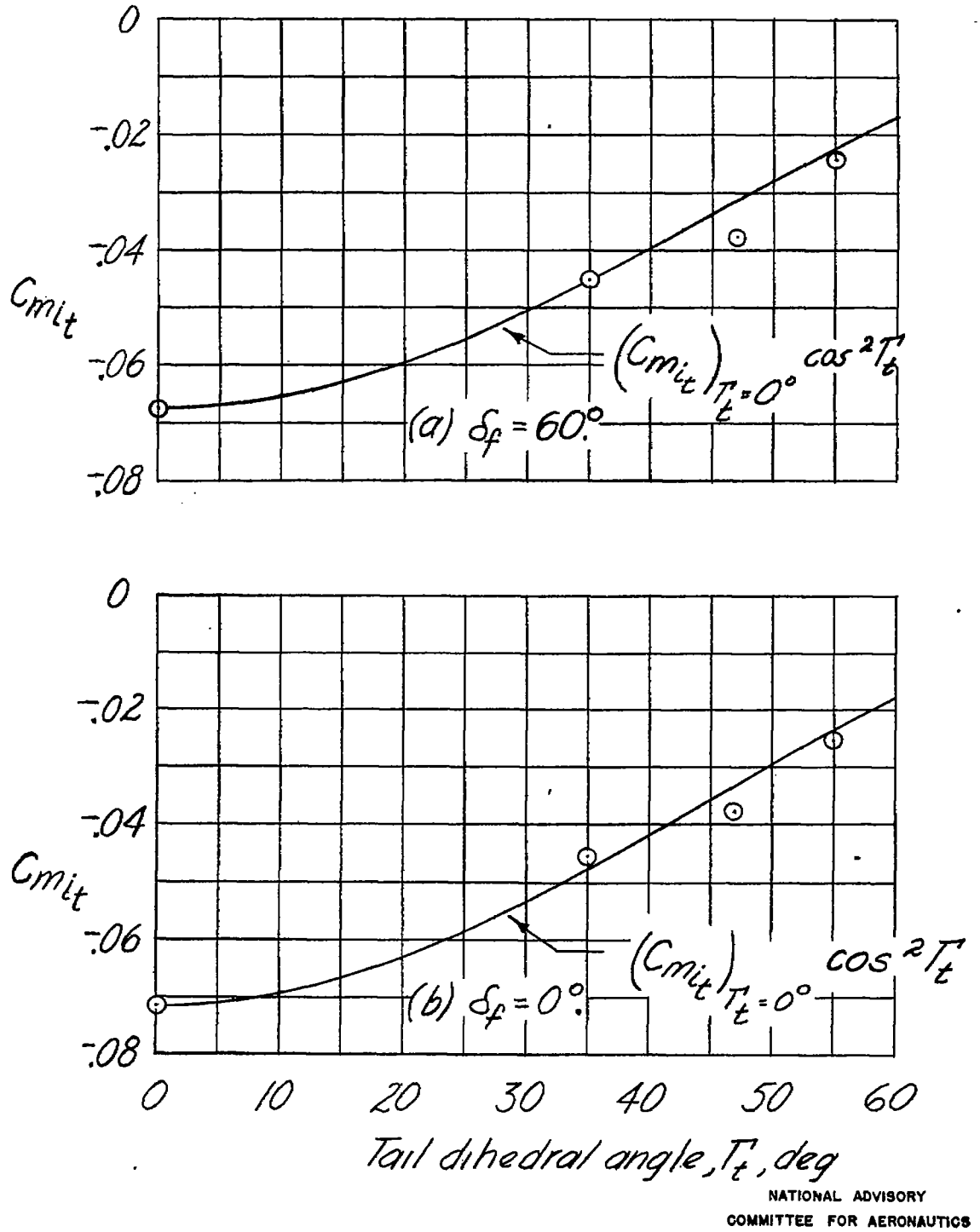

Figure 20. - Variation of stabilizer effectiveness with tail dihedral angle.

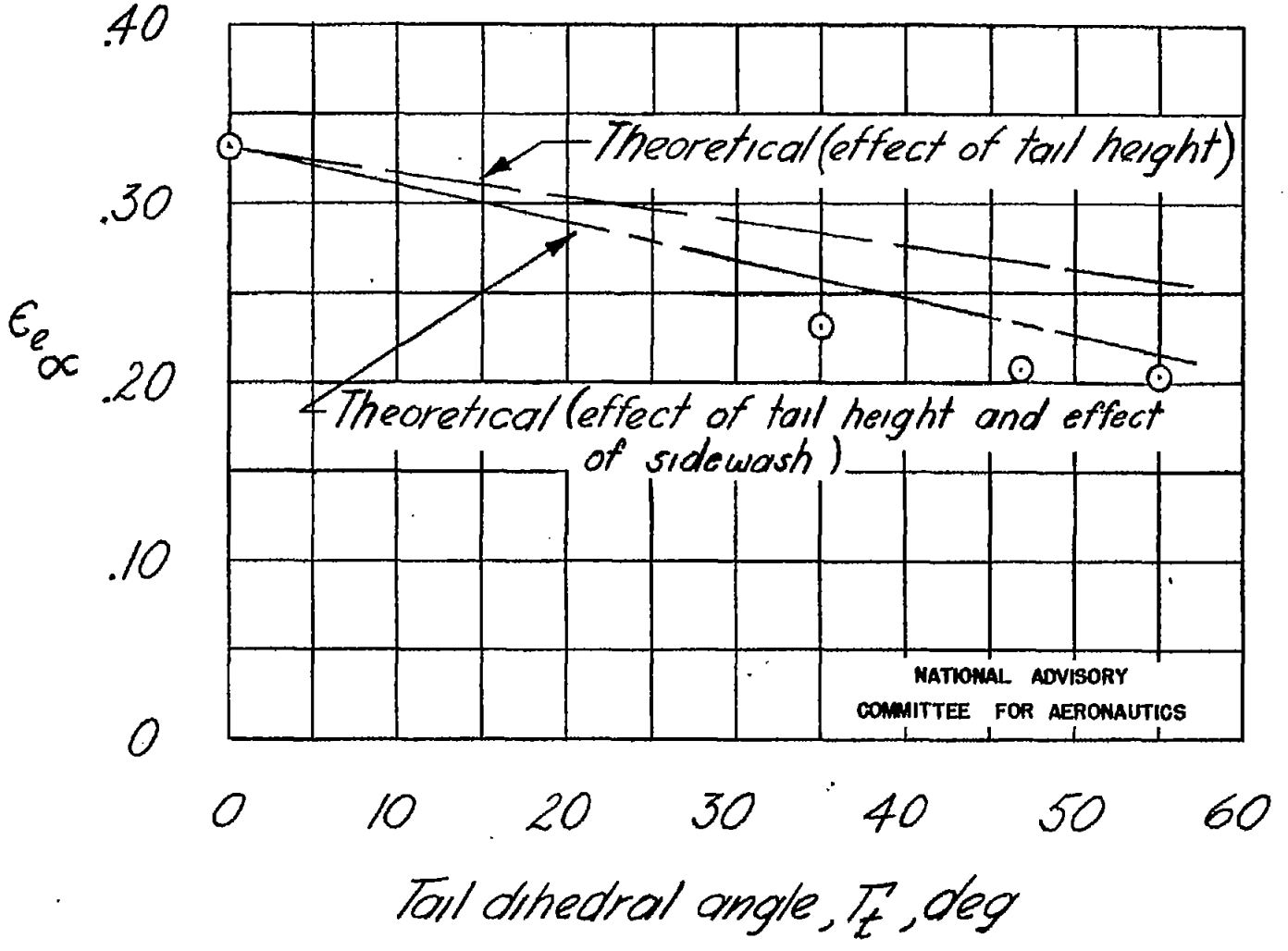

Figure 21.-. Variation of rate of change of downwash with tail dihedral angle. $\delta_f = 0^\circ$; $\alpha = 0^\circ$.

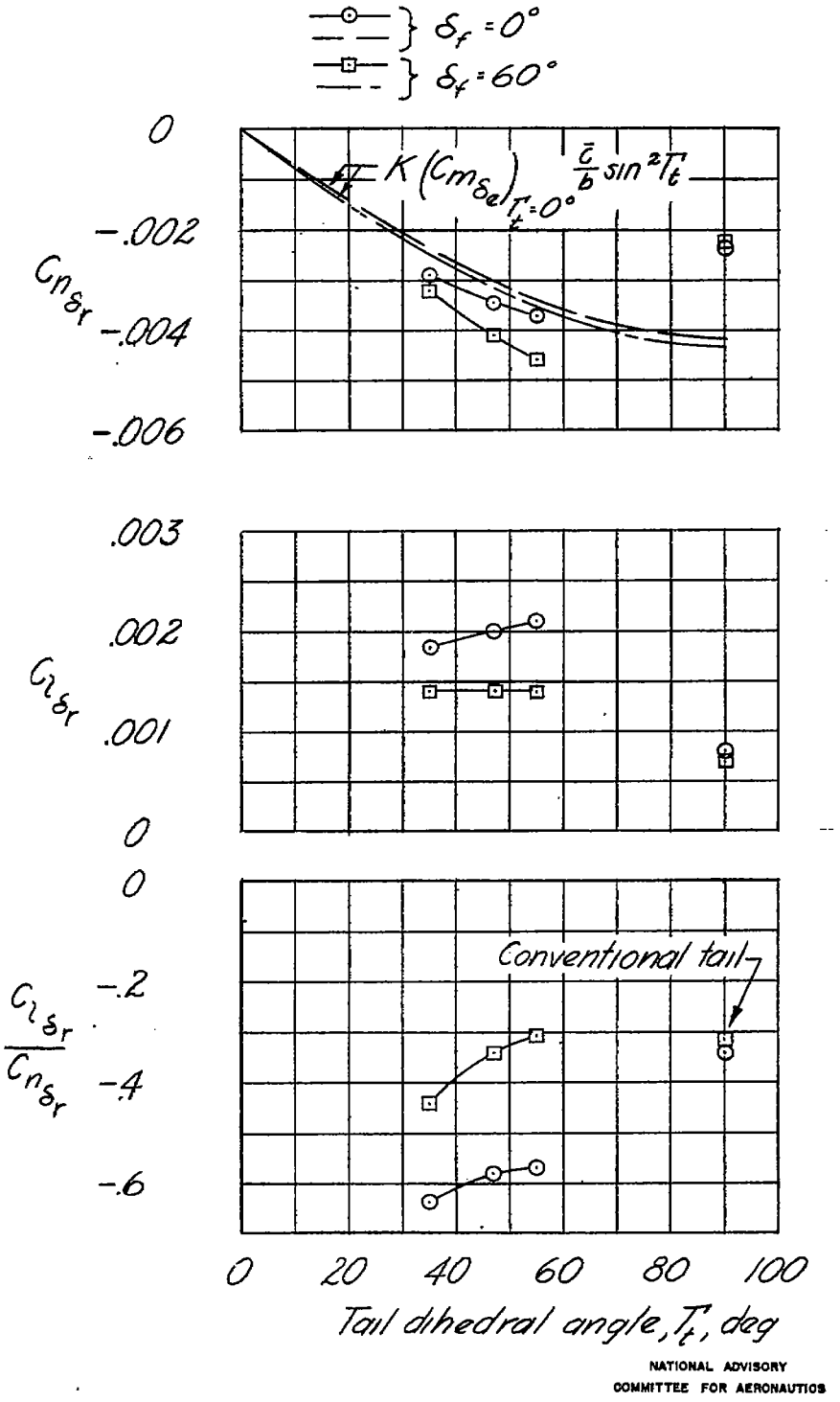

Figure 22.- Variation of rudder effectiveness with tail dihedral angle.

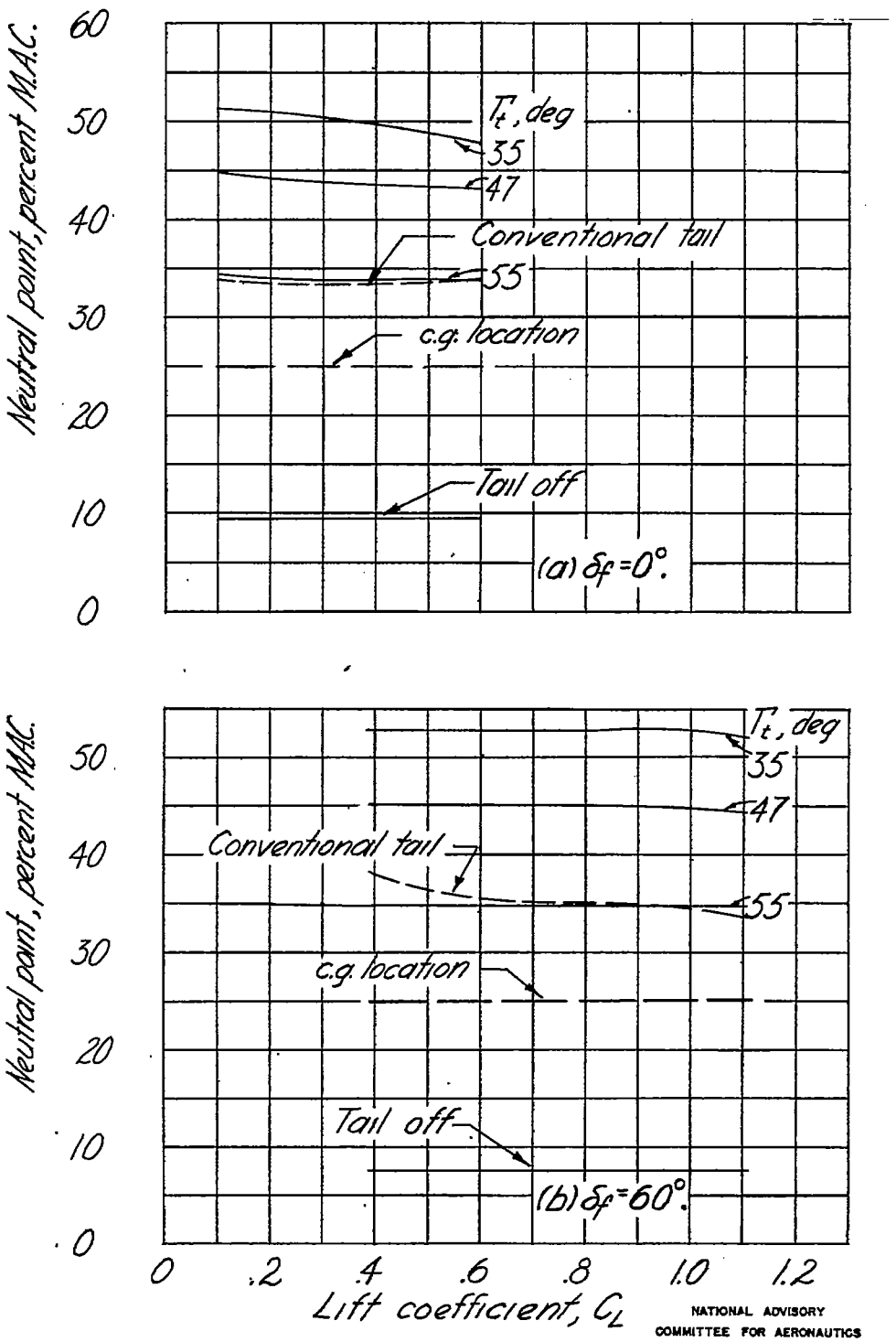

Figure 23.- Variation of neutral points with lift coefficient.

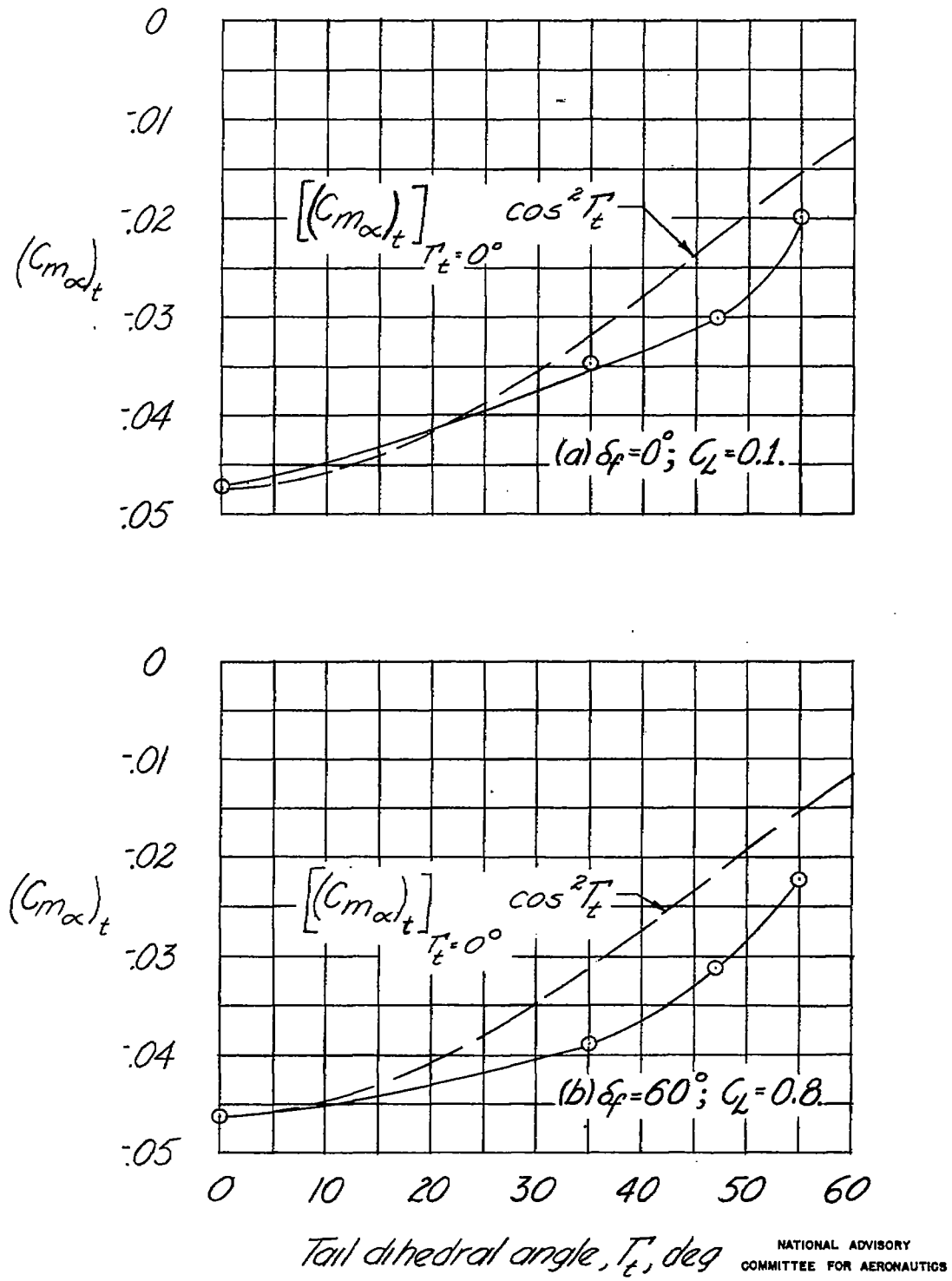

Figure 24.- Variation of $\left(C_{m_a}\right)_t$ with tail dihedral angle.

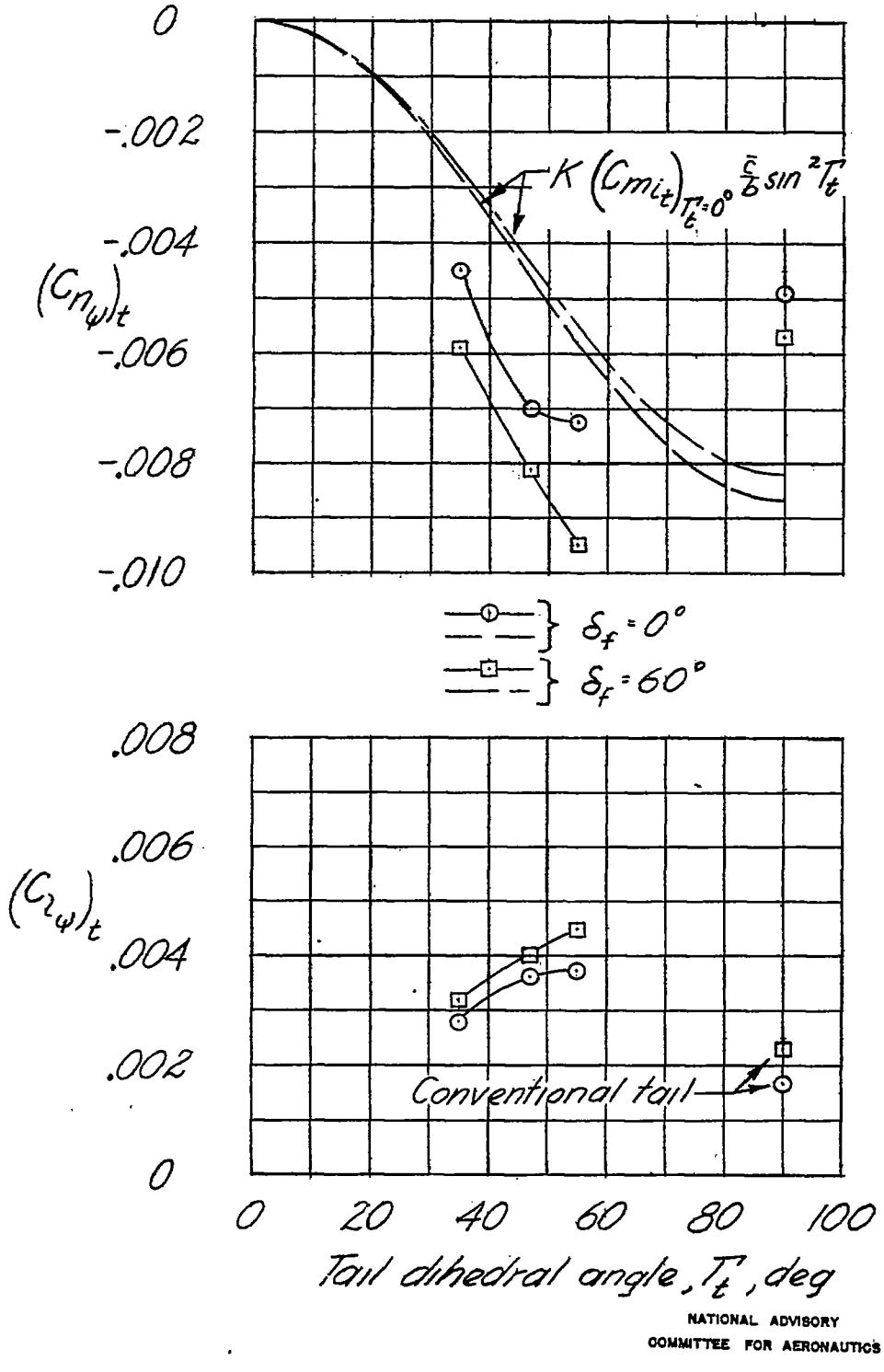

Figure 25.- Variation of tail contribution to lateral stability with tail dihedral angle. $\alpha = 0^\circ$.

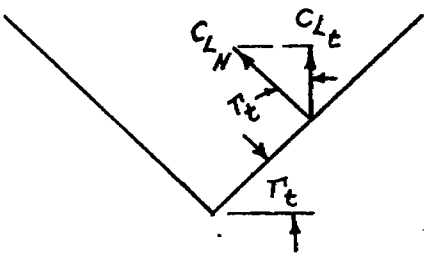

$$C_{L_t} = C_{L_N} \cos T_t$$

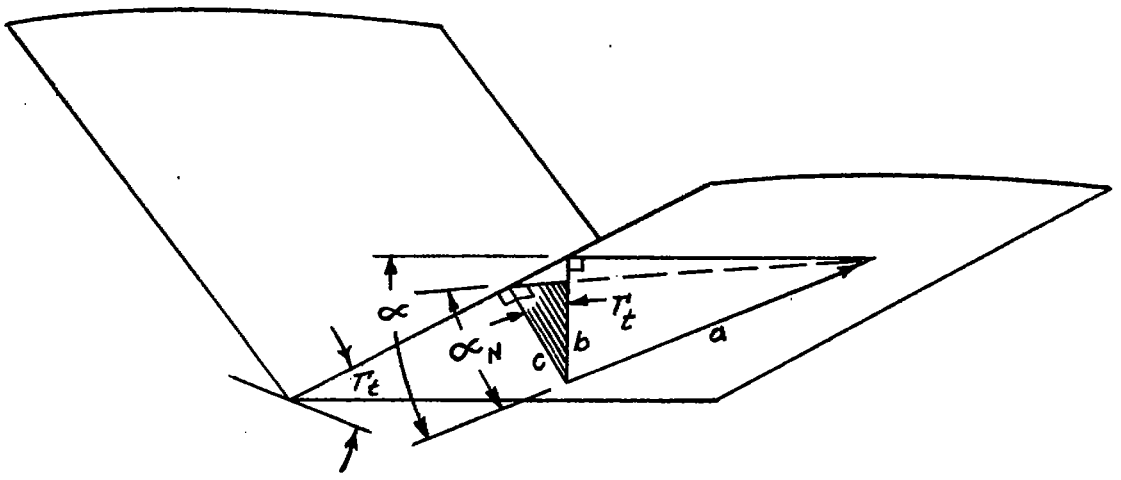

$$\sin \alpha = \frac{b}{a} \text{ , or } a = \frac{b}{\sin \alpha}$$

$$\sin \alpha_N = \frac{c}{a} \text{ , or } a = \frac{c}{\sin \alpha_N}$$

If α and α_N are small

$$a = \frac{b}{\alpha} = \frac{c}{\alpha_N} \text{ , or } \frac{c}{b} = \frac{\alpha_N}{\alpha}$$

but $\frac{c}{b} = \cos T_t$

Therefore, $\frac{\alpha_N}{\alpha} = \cos T_t$, or $\alpha_N = \alpha \cos T_t$

NATIONAL ADVISORY
COMMITTEE FOR AERONAUTICS

Figure 26.- Relations of angles and force coefficients for vee tail in pitch.

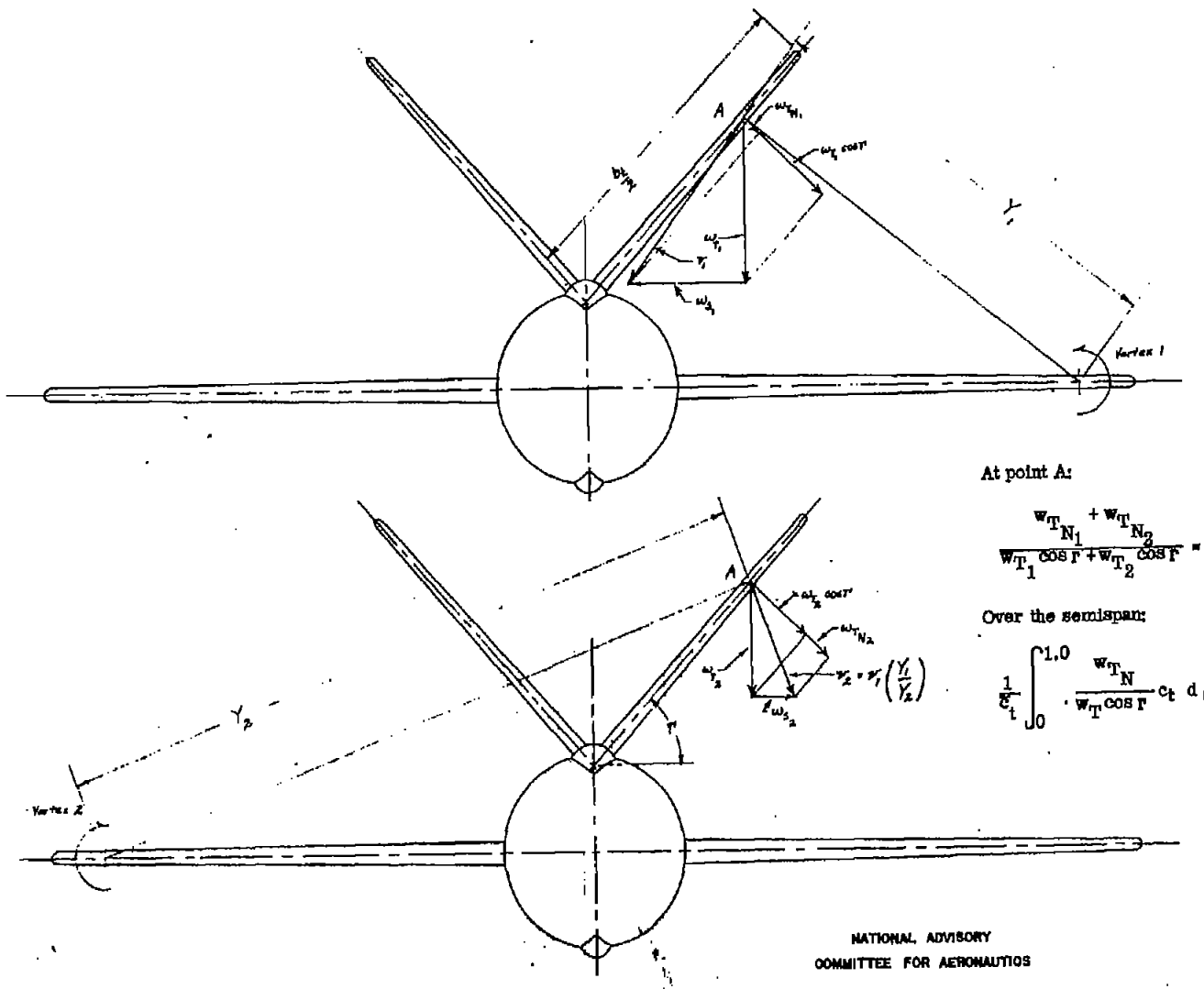

At point A:

$$\frac{w_{T_{N_1}} + w_{T_{N_2}}}{w_{T_1}\cos\Gamma + w_{T_2}\cos\Gamma} = 0.696$$

Over the semispan:

$$\frac{1}{c_t}\int_0^{1.0} \frac{w_{T_N}}{w_T \cos\Gamma} c_t \, d\left(\frac{y}{b_t/2}\right) = 0.798$$

Figure 27.- Effect of sidewash on longitudinal stability. (Subscripts 1 and 2 refer to vortices.)